NUREG/CR-6911

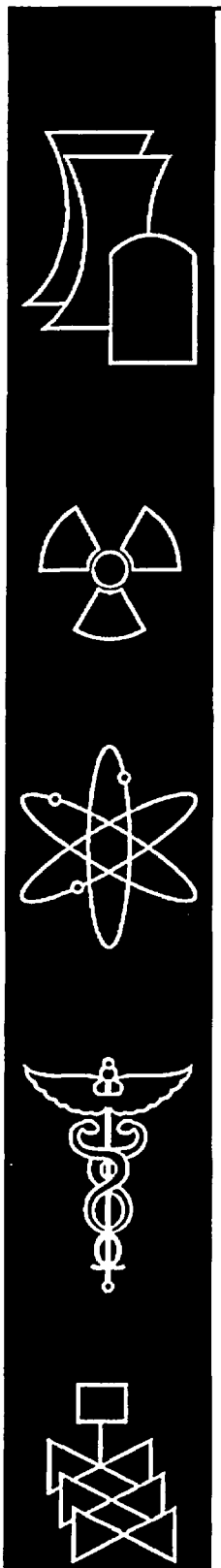

Tests of Uranium (VI) Adsorption Models in a Field Setting

U.S. Geological Survey

U.S. Nuclear Regulatory Commission
Office of Nuclear Regulatory Research
Washington, DC 20555-0001

AVAILABILITY OF REFERENCE MATERIALS IN NRC PUBLICATIONS

NRC Reference Material

As of November 1999, you may electronically access NUREG-series publications and other NRC records at NRC's Public Electronic Reading Room at http://www.nrc.gov/reading-rm.html. Publicly released records include, to name a few, NUREG-series publications; *Federal Register* notices; applicant, licensee, and vendor documents and correspondence; NRC correspondence and internal memoranda; bulletins and information notices; inspection and investigative reports; licensee event reports; and Commission papers and their attachments.

NRC publications in the NUREG series, NRC regulations, and *Title 10, Energy*, in the Code of *Federal Regulations* may also be purchased from one of these two sources.

1. The Superintendent of Documents
   U.S. Government Printing Office
   Mail Stop SSOP
   Washington, DC 20402–0001
   Internet: bookstore.gpo.gov
   Telephone: 202-512-1800
   Fax: 202-512-2250
2. The National Technical Information Service
   Springfield, VA 22161–0002
   www.ntis.gov
   1–800–553–6847 or, locally, 703–605–6000

A single copy of each NRC draft report for comment is available free, to the extent of supply, upon written request as follows:

Address: Office of Administration
Reproduction and Distribution
Services Section
U.S. Nuclear Regulatory Commission
Washington, DC 20555-0001
E-mail: DISTRIBUTION@nrc.gov
Facsimile: 301–415–2289

Some publications in the NUREG series that are posted at NRC's Web site address http://www.nrc.gov/reading-rm/doc-collections/nuregs are updated periodically and may differ from the last printed version. Although references to material found on a Web site bear the date the material was accessed, the material available on the date cited may subsequently be removed from the site.

Non-NRC Reference Material

Documents available from public and special technical libraries include all open literature items, such as books, journal articles, and transactions, *Federal Register* notices, Federal and State legislation, and congressional reports. Such documents as theses, dissertations, foreign reports and translations, and non-NRC conference proceedings may be purchased from their sponsoring organization.

Copies of industry codes and standards used in a substantive manner in the NRC regulatory process are maintained at—

The NRC Technical Library
Two White Flint North
11545 Rockville Pike
Rockville, MD 20852–2738

These standards are available in the library for reference use by the public. Codes and standards are usually copyrighted and may be purchased from the originating organization or, if they are American National Standards, from—

American National Standards Institute
11 West 42nd Street
New York, NY 10036–8002
www.ansi.org
212–642–4900

Legally binding regulatory requirements are stated only in laws; NRC regulations; licenses, including technical specifications; or orders, not in NUREG-series publications. The views expressed in contractor-prepared publications in this series are not necessarily those of the NRC.

The NUREG series comprises (1) technical and administrative reports and books prepared by the staff (NUREG–XXXX) or agency contractors (NUREG/CR–XXXX), (2) proceedings of conferences (NUREG/CP–XXXX), (3) reports resulting from international agreements (NUREG/IA–XXXX), (4) brochures (NUREG/BR–XXXX), and (5) compilations of legal decisions and orders of the Commission and Atomic and Safety Licensing Boards and of Directors' decisions under Section 2.206 of NRC's regulations (NUREG–0750).

NUREG/CR-6911

Tests of Uranium (VI) Adsorption Models in a Field Setting

Manuscript Completed: August 2006
Date Published: August 2006

Prepared by
G. P. Curtis, J. A. Davis

Water Resources Division
U.S. Geological Survey
Menlo Park, CA 94025

A. L. Schwartzman, NRC Project Manager

Prepared for
Division of Fuel, Engineering, and Radiological Research
Office of Nuclear Regulatory Research
U.S. Nuclear Regulatory Commission
Washington, DC 20555-0001
Job Code Y6462

ABSTRACT

Field-based techniques were tested for determining K_d values or for validating surface complexation model-derived K_d values. The field site used for the study was a uranium mill tailings site at Naturita, Colorado. The techniques tested included: 1) the use of downhole *in-situ* devices that held a sample of a single mineral or sediment that were deployed in the aquifer contaminated with uranium, 2) *in-situ* push-pull tracer tests conducted within the contaminated aquifer, and 3) small-scale U(VI) migration tracer tests conducted within the aquifer. The experiments were conducted on scales that ranged from centimeters for the downhole devices to several meters for the small-scale tracer tests.

The tracer test results showed that U(VI) that has been present in the Naturita aquifer for several decades could be readily desorbed by perturbing groundwater chemical conditions. The experimental observations clearly demonstrated that in aquifers where U(VI) concentrations are controlled by adsorption, dissolved U(VI) concentrations can be rapidly impacted by increases or decreases in alkalinity. The experimental results in U(VI) migration tests were reasonably well described by a reactive transport model that simulated adsorption reactions using a semi-mechanistic surface complexation modeling approach. The model predicted both increases and decreases of U(VI) concentration reasonably well when the transport parameters were calibrated to observed Br transport. The results demonstrate the adequacy of the model for simulation of transient geochemical effects under the influence of a natural gradient. In contrast, a constant-K_d model would have predicted neither the observed increases nor decreases in U(VI) concentration in tests in which only the alkalinity of the groundwater was perturbed. This indicates that the uncertainty of predictions using the SCM approach were much smaller than those that would have been obtained if a constant-K_d approach had been used to model U(VI) adsorption. A detailed understanding of U(VI) surface and aqueous speciation is required to predict changes in U(VI) concentration in the Naturita aquifer, and likely in other aquifers contaminated with U(VI).

It was concluded that push-pull test results were not useful in the Naturita aquifer for evaluating adsorption model parameters. The limitation results from the nearly reversible nature of the reactive transport simulations when applied to cases where sorption processes are probed by manipulating groundwater alkalinity. Velocity and/or dispersive processes in the aquifer were sufficiently large that geochemical effects were dampened by dilution in most of the experiments. Push-pull tests may be useful for studying *rates* of sorption and desorption in aquifers.

The results with downhole in-situ devices for measuring K_d values suggest that the method needs further improvement. Furthermore, the experiments suggest that surface complexation models for single minerals need to be calibrated in solutions with high dissolved carbonate concentrations in order to be applied to aquifers that contain groundwaters in equilibrium with partial pressures of carbon dioxide gas greater than 0.01 atmospheres, such as the Naturita aquifer.

FOREWORD

The U.S. Nuclear Regulatory Commission (NRC) is responsible for the regulatory oversight of remediation and cleanup of sites contaminated with radionuclides. Regulatory decisions associated with this responsibility are based, in part, on performance assessment (PA) calculations that utilize numerical models to estimate radioactive exposure at selected locations. Determining the radioactive exposure risk in PA requires the calculation of total radionuclide concentrations present at a specific site. Subsurface transport models used by the NRC and its licensees estimate the effects of the anticipated interactions between radionuclides and solids in the ground. In practice, however, most reactive transport models summarize the chemical complexity of aqueous complexation and sorption processes by utilizing a single constant distribution coefficient (i.e., K_d value) approach. This approach defines the distribution coefficient as the proportion of radionuclide in the groundwater compared to the radionuclide associated with the solids in the ground. Uncertainties in these distribution coefficients for various soil types are the result of their sensitivities to water chemistry and mineralogy. Distribution coefficients used to characterize the adsorption of radionuclides in soils have been identified as potential sources of uncertainty in decommissioning, uranium recovery, and radioactive waste disposal cases.

The NRC has worked with the U.S. Geological Survey (USGS), through interagency agreements, to develop more realistic models for site-specific chemical sorption processes. The ultimate goal of this work is to create more realistic PA models that can adequately represent the effects of natural processes at chemically complex sites on radioactive materials movement through the environment. One way the NRC and its licensees assess the potential movement of radioactive materials in the subsurface is by modeling the transport of radionuclides on specific sites. Therefore, techniques for determining site-specific distribution coefficients are necessary to both implement and test the results of models that are sensitive to changes due to mineralogy and water quality from point-to-point and over time. This report evaluates field-based techniques for determining K_d values or for validating laboratory- or model-derived K_d values. The site used for this study was a uranium mill tailings site at Naturita, Colorado.

This report is one in a series of reports documenting a field demonstration using surface complexation models to obtain a more realistic and site-specific estimate of the movement of radioactive materials in soil. This report investigates three field-based techniques for determining K_d values for a specific field site. Section 1 provides a detailed description of the Naturita field site and a general description of the project. Section 2 compares the K_d values determined in the field with K_d values predicted using surface complexation models. Section 3 describes two types of tracer tests used to evaluate the applicability of semi-mechanistic surface complexation modeling (SCM) for describing uranium (VI) adsorption and desorption under field conditions. Section 4 provides observations and modeling descriptions associated with the use of push-pull tracer tests, and Section 5 focuses on the use of small-scale migration tracer tests to model the site.

Included in this report are detailed discussions of the physical and hydrological characteristics of the Naturita site, physical and chemical processes that can influence the adsorption and desorption of radionuclides associated with aquifers on the site, and detailed descriptions of field-scale techniques that can be used to calculate site-specific radionuclide distribution coefficients. An evaluation of the field techniques discussed in this report indicates that some techniques are more applicable to certain sites then others.

Brian W. Sheron, Director
Office of Nuclear Regulatory Research

CONTENTS

FIGURES

TABLES

1 TESTS OF URANIUM(VI) ADSORPTION MODELS IN A FIELD SETTING: INTRODUCTION AND FIELD SITE DESCRIPTION

1.1 Introduction

Numerous sites throughout the United States are contaminated by radionuclides, especially uranium (U) and thorium (Th) and their by-products, due to mining, milling, and other industrial processes (Morrison and Cahn, 1991). The United States Nuclear Regulatory Commission (USNRC) is responsible for the regulatory oversight of site remediation and clean up, and possible release of sites for public or unrestricted use. Licensing decisions are made based on performance assessment (PA) calculations that utilize numerical models to estimate the increase in radioactivity exposure to the biosphere at selected locations. Contamination is often limited to the soils, subsurface sediments, and shallow aquifers at these sites.

Prediction of the fate and transport of radionuclides is of paramount importance in evaluating remediation schemes and in quantifying the risk of contamination to human or ecosystem health (Davis et al., 2004a; USEPA, 1999). To make a calculation of radioactive exposure risk in PA, it is necessary to calculate the total amount of each radionuclide that will be present at selected locations as a function of time. A solute transport model is typically used to describe the physical processes of advection and dispersion that may transport radionuclides in groundwater from the source location to a site of ingestion. In addition to these hydrophysical processes, the transport of many radionuclides can be strongly influenced by reactive chemical processes, including aqueous complexation, sorption, precipitation and dissolution, and redox reactions. However, in practice, most reactive transport models ignore the chemical complexity of aqueous complexation and sorption processes and utilize the distribution coefficient (constant K_d) approach to describe the retardation of radionuclide contaminants (Curtis et al., 2006; Davis and Curtis, 2003; USEPA, 1999). Although sorption is only a part of the overall PA calculations, retardation of radionuclide transport in the far-field geosphere zone may be extremely important in reducing the risk of biosphere exposure of certain radionuclides to levels that are in compliance with regulations. In order to be "conservative", large ranges of K_d values may need to be estimated by expert judgement in order to account for possible changes in chemical conditions and for other sources of error. The uncertainties in these ranges are difficult to assess quantitatively without doing large numbers of experiments.

In this study, field-based techniques were tested for determining K_d values or for validating laboratory- or model-derived K_d values. The field site used for the study was the uranium mill tailings site at Naturita, Colorado (Davis and Curtis, 2003). The techniques included: 1) the use of downhole *in-situ* devices that held a sample of a single mineral or sediment that were deployed in the aquifer contaminated with uranium, 2) *in-situ* push-pull tracer tests conducted within the contaminated aquifer, and 3) small-scale U(VI) migration tracer tests conducted within the aquifer. The experiments were conducted on scales that ranged from centimeters for the downhole devices to several meters for the small-scale tracer tests.

1.2 The Naturita UMTRA Site

Uranium (U) ore processing on the Colorado Plateau resulted in a number of inactive mill tailing sites at which there is contamination of groundwater (USDOE, 1996). The groundwater at many of these sites is contaminated with U and often other species including vanadium (V), selenium and molybdenum. The USDOE is responsible for clean up of many of these sites as dictated by the Uranium Mill Tailings Remediation Act (UMTRA).

Uranium occurs in the environment predominantly as U(IV) in reducing systems and U(VI) in oxic systems. In reducing waters, U(IV) forms insoluble phases and thus is

relatively immobile (Langmuir, 1997). In oxic waters, U(VI) forms many soluble hydroxide and carbonate complexes which lead to increased solubility and mobility. Precipitation of U(VI) phases usually occurs only within and near uranium ore bodies or near concentrated waste sources. Adsorption of U(VI) in oxic waters is sensitive to pH and partial pressure of carbon dioxide gas (pCO_2). Adsorption is generally negligible at low pH values where the uranyl cation (UO_2^{+2}) is the dominant species and increases with increasing pH usually in the pH range of 4 to 6. In the alkaline region, U(VI) is strongly adsorbed in the absence of dissolved CO_2 (Hsi and Langmuir, 1985; Prikryl et al., 2001) but in the presence of dissolved CO_2, the formation of U(VI)-carbonate complexes reduces adsorption (Davis et al., 2004b; Waite et al, 1994). At intermediate values of pH and CO_2, the extent of adsorption is determined by competition between the formation of aqueous U(VI)- carbonate complexes and surface U(VI)-carbonate complexes (Bargar et al., 1999; Bargar et al., 2000; Bostick et al., 2002; Arai et al., 2006). The importance of CO_2 in the formation of both aqueous and surface complexes with U(VI) illustrates that adsorption and transport of U(VI) can be strongly impacted by variable alkalinity.

Dissimilatory Fe(III)-reducing bacteria (DIRB) play an important role in the geochemistry of many subsurface groundwater and sediment environments. Many DIRB are able to reduce the highly soluble and mobile U(VI) species to highly insoluble U(IV), which precipitates as uraninite (Lovely et al., 1991). Microbial Fe(III) reduction can also lead to an increase in radionuclide mobility if sorbed or co-precipitated U(VI) is released following Fe(III) oxide reduction. Sorbed Fe(II) on mineral surfaces (Jeon et al., 2005; Liger et al., 1999) and mineral phases containing Fe(II) (O'Loughlin et al., 2003; Wersin et al., 1994) can also reduce U(VI) to U(IV).

The Naturita UMTRA site is useful for studying the influence of the processes mentioned above on U fate and transport (Curtis et al., 2006; Davis et al., 2006). The site has both variable alkalinity and redox conditions, resulting in complex U(VI) transport behavior.

1.2.1 Site Description

The former U mill tailings site is approximately 3 km northwest of the town of Naturita, CO along the San Miguel River in southwestern Colorado as shown in Figure 1.1. The San Miguel River is the only perennial surface water body at the site. The Naturita area is semi-arid; the estimated average annual precipitation is 9 inches (23 centimeters) and grasses and sagebrush dominate the vegetation, except near the river where cottonwoods are common.

The ore mill processed U and V ores at the site beginning in 1939 almost continuously until the mill was shut down in 1958. From 1961 until 1963, a U ore upgrader was operated at the site. Uranium and V were extracted from the ore by salt roasting followed by carbonate leaching in percolation tanks. Carbonate leach tails were slurried to the western half of the Naturita site to an area of the site farthest (200 meters) from the San Miguel River and closest to highway 141. Carbonate leaching residues were later sent to a second stage of sulfuric acid leaching. Acid leach tails were deposited closer to the river. Between 1977 and 1979, the mill tailings were removed from the site, and between 1996 and 1998 the contaminated surface soils were excavated and transported offsite.

1.2.2 Hydrogeology

Contaminated groundwater at the Naturita site occurs in the thin alluvial deposits of the San Miguel River floodplain. The aquifer is recharged by the river to the southeast of the site and discharges into the river north of the site. Ground water flows approximately parallel to the river. The alluvial aquifer is separated from an underlying, moderately permeable sandstone aquifer (the Salt Wash Member) by a fine-grained shale (the Brushy Basin Member), which is approximately 30 m thick. The average saturated thickness is 1.8 m when the river is at low flow conditions. The alluvial aquifer consists of sand, gravel and cobbles and the mineralogy consists of primarily quartz with

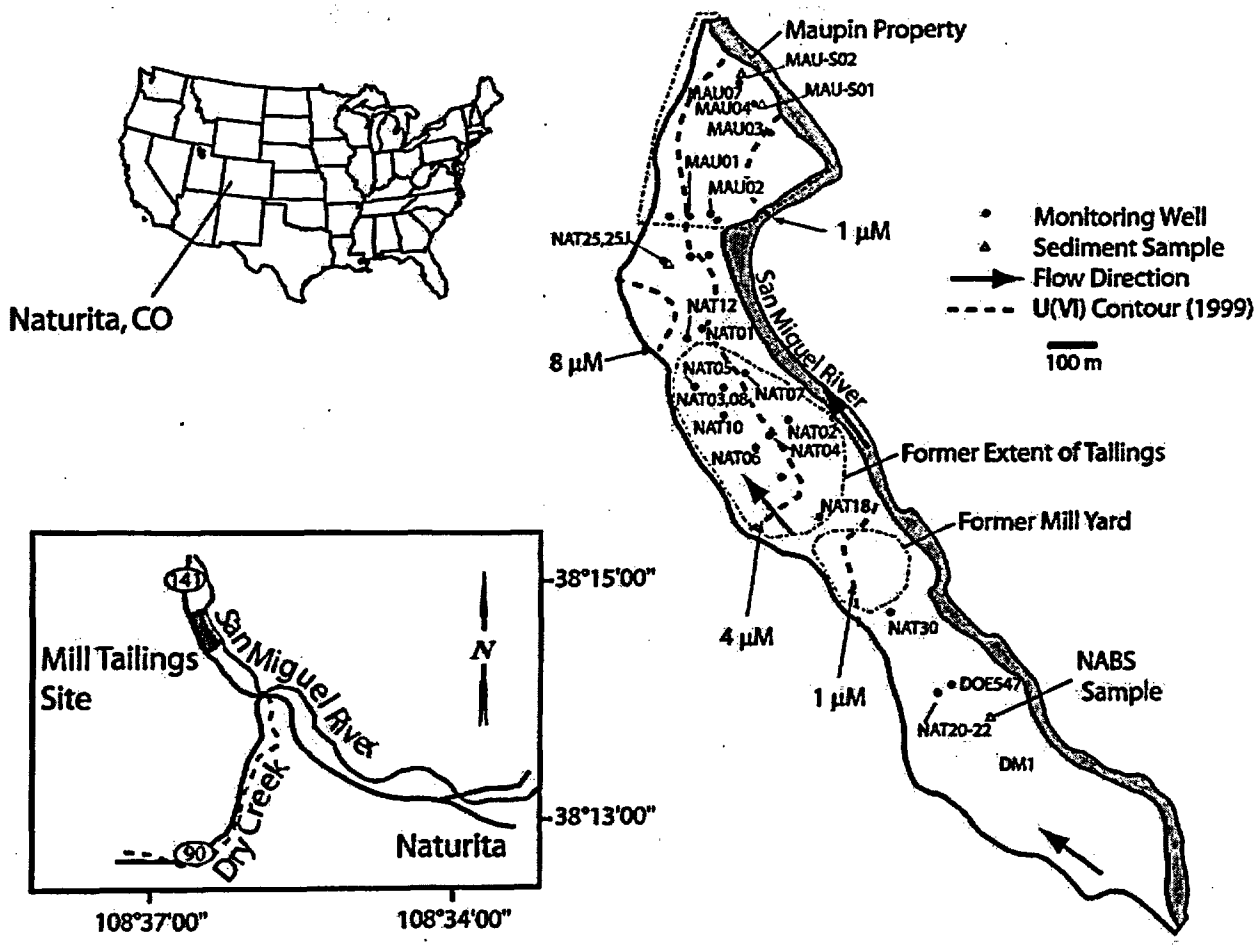

Figure 1.1. Locality Map of Naturita, Colorado, U.S.A, showing locations of groundwater monitoring wells, sediment sampling locations, groundwater flow direction, locations of the former uranium mill yard and tailings pile, and U(VI) concentration contours in 1999.

lesser amounts of detrital feldspars, carbonates, magnetite, and fine clay-size materials (Davis et al., 2004b).

Figure 1.1 shows a map of the Naturita site that illustrates the location of the former mill yard, the extent of the former tailings pile, and all of the monitoring wells at the site. Between 1986 and 1997, USDOE installed 12 wells in the alluvial aquifer and 2 wells in the Salt Wash aquifer. All of these wells except DOE-547 and DOE-548, which are in the alluvial aquifer, were removed by the end of 1998. In 1998 and 1999, the USGS installed wells at 39 new locations and some of these new wells were clusters that included some multilevel wells. High concentrations of U(VI) are found in the ground water below and downgradient of the former tailings pile. Both water used to process the U ore and mill tailings and rain and snow that leached U from the deposited tailings could have caused the transport of U(VI) to the ground water at the site.

A well that was installed in the Salt Wash aquifer in the 1980's and subsequently abandoned by USDOE had heads that exceeded those in the alluvial aquifer indicating the potential for vertically upward flow and transport. The deep groundwaters had an average chloride (Cl) concentration of 20 mM, which was 200 times higher than Cl in background alluvial wells, indicating minimal

upward flow. The U(VI) concentration in the deep groundwaters was 0.16 μM.

1.2.3 Geochemical Characterization

Spatial concentration contours for alkalinity, pH, and dissolved U(VI), Ca, Fe, Mn, and O_2 in the Naturita alluvial aquifer in March 2004 are shown in Figure 1.2. Elevated concentrations of U(VI) and alkalinity were observed below and downgradient of the former uranium mill tailings, and the concentrations were generally lower near the San Miguel River and higher near the western edge of the aquifer. The average U(VI) concentration in the wells upgradient of the former mill site was 0.02 μM, and a peak concentration of 7 μM was observed at well NAT-26. Most of the impacted groundwater had U(VI) concentrations between 2 and 6 μM. Alkalinity had a similar spatial pattern as the U(VI) concentration, but the range in concentration was smaller. Alkalinity values ranged from approximately 4.7 meq/L upgradient to peak values of 10.5 meq/L at well NAT-26. Calcite saturation indices generally range from –0.25 to 0.35 suggesting that the groundwaters were in equilibrium with calcite, which is present in the sediments (Davis and Curtis, 2003). Computed pCO_2 values range from 0.0024 to 0.14 atm. The distribution of sulfate at the site in 1999 was very similar to that observed for the alkalinity (Fig. 1.2); sulfate concentrations were 1.7 mM at wells DOE-547 and MAU-03, 7.0 mM at NAT-19, and 10.6 mM at MAU-07. The highest sulfate concentration observed was 15.8 mM at well NAT-26.

The pH values from wells DM-1, DOE-547, and NAT-20, -21, -22, which are upgradient of the former mill site are approximately 1 pH unit less than that observed in the San Miguel River. Upgradient alkalinity values have been nearly constant over time (average value of 4.7 meq/L), whereas the alkalinities in the San Miguel River varied seasonally with a range of 1.3 meq/L at high river stage to 2.6 meq/L at low river stage (Davis and Curtis, 2003). The decrease in the pH and the increase in alkalinity within the aquifer are consistent with biological activity. This activity is assumed to occur in the riverbank and possibly in the root zone of cottonwoods and willows near the river because water samples from well DM-1, which is ~10 m from the river, are similar to those from well DOE-547 which is ~120 m from the river. There were also high V concentrations close to highway 141, where concentrations approached 100 μM, whereas outside of this plume dissolved V was below detection limits (Davis and Curtis, 2003).

The groundwaters at the Naturita site are generally not in equilibrium with respect to redox conditions. This is indicated by the co-occurrence of low, but measurable dissolved O_2 and Fe(II) in water pumped from wells (Fig. 1.2), which is not expected under equilibrium conditions at near neutral pH values (Langmuir, 1997). Since 1998, nitrate has only been consistently detected at well NAT-26, where the average concentration was 40□ μM, and dissolved Mn(II) is present in the range of 20-50 μM throughout much of the site. Sulfide was absent in groundwater from all wells sampled in March 2004. The concentration of Fe(II) is relatively small (≤10 μM) in the upgradient portion of the site, including the area beneath the former mill and tailings (Fig. 1.2). The relative constancy of the dissolved Fe(II) and O_2 concentrations over this portion of the site suggest that the extent of microbiological activity may be limited, perhaps by carbon limitation. However, in the extreme downgradient portion of the site, Fe(II) concentrations increase to as high as 50 μM. This area of the site has a thick stand of cottonwood trees, and studies have reported that mild reducing conditions and active microbial populations occur in the vicinity of tree roots, possibly because of microbial degradation of root exudates (Lee et al., 2000; Godsy et al., 2003). Carbonate extractions on freshly collected sediments from near well NAT-25 under an inert atmosphere demonstrated that U(IV) phases were probably not important at that location (Kohler et al., 2004), however, reducing conditions in the downgradient portion of the aquifer appear to be sufficient for bacteria to reduce U(VI), leading to precipitated U(IV) (Davis et al., 2006). Historical data (Davis and

Curtis, 2003) clearly indicate that the plumes of dissolved U(VI) and alkalinity are moving

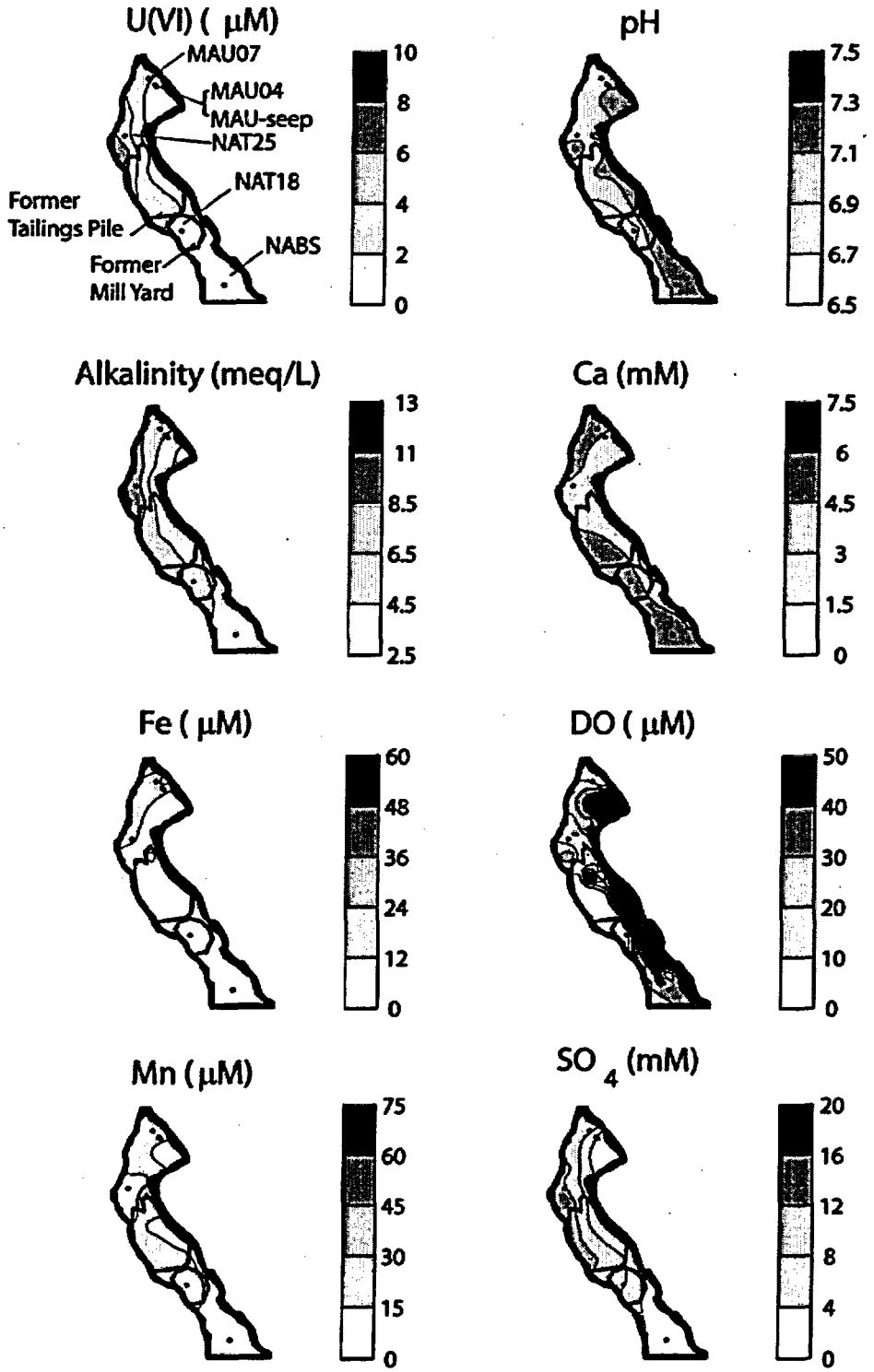

Figure 1.2. Alkalinity, pH, and the concentrations of dissolved U(VI), Ca, Fe, Mn and O_2 in the Naturita alluvial aquifer in March 2004 and sulfate in 1999. Locations of the wells MAU-04, MAU-07, NAT-18, and NAT-25 are shown.

downgradient, while Fe(II) concentrations in the downgradient area with reducing conditions have remained relatively stable (Fig. 1.2).

Determining the relative importance of U(VI) adsorption and U(IV) precipitation as processes that influence uranium fate and transport under suboxic conditions is difficult. Bacterial studies demonstrated that known Fe(III)-reducing bacteria are present in the downgradient MAU-04 and –07 groundwater samples, but not in an upgradient NAT-18 groundwater sample (Davis et al., 2006). A wide variety of Fe(III)-reducing bacteria were isolated from MAU-04 and -07 enrichment cultures, indicating that there is significant diversity among the Fe(III)-reducing bacteria in the subsurface in the downgradient region of the aquifer. An organism closely related to the Fe(III)- and U(VI)-reducing bacterium, *Geobacter sulfurreducens,* (Caccavo et al., 1994) was identified in MAU-04 groundwater, where it accounted for about 2% of the microbial community (Davis et al., 2006). The overall microbial composition is similar to the groundwater community structure at another UMTRA site at Rifle, Colorado, USA (Anderson et al., 2003). At the Naturita site, it appears that U(IV) precipitation may occur in the downgradient region, where significant dissolved Fe(II) is present and Fe(III)-reducing bacteria are detected in the microbial community.

Saturation indices (SI) have been computed to assess if the solubility of U(VI) minerals might be controlling U(VI) transport (Davis and Curtis, 2003). The computed SI values were found to be well below saturation for several U(VI) phases including uranophane, soddyite, schoepite, and rutherfordine. Calculations were also performed to evaluate the stability of the U(IV) phases, uraninite and U_3O_8. The calculations assumed that the Fe(III)/Fe(II) couple was at equilibrium with the U(VI)/U(IV) couple and that Fe(III) activity was controlled by the solubility of either ferrihydrite or goethite. The U(IV) phases were below saturation (SI<-5) if equilibrated with ferrihydrite and at or near saturation (-2<SI<2) if equilibrated with goethite (Davis and Curtis, 2003).

1.3 Project Approach

Simulations of reactive transport processes in groundwater often require many parameters as model inputs. These parameters include hydrologic parameters that describe flow and transport as well as reaction parameters that describe the chemical reaction network. While hydrologic parameters are most often determined from field tests such as pump tests, slug tests, or tracer tests coupled with model calibration, there is less agreement on how chemical reaction parameters should be determined. For chemical reaction processes, such as adsorption reactions, parameter values could be based on a variety of sources including tabulated thermodynamic data, laboratory experiments using site-specific materials, or field-determined values.

Surface complexation models (SCMs) are a useful approach for simulating adsorption in reactive transport models, especially in instances where geochemical conditions vary spatially and temporally (Curtis et al., 2006; Kent et al., 2000). One approach for developing an SCM for use in field-scale reactive transport simulations is to use published SCMs for well-characterized mineral surfaces coupled with detailed soil characterization for the field medium. This approach has been termed the component additivity method, in which SCM for single mineral phases are assembled in an additive fashion to predict adsorption by a whole sediment. Our previous work (Davis et al., 2004b) identified four significant sources of uncertainty in using this approach: (1) estimation of surface site types and surface area abundances, even for well-characterized sediments, (2) a lack of fundamental data on the effects of competitive adsorption of common groundwater solutes, (3) a lack of fundamental data on the effects of common groundwater solutes on surface charge and potentials, and (4) inconsistencies that could result when combining SCMs that use different electrical double layer formulations. In the current project, we addressed the second of these

uncertainties by conducting *in-situ* experiments with well-characterized mineral phases: kaolinite, quartz, and hematite.

A second approach for developing an SCM for a natural sediment is to calibrate a model to measured adsorption data. In this approach, adsorption is postulated to occur on generic surface sites that represent average properties of the sediment surfaces rather than specific mineral surfaces. Model parameters are calibrated to adsorption data for postulated reaction stoichiometries and different model formulations, and are selected based on simplicity and goodness of fit. An advantage of this approach is that the electrical double layer is not considered explicitly; adsorption reaction stoichiometry and binding constants are derived by fitting the macroscopic dependence of adsorption as a function of pH. This is important because of the difficulty in quantifying electrical field and charge at the mineral-water interface in mixtures of mineral phases with associated surface coatings. In the current work, we refer to this approach as a semi-mechanistic approach; in previous work it has been called a generalized composite approach. For the Naturita field site, laboratory experiments using site-specific materials obtained upgradient of the contaminated zone were used to develop a semi-mechanistic SCM that described U(VI) reaction stoichiometry and apparent stability constants with the sediments (Davis et al., 2004b). This SCM did a good job of predicting U(VI) K_d values for both contaminated sediments that were collected during the installation of groundwater monitoring wells (Kohler et al., 2004), with the exception of two downgradient wells where U(VI) reduction may have occurred (Davis et al., 2006). In addition, the SCM successfully predicted K_d values measured on uncontaminated sediments suspended in groundwater wells that had variable U(VI) concentrations and alkalinity values (Curtis et al., 2004).

The suitability of the semi-mechanistic SCM for simulating U(VI) migration in a reactive transport model was evaluated previously for the Naturita site (Curtis et al., 2006; Davis and Curtis, 2003). The reactive transport model could be fit to the site data, although some uncertainties remain regarding the applicability of the SCM to describe U(VI) transport in the field. The most significant uncertainty results because the source term was so poorly understood that the composition of the source had to be included in the model calibration. The uncertainty related to the source term would likely dominate an uncertainty analysis of the transport of U(VI). Thus, to achieve the goal of reducing uncertainty of the simulated long-term fate on U(VI) concentration in the aquifer, it is important to demonstrate the applicability of the SCM to describe U(VI) transport under field conditions. To achieve this goal, reactive transport experiments were conducted in the field at scales of 0.5 to 3 m. Uranium migration tests were conducted that considered variable U(VI) concentrations and alkalinity, and included Br as an inert tracer. The field experiments also included several single-well push-pull tests that were conducted at increased and decreased U(VI) concentrations and alkalinity values. The tracer tests demonstrated that the sediment readily releases U(VI) even after many years of contact with the contaminated groundwater, suggesting that U(VI) migration is controlled by adsorption reactions. Reactive transport simulations used the SCM developed with uncontaminated Naturita sediments (Davis et al., 2004b).

2 COMPARISON OF IN-SITU K_D VALUES FOR URANIUM(VI) SORPTION WITH VALUES PREDICTED FROM SURFACE COMPLEXATION MODELS

2.1 Introduction

In previous experiments, mesh bags constructed of 50 micron nylon filter fabric containing a composite of uncontaminated Naturita sediment (NABS) were suspended in well casings in various wells throughout the Naturita field site (Curtis et al., 2004). The mesh bags were removed periodically and analyzed for U uptake. K_d values (or distribution coefficients) observed for these samples were compared with model-predicted K_d values from a surface complexation model calibrated with uncontaminated Naturita sediments in laboratory experiments (Davis et al., 2004b).

In the experiments described in this section, a similar approach was taken using pure reference minerals for which surface complexation models have been developed that describe U(VI) sorption as a function of water chemistry. The purpose of these experiments was to determine the applicability of laboratory-derived models for reference minerals (which can be found in the literature) to field conditions. This study was conducted by contacting well-characterized mineral phases with Naturita groundwater in wells that had variable U(VI) concentrations and alkalinity. U(VI) adsorption measured in the field could be different from that in laboratory conditions because laboratory conditions typically do not consider competitive adsorption of common groundwater solutes, nor do they consider conditions that could lead to the formation of surface coatings containing aluminum and silicon. Such coatings may be difficult to characterize yet significantly change adsorption properties.

The following materials were chosen for down-hole studies: kaolinite, hematite, quartz, clinoptilolite, and a sediment composite prepared from cores collected in the saturated zone of the 40-Mile Wash (FMW) aquifer, Nye County, Nevada.

2.2 Materials and Methods

2.2.1 Preparation, Installation, and Retrieval of Samples

Because of the small particle sizes of the reference materials, two new types of sample holders were investigated. Previous experiments with the Naturita uncontaminated composite (NABS) utilized 50 μm filter fabric (Curtis et al., 2004). Kaolinite was used to test the effects of exposure time in the wells on measurements of U(VI) sorption and to test the two new sample holders: a) dialysis tubing (KDT) and b) nylon vials (KNV). Kaolinite (KGA-1), obtained from the Source Clays Repository of the Clay Minerals Society, was prepared as a slurry (200 g/L) in MilliQ water, which had been purged with $N_2(g)$ to displace any $O_2(g)$ which might oxidize and precipitate Fe(II) present in the well waters. The slurry (5 mL, corresponding to 1 g kaolinite) was then pipetted into either a 5-mL nylon vial or a short length (~4.5 cm) of dialysis tubing (SpectraPor7, 8K Dalton, 7.5 mm diameter). The mouths of the nylon vials (1.25 cm in diameter) were covered with dialysis tubing. At the same time, "blank" nylon vials containing only water and covered with dialysis tubing (BNV) were also prepared. The samples were placed into mason jars containing N_2-purged deionized water. The mason jars were purged with $N_2(g)$ several times over 24 hr in order to remove as much $O_2(g)$ as possible. Duplicates of each sample type were prepared for installation into each of 10 wells that had variable water chemistry. The samples were placed into 35.5 cm lengths of 3.2 cm diameter PVC pipe that had been drilled with 1.25 cm diameter holes and lined with nylon mesh. The sample holders were lowered into the wells to within about 23 to 30 cm of the well bottom. Samples were installed in the following wells on March 24, 2004 and retrieved on March 26 (1 dialysis sample) or April 23-24, 2004 (remaining samples): NAT-05, NAT-09, NAT-11, NAT-19,

NAT-20, NAT-24, NAT-25, NAT-26, MAU-07, and MAU-08. After the dialysis bags were sampled, the bags were opened and the slurry was transferred to a pre-weighed vial, removing as much water as possible. The nylon vials were simply capped and transported back to the lab.

Water samples from each well were collected by low-flow sampling at the elevation where the mineral bags were deployed within the borehole. Alkalinity and pH were measured in the field. Concentrations of U(VI) and other metals were determined in the laboratory by kinetic phosphorescence analysis (KPA) and inductively-coupled plasma spectroscopy (ICP-AES), respectively.

From initial experiments with kaolinite, we determined that the dialysis tubing with an exposure time of 1-month was the best method for placing mineral samples in the wells. Subsequent experiments with quartz, hematite, clinoptilolite and the 40-Mile Wash sediment composite (FMW) were performed using a 1-month exposure time.

The quartz used was a commercially obtained crushed quartz powder, Min-U-Sil 30 (Pennsylvania Glass & Sand Company). Quartz was treated to remove contaminants as described by Kohler et al. (1996). Grain sizes were 8-30 μm and the specific surface area as measured by 5 point BET nitrogen gas adsorption was 0.29 m^2/g. Dialysis tubing was filled with about 4 g quartz and 3 mL of N_2-purged deionized water. Duplicate quartz bags were installed in the wells listed above (except MAU-01 was substituted for NAT-25) on 10/9/2004 and retrieved on 11/10/2004.

Hematite was synthesized following the method of Bargar et al. (1997). The hematite had a surface area of 50 m^2/g as measured by 5 point BET nitrogen adsorption. Hematite was stored as a slurry in MilliQ water containing 171 g/L and transferred to dialysis tubing by pipet. Duplicate hematite bags were installed in the wells listed above for quartz on 3/27 and 3/28/2005 and retrieved on 4/28 and 4/29/2005.

Clinoptilolite was obtained courtesy of Paul Bertetti of the Southwest Research Institute, San Antonio, TX. The material was similar to that used in Bertetti et al. (1998), and had been cleaned and processed in order to generate Na-clinoptilolite as described by Pabalan et al. (1998, 1994). The clinoptilolite sample had a surface area of 10.1 m^2/g.

The 40-Mile Wash composite (FMW) was prepared from samples collected as part of the Nye County (Nevada) Early Warning Drilling Program. Core materials were subsampled during the drilling of Borehole NC-EWDP 19PB at depths from 350-587 feet below ground surface on December 2-5, 2003. The water table was located at approximately 350 feet below ground surface at the location of sampling. The core materials were dry sieved to remove particles greater than 3 mm in size. The composite was prepared by mixing sediments in roughly equal weights per unit vertical length.

Approximately 1 g samples of clinoptilolite or FMW composite were placed in dialysis tubing along with 5 mL of N_2-purged deionized water. Duplicate samples of each were installed in the wells listed above (except NAT-26) on 11/3 and 11/4/2005 and retrieved on 12/6 and 12/7/2005. All samples were stored in N_2-purged deionized water in mason jars as discussed above prior to installation in the wells. During retrieval of clinoptilolite and FMW bags, excess water from inside the bags was retained, transported back to the lab and centrifuged at 6876 *g* for 20 min to completely separate the solid and liquid phases. These samples were analyzed and compared with bulk groundwater samples collected from each well at the same time.

2.2.2 Extraction and Analysis of Samples

With the exception of hematite, all mineral bag samples were weighed and dried to determine the amount of water present in each sample. Dried samples were then extracted with 20-mL of bicarbonate-carbonate solution (20 meq/L alkalinity, pH 9.4, hereafter referred to as 'carbonate solution') for 3 weeks (quartz was extracted for 4 weeks), followed by an extraction with 20 mL of hot, concentrated nitric

acid for 3 days. The hematite samples were not dried, but simply extracted as a slurry with 40 mL of carbonate solution, adjusting the pH to 9.4. The volume of water associated with each hematite sample was determined by weighing the samples and calculating volume based on the known density of the hematite slurry. The carbonate extraction will desorb U(VI) that was adsorbed after deploying the samples in the wells, while the nitric acid can dissolve any U remaining that is more tightly bound (Kohler et al., 2004). Clinoptilolite samples were also extracted with 0.1 M sodium formate at pH 3.5 ('formate solution') after the carbonate extraction, in order to determine the amount of adsorbed U(VI), for reasons that will be discussed in more detail below. Samples were diluted as necessary and analyzed for dissolved U(VI) (by KPA or ICP-MS) and selected other elements (by ICP-AES). Water samples collected for alkalinity were titrated with sulfuric acid using the Gran titration. All other water samples were acidified with nitric acid to 0.15 M HNO_3 and analyzed by KPA and ICP-AES.

2.3 Laboratory Kinetics

Kinetics experiments investigating the amount of time required for U(VI) sorption to reach equilibrium have been performed by others for the minerals used in these experiments (Pabalan et al., 1998; Fox et al., 2006). These studies have demonstrated that equilibration times of 48-72 hr are sufficient in well-mixed batch experiments. However, in our studies the equilibration time required should be longer because the minerals were held within dialysis tubing, and additional time is needed for the water inside the bag to equilibrate with the water composition outside of the bag. We performed experiments in the laboratory to determine the appropriate equilibration time for samples held in the dialysis bags. Mineral bag samples of quartz, kaolinite, and FMW composite were prepared in the same manner as the field samples, placed in a 1 L bottle filled with an artificial groundwater (AGW) solution containing 750 µg/L U(VI), 6.64 mM Ca^{2+}, 1.52 mM Mg^{2+}, 0.064 mM K^+, 2.41 mM Na^+, 4.79 mM SO_4^{2-}, 4.50 mM Cl^-, and an alkalinity of 4.71 meq/L. The bottle was bubbled continuously with a 2% CO_2/ 98% N_2 gas mixture in a glove bag in order to maintain a pH of 6.9. Dialysis bag samples were removed periodically for up to 30 days, and the solid and liquid phases were separated by centrifugation (16,270 *g* for 5 minutes). The supernatant samples were then acidified to 0.15 M with nitric acid and analyzed for U(VI) concentration by KPA, along with a sample of the AGW outside of the dialysis bags. Due to some evaporation during the experiments, U(VI) concentrations in the bulk solution outside of the bag changed slightly over time, and therefore, a sample of water outside of the dialysis bags was collected each time a bag was sampled. In the cases of kaolinite and FMW, the solid phase was retained and extracted with carbonate solution for 3 weeks in order to determine the total U(VI) sorbed.

Figure 2.1 shows the ratio of U(VI) concentrations in water inside and outside the dialysis bags as a function of time for the quartz, kaolinite, and FMW composite experiments. In the cases of quartz and FMW, the U(VI) concentration inside the bags reaches identical concentrations with the water outside the bags after only 1 day of exposure. However, kaolinite, which adsorbed more U(VI) than either quartz or FMW, required 7 days of equilibration before reaching identical concentrations.

Kaolinite and FMW sediments removed from the dialysis bags were extracted with carbonate solution in order to desorb U(VI). The amount of U(VI) extracted reached a maximum after 14 days of dialysis bag equilibration in kaolinite experiments and 7 days in FMW composite experiments (Figure 2.2). In both cases, this is slightly longer than the equilibration times measured for water equilibration inside and outside the bags (Figure 2.1). U(VI) extracted with carbonate solution decreased over longer exposure times (30 days for kaolinite, and 14-30 days for FMW composite). This may be an indication that U(VI) is becoming more tightly bound over time, with less U(VI) desorbed in the carbonate extraction. All of the mineral samples

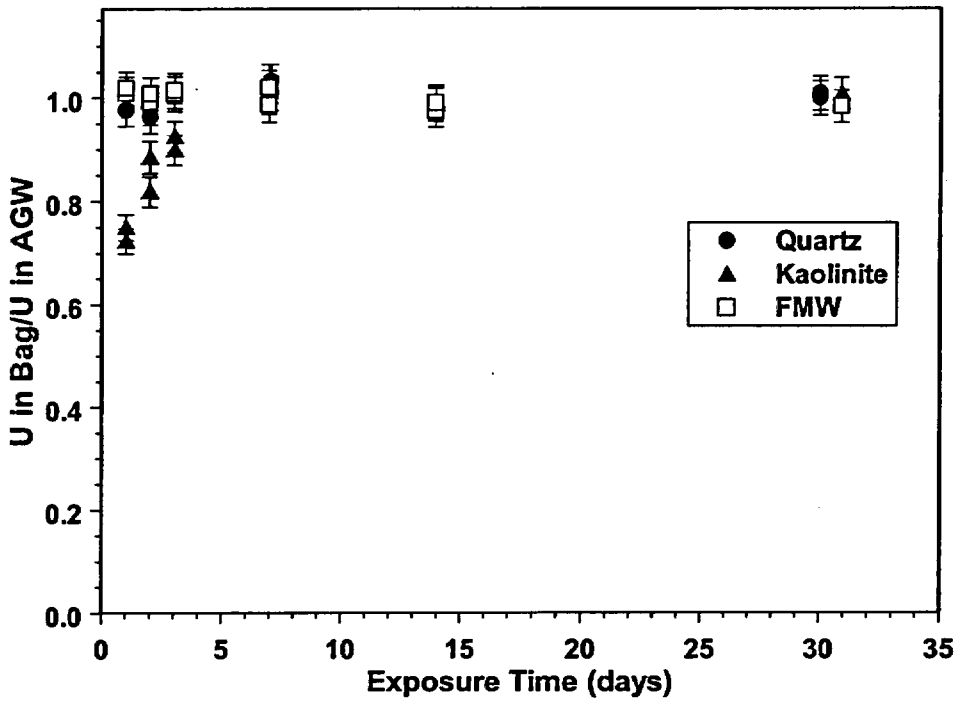

Figure 2.1. The ratio of U(VI) concentrations inside and outside of dialysis bags as a function of time in test experiments with quartz, kaolinite, and 40-Mile Wash composite sediment.

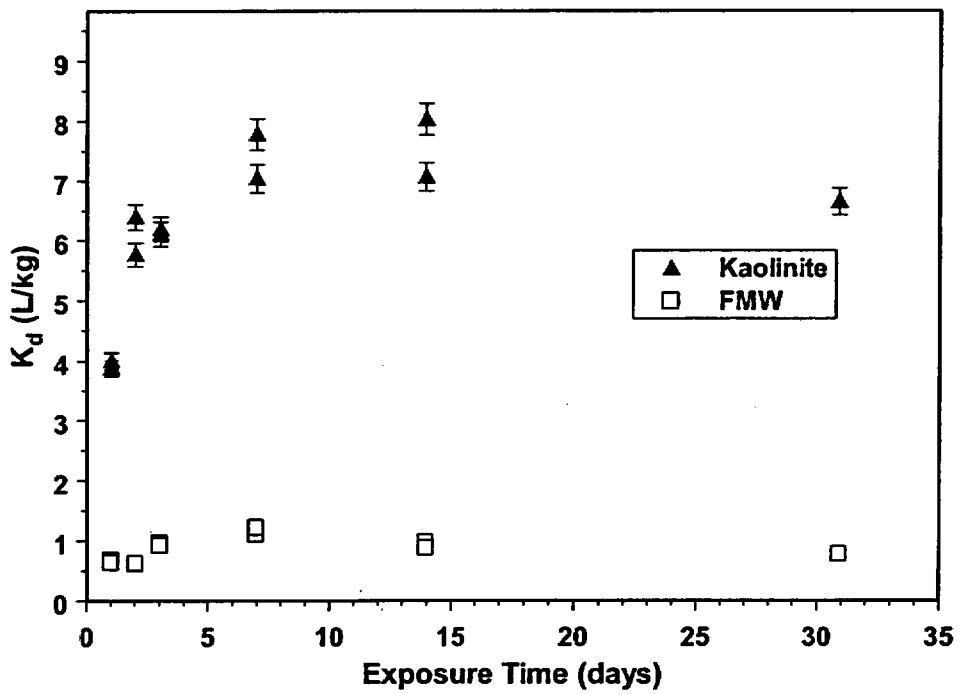

Figure 2.2. U(VI) desorbed from kaolinite or the FMW sediment composite by the bicarbonate-carbonate solution as a function of time, expressed as a K_d value. Error bars for the FMW experiment are smaller than the data points.

collected after field exposure were extracted with hot concentrated nitric acid in order to fully recover any U(VI) that was not extracted with the carbonate solution. We chose a field exposure time of about 30 days based on the results of the laboratory experiments.

2.4 Groundwater Chemistry

Table 2.1 shows the concentrations of various elements measured in groundwater samples at the wells studied. Groundwater was sampled at each well when each mineral bag deployment was sampled. There was very little change in the concentrations over the 1-month exposure time for each mineral bag. While most elemental concentrations remained fairly constant over the entire 2-year period of this study, Fe and Mn concentrations in wells MAU-07 and MAU-08 varied considerably, demonstrating changing redox conditions in these wells. The values presented in Table 2.1 represent typical groundwater concentrations. Table 2.2 shows the Fe and Mn concentrations in MAU-07 and MAU-08 wells over the entire study period. Fe and Mn concentrations in MAU-08 were particularly variable, and seemed to vary seasonally, being lower in the spring and higher in the fall. However, the presence of dissolved Fe(II) in these wells is an indication that in addition to U(VI) sorption, U(IV) precipitation might occur in these wells, increasing the apparent K_d values (Davis et al., 2006).

Table 2.1. Typical chemical compositions of groundwater in the wells used for mineral bag deployment. The values are from samples collected on 11/10/2004, except for well NAT-25, which was sampled on 4/23/2004.

	pH	Alk‡	U	Ca	Fe	Mg	Mn	Na	Si	V
		meq/L	µg/L	mg/L						
MAU-01	7.10	6.98	608	154	BDL†	43.8	0.72	217	8.39	0.16
MAU-07	7.02	7.57	485	173	2.05	51.7	0.91	171	8.07	0.18
MAU-08	7.16	9.91	923	191	0.90	65.9	1.19	474	8.66	0.23
NAT-05	7.02	7.57	878	168	BDL	59.8	1.07	315	9.85	3.80
NAT-09	7.26	6.66	476	163	BDL	47.9	0.06	189	9.81	1.99
NAT-11	7.09	6.65	639	227	BDL	64.8	1.11	217	9.65	1.94
NAT-19	6.98	5.60	32	215	BDL	53.9	1.44	144	7.53	0.38
NAT-20	7.11	4.33	12	208	BDL	43.4	BDL	65	6.33	0.17
NAT-24	7.08	6.76	629	170	BDL	45.0	0.20	166	8.42	0.17
NAT-25	7.02	9.23	1256	178	1.10	56.8	0.30	450	8.81	0.20
NAT-26	7.21	9.97	1782	133	BDL	60.3	0.10	726	7.01	0.21

†BDL: Below detection limit
‡Alk: Alkalinity

Table 2.2. Iron and manganese concentrations in wells MAU-07 and MAU-08 at various sampling times.

	Mar04	Apr04	Oct04	Nov04	Mar05	Apr05	Nov05	Dec05
	Fe Concentrations (mg/L)							
MAU-07	2.02	2.02	1.74	2.05	1.87	1.70	1.35	1.68
MAU-08	0.12	BDL†	1.97	0.90	BDL	BDL	0.48	0.52
	Mn Concentrations (mg/L)							
MAU-07	1.23	1.15	0.74	0.91	1.09	1.02	0.82	1.02
MAU-08	0.35	0.27	1.14	1.19	0.06	0.87	1.10	0.60

†BDL: Below detection limit

Water collected from inside the clinoptilolite and FMW dialysis bags is compared with the bulk groundwater collected at the same time (December 2005) in Figure 2.3. The concentrations of U, K, Mg, and Na inside the bags agreed within measurement error with the concentrations in bulk groundwater. Calcium concentrations inside the bags were either the same or slightly lower inside the bags in comparison to the bulk groundwater. Measured values for Fe and Mn were much more variable, with no clear trend.

2.5 In-situ Kaolinite Field Measurements

2.5.1 Effect of Residence Time in Wells

A comparison of the KDT samples retrieved after 2 days and 1 month of exposure time in the wells demonstrates that U(VI) concentrations did not reach equilibrium after only 2 days in the wells (Fig. 2.4). More U(VI) was extracted by carbonate solution in every well after 1 month of exposure time versus 2 days (Fig. 2.4A). However, in the case of the nitric acid extractions, only two wells with the highest overall U(VI) concentrations (NAT-24 and NAT-26) showed higher U(VI) extracted after 1 month of exposure time (Fig. 2.4B). This trend is a reflection of the lack of equilibrium between the water inside and outside of the dialysis tubing. Because there was some water entrained with the kaolinite sample before it was dried (up to 5 mL/g), a fairly large correction was required to the raw carbonate extraction data in order to account for dissolved U(VI) present within the dialysis bag. This correction was made by assuming that the U(VI) concentration measured in the groundwater from each well was the same as that present inside the dialysis bag. Our kinetics experiments indicated that 7 days were required to reach identical U(VI) concentrations in water inside and outside the bags in kaolinite experiments, and up to 14 days of equilibration were required to achieve steady-state carbonate-extractable U(VI) (Figs. 2.1 and 2.2). The data in Figure 2.4 supports our kinetic data produced in the laboratory, which shows that longer exposure times (e.g., 1 month) are necessary to achieve equilibrium concentrations of adsorbed U(VI) within the dialysis bags.

2.5.2 Effect of Sample Holder Type

Two sample holder types were tested with kaolinite in the field, dialysis tubing and nylon vials with the tops covered with dialysis membrane. U(VI) extracted by carbonate solution and nitric acid for the two types of sample holder deployments are shown in Figure 2.5. While it appears that more U(VI) was sorbed in the samples placed in the nylon vials than in the dialysis tubing, the sorbed U(VI) values calculated for the nylon vials have much greater error due to the correction for dissolved U(VI) present in entrained water (nylon vials had about 2.5-5 mL water per g of kaolinite). For many samples, this correction was very large, accounting for over 100% of the carbonate extracted U(VI) (e.g. NAT-24, KNV2). It appears that water inside the nylon vials was not in equilibrium with water outside the nylon vials (groundwater). Two nylon vial samples containing only water (no kaolinite) were also sampled for each well and the U(VI), Ca, Mg Na, and V concentrations in each are compared in Figure 2.6. As shown in Figures 2.5 and 2.6, the concentrations measured in replicate samples do not agree very well for these samples, particularly for U(VI) and Ca, and also do not agree with concentrations measured in the bulk groundwater. It was concluded that the dialysis bags were a much better method for deployment in wells, because of better agreement between replicate samples and better equilibration between the bulk groundwater and water inside the dialysis bags.

2.5.3 Carbonate Extraction Kinetics

Kaolinite samples were extracted with carbonate solution for a period of 3 weeks. The amount of U(VI) extracted increased between 24 hr and 2 weeks, but was not significantly different between 2 and 3 weeks. The concentrations of elements extracted from kaolinite by the carbonate solution data are shown in Figure 2.7. Significant amounts of V (well above background for the kaolinite used in this study) were extracted from samples placed in wells

NAT-05, NAT-09, NAT-11, and NAT-19. All other samples had low levels of V, equivalent to that extracted from kaolinite before deployment in dialysis bags in the wells.

2.5.4 Comparison of Carbonate and Nitric Acid Extractions

Surprisingly, a significant amount of U(VI) was also extracted by nitric acid following the carbonate solution extraction. Some of this was due to background U(VI) present in the kaolinite prior to exposure to groundwater. A comparison of the carbonate and nitric acid extracted U(VI) is shown in Figure 2.8. The "blanks" show data for extractions of kaolinite without exposure to groundwater. After the amount of U(VI) present in the kaolinite is subtracted out, the nitric acid extracted U(VI) is less than that extracted by carbonate, but in most cases the amount is still significant.

2.5.5 Comparison with Predictions of Kaolinite Surface Complexation Model

Adsorbed U(VI) on the kaolinite samples was estimated from the amount of U(VI) desorbed in the carbonate solution extractions. K_d values for U(VI) adsorption by kaolinite were then calculated from the estimated adsorbed U(VI) concentration divided by the dissolved U(VI) concentration in the groundwater sampled at the same depth in the well. Model-predicted K_d values were calculated from the calibrated SCM reported for kaolinite by Payne et al. (2004). The two sets of K_d values are shown in Table 2.3. The measured K_d values ranged from 0.6 mL/g to 2.4 mL/g for the kaolinite deployed in the wells, with K_d values generally increasing with decreasing alkalinity and U(VI) concentration. The kaolinite model-predicted K_d values ranged from 15 to 45, approximately 20 times larger than the measured values. The reason for the discrepancy between the measured and model-predicted values is unknown, but it is suspected that the SCM overpredicts U(VI) adsorption because of the lack of experimental data at high partial pressures of $CO_2(g)$ in the study by Payne et al. (2004). The partial pressures of $CO_2(g)$ in groundwater ranged from 2-5% based on the measured pH and alkalinity values at the wells at which kaolinite was deployed (Table 2.1). Another possible reason for the disagreement between the model and measurements of K_d values is that aqueous chemical conditions (e.g., pH, alkalinity) were different inside the dialysis bags than in the groundwater despite the 30-days of equilibration, perhaps due to microbial fouling. However, microbial fouling was not visually observed and the test of U(VI) concentrations inside and outside the dialysis bags showed little difference. This suggests that the difference between the measured and model-predicted K_d values may be more likely impacted by the accuracy of the SCM under conditions of high partial pressures of $CO_2(g)$.

The measured K_d values for wells MAU-07 and MAU-08 did not seem unusually larger than other wells, suggesting that U(IV) precipitation onto the samples was likely insignificant.

Table 2.3. Comparison of measured and model-predicted U(VI) K_d values for kaolinite samples in contact with Naturita groundwater

Well	Measured K_d (mL/g)	Model-Predicted K_d value (mL/g)
MAU-07	0.86	28
MAU-08	0.65	15
NAT-05	0.93	33
NAT-09	1.0	22
NAT-11	0.79	23
NAT-19	1.6	45
NAT-24	2.4	29
NAT-25	1.1	24
NAT-26	1.0	23

2.6 In-Situ Quartz Field Measurements

2.6.1 Carbonate Extraction Results

In contrast to the kaolinite samples, U(VI) accumulation on quartz was not measurable within the errors of the experimental approach.

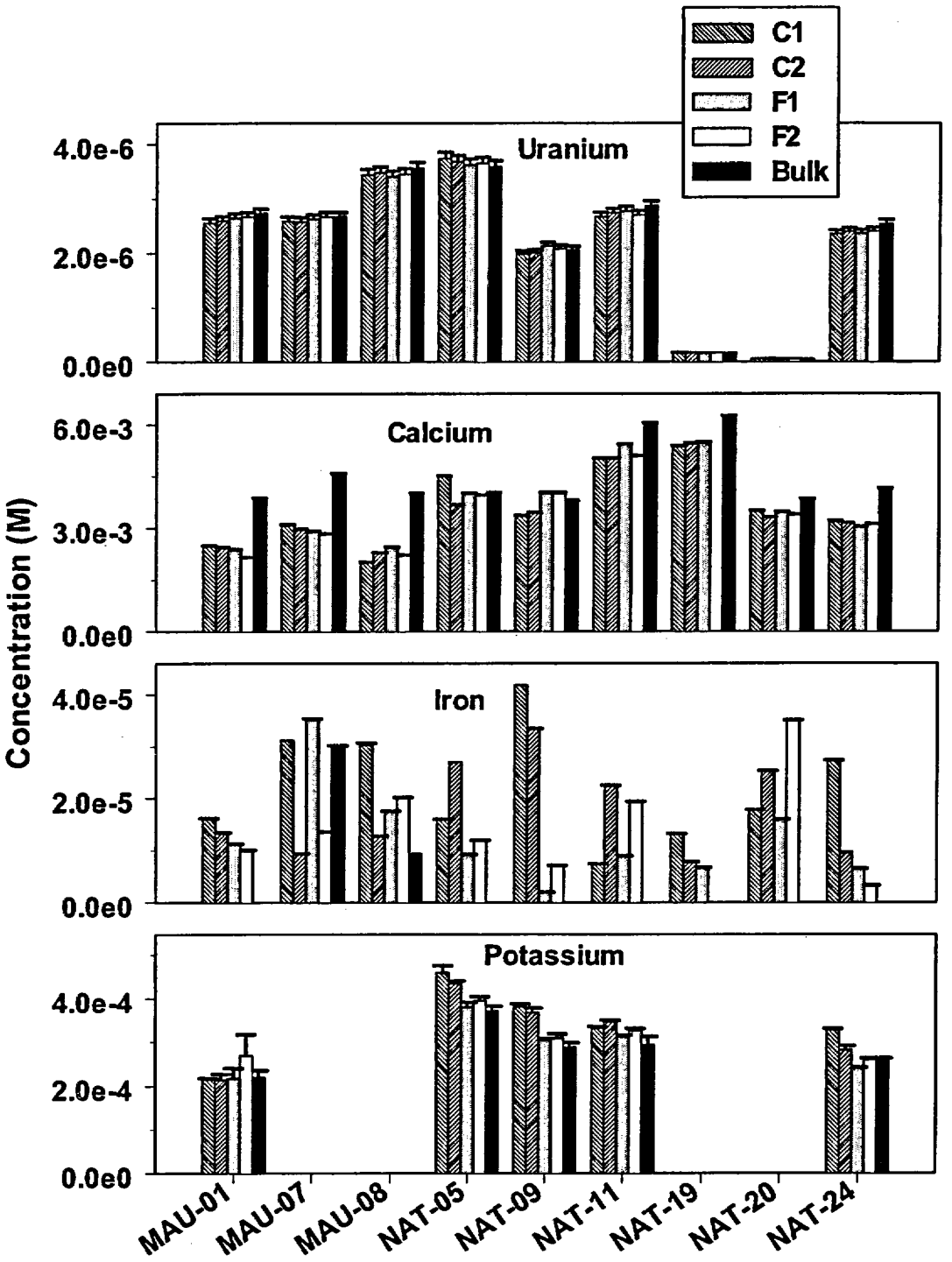

Figure 2.3. Comparison of various elemental concentrations measured in replicate clinoptilolite (C1, C2) and 40-Mile Wash composite (F1, F2) dialysis bags compared with bulk groundwater (bulk) in December 2005. Data below the detection limit for Fe (1.8×10^{-6} M), K (2.0×10^{-4} M), and Mn (2.5×10^{-7} M) is not plotted.

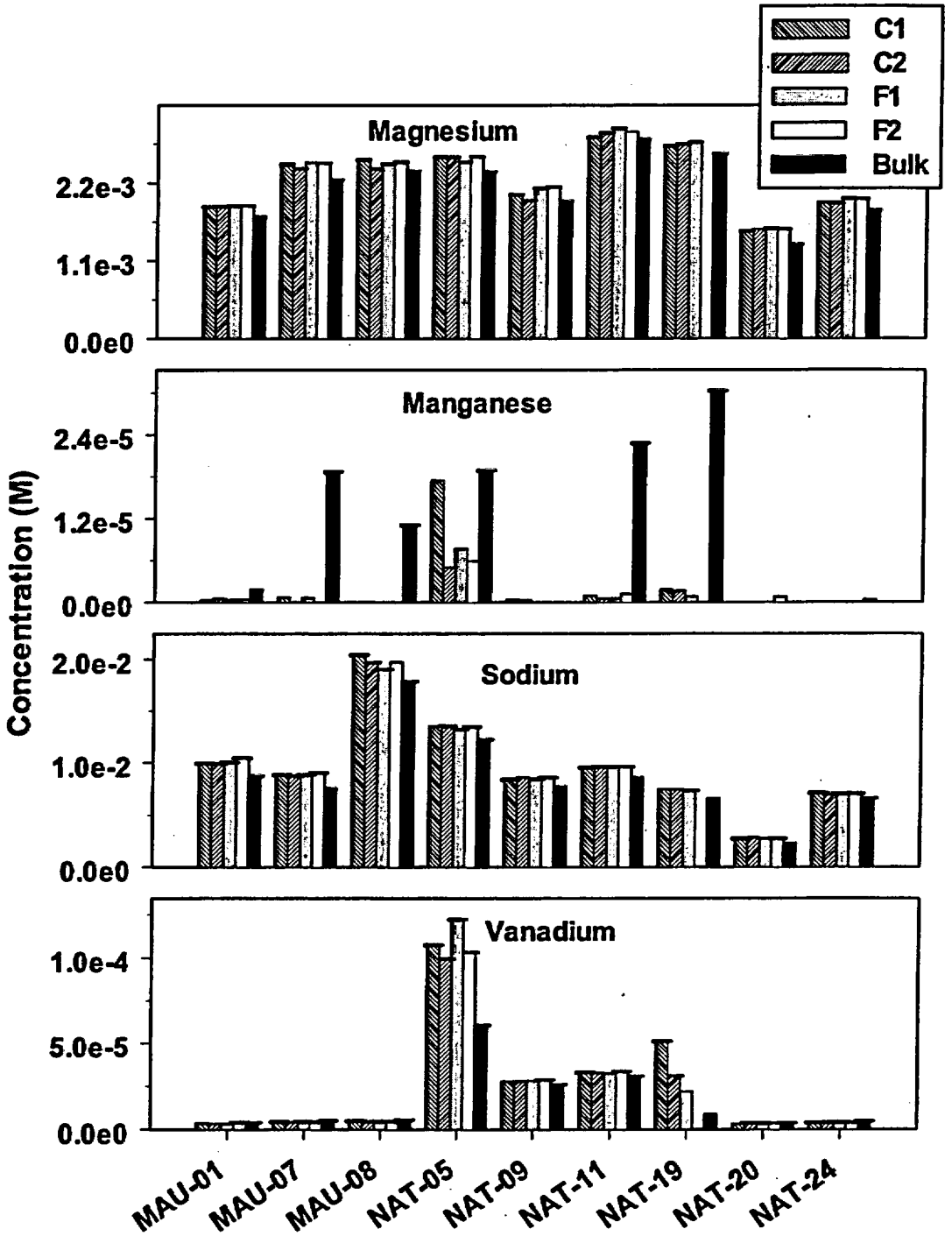

Figure 2.3 (continued). Comparison of various elemental concentrations measured in replicate clinoptilolite (C1, C2) and 40-Mile Wash composite (F1, F2) dialysis bags compared with bulk groundwater (bulk) in December 2005. Data below the detection limit for Fe (1.8×10^{-6} M), K (2.0×10^{-4} M), and Mn (2.5×10^{-7} M) is not plotted.

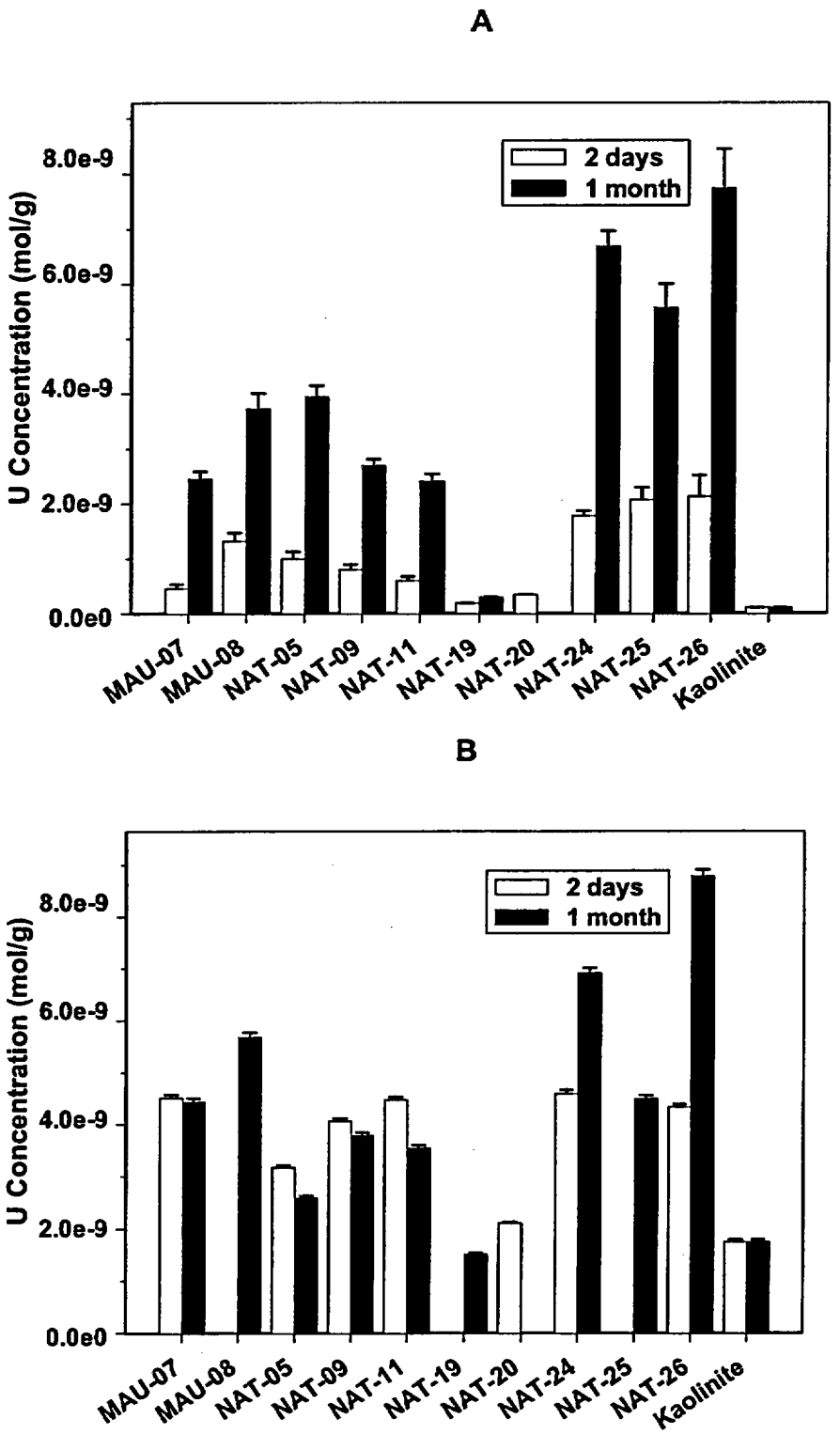

Figure 2.4. Comparison of U(VI) concentrations for kaolinite samples deployed in dialysis tubing and placed in wells for 2 days or 1 month. U(VI) concentrations in (A) carbonate solution extracts, and (B) nitric acid extracts. Sample labeled 'Kaolinite' shows data for extractions without field deployment.

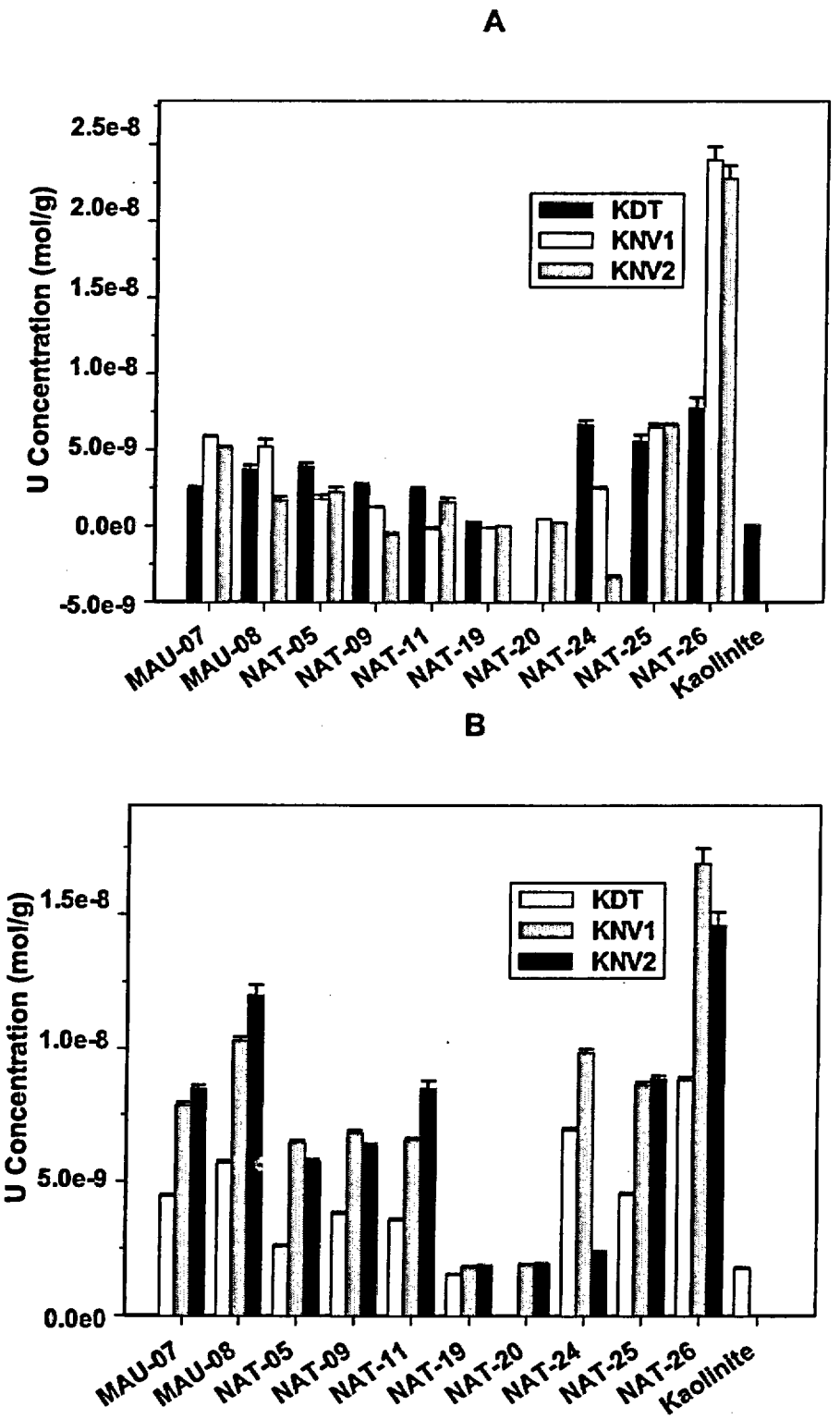

Figure 2.5. Comparison of U(VI) extracted from kaolinite deployed in different sample holder types: KDT (dialysis tubing) and KNV (nylon vial), with U(VI) extracted by carbonate solution (A) and nitric acid (B). Sample labeled 'Kaolinite' shows data for extractions without field deployment.

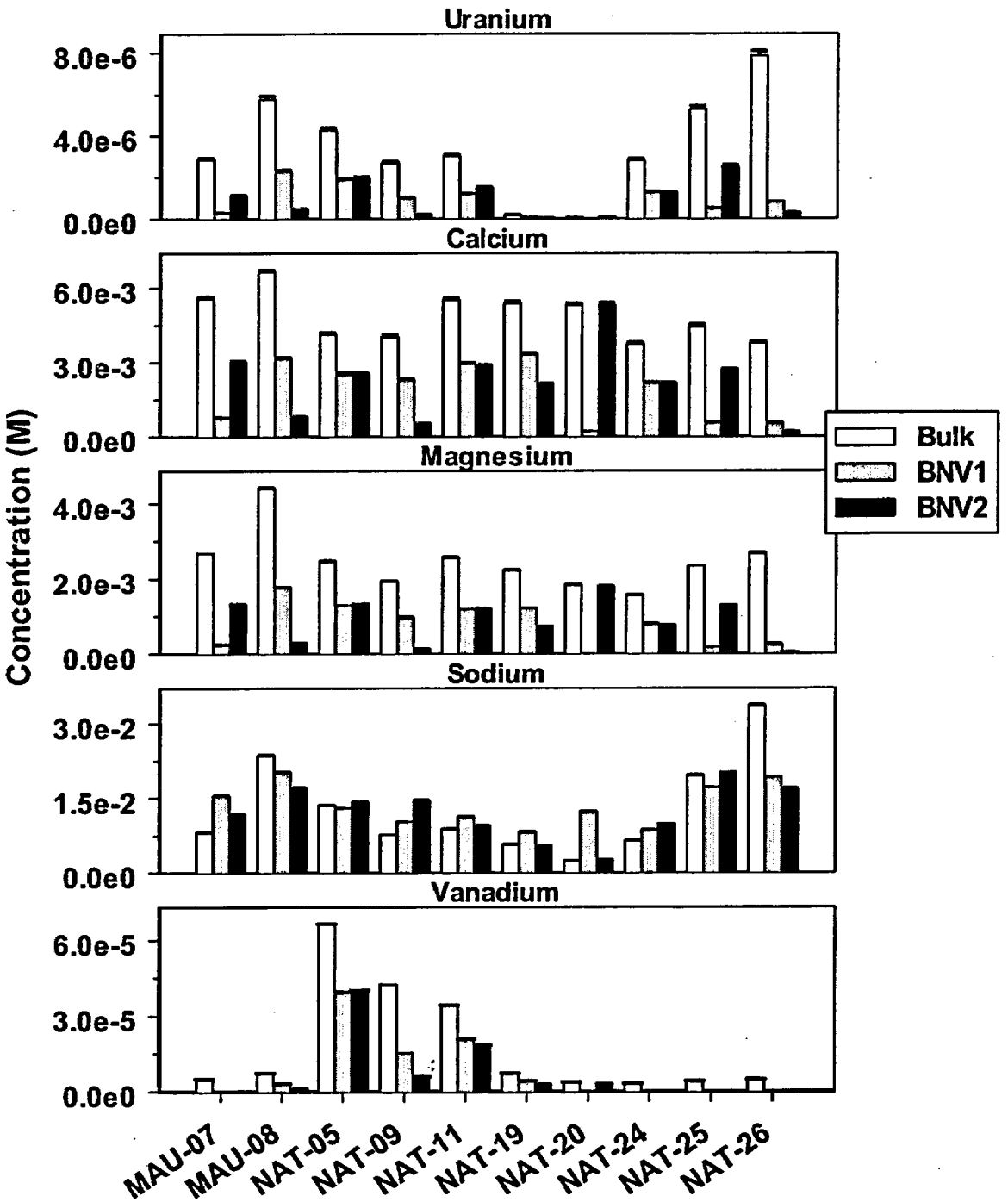

Figure 2.6. Comparison of dissolved concentrations of U(VI), Ca, Na, and V in bulk groundwater samples (sampled April 23, 2004) and replicate nylon vials without kaolinite (BNV).

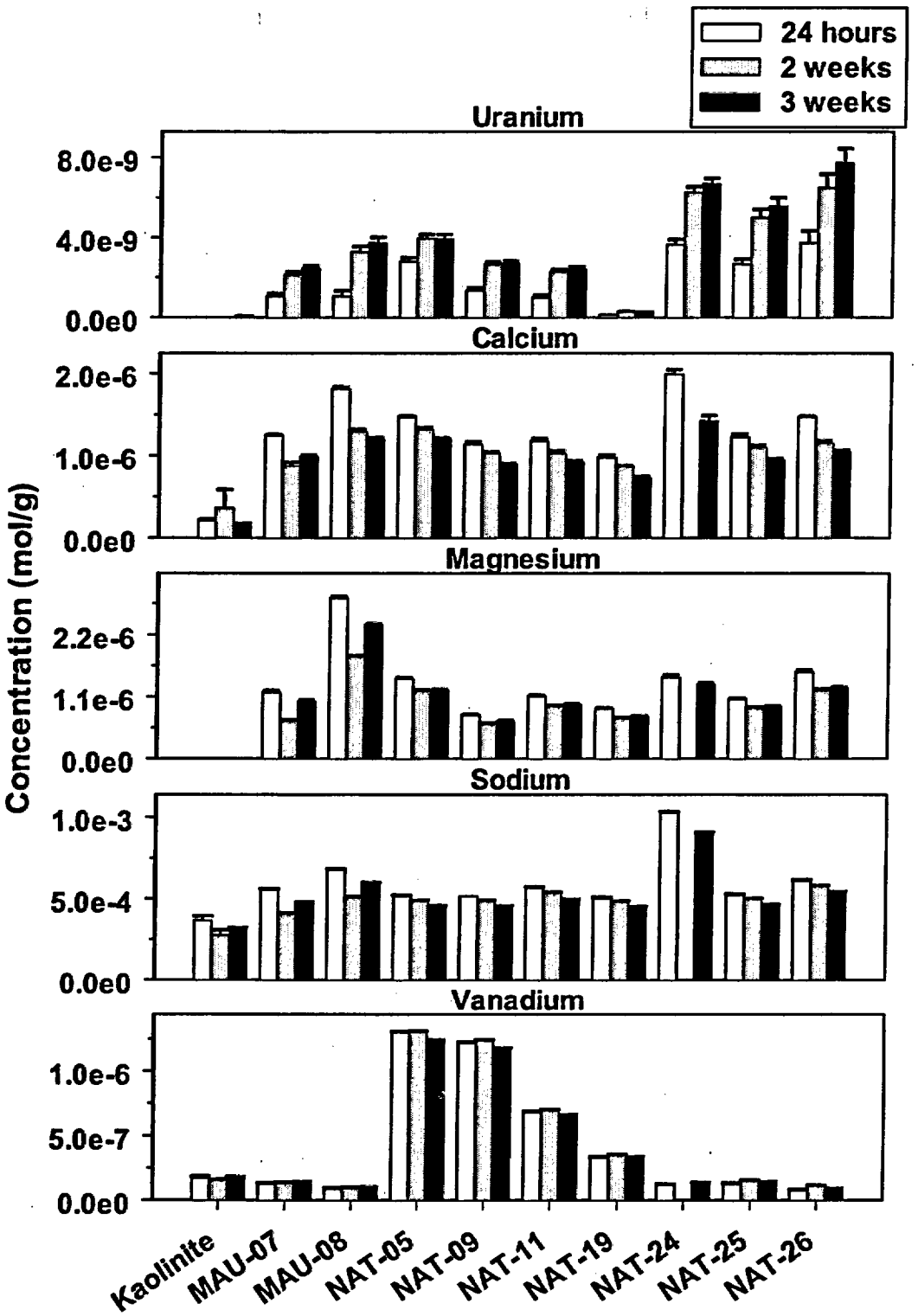

Figure 2.7. Concentrations of elements extracted at various times from kaolinite after exposure to groundwater for 1 month. For U(VI) and V, the data are corrected for the amounts of U(VI) and V that were present in entrained water when the kaolinite samples were collected. None of the other elements were corrected for the amount present in entrained water. Sample labeled 'Kaolinite' shows data for extractions without field deployment.

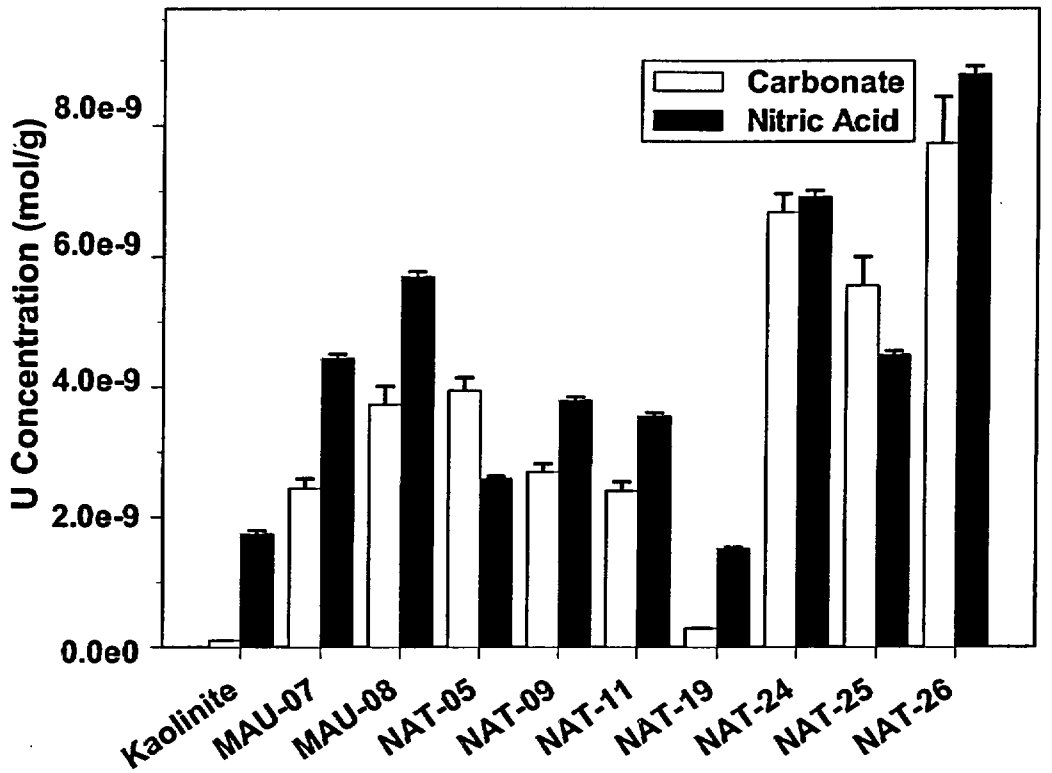

Figure 2.8. Comparison of U(VI) concentrations extracted from kaolinite exposed to groundwater for 1 month by the carbonate solution and nitric acid. The carbonate data presented is for 3 weeks of extraction time and is corrected for U(VI) in entrained water associated with the sample. Sample labeled 'Kaolinite' shows data for extractions without field deployment.

A small amount of U(VI) was extracted by the carbonate extraction (Fig. 2.9A), however, when the amounts of U(VI) present from entrained water associated with the quartz samples are subtracted out, the net U(VI) extracted drops to zero or below, as shown in Figure 2.9B. Quartz has a much lower surface area than other minerals used in this study (0.29 m^2/g for quartz versus 8.4 and 50 m^2/g for kaolinite and hematite, respectively). Thus, we would expect a much lower amount of U(VI) to adsorb to the quartz surface per unit weight. Because the amount of adsorbed U(VI) is determined by subtraction of two numbers that are of similar value, the experimental errors in determining these two numbers are greater than the actual amount of adsorbed U(VI). There is also the possibility that the correction factor applied is too large if the U(VI) concentrations within the entrained water were actually lower than the concentrations in groundwater outside the bag. However, the kinetics experiments performed in the laboratory showed that U(VI) in water inside dialysis bags containing quartz reached equilibrium in only 3 days.

Other elements were measured in the carbonate extraction solution (Fig. 2.10). These data have not been corrected for amounts present in entrained water associated with the quartz samples, except as indicated in Figure 2.10 for V. It is interesting to note that while the correction for U(VI) present in entrained water was very large compared to extracted U(VI), the correction factor was not too large for vanadium. Vanadium accumulated on samples deployed in wells NAT-05, NAT-09, NAT-11, and NAT-19, even when correcting for the amount of V present in entrained water. This observation suggests that there was likely good contact between the quartz and groundwater within the dialysis tubing.

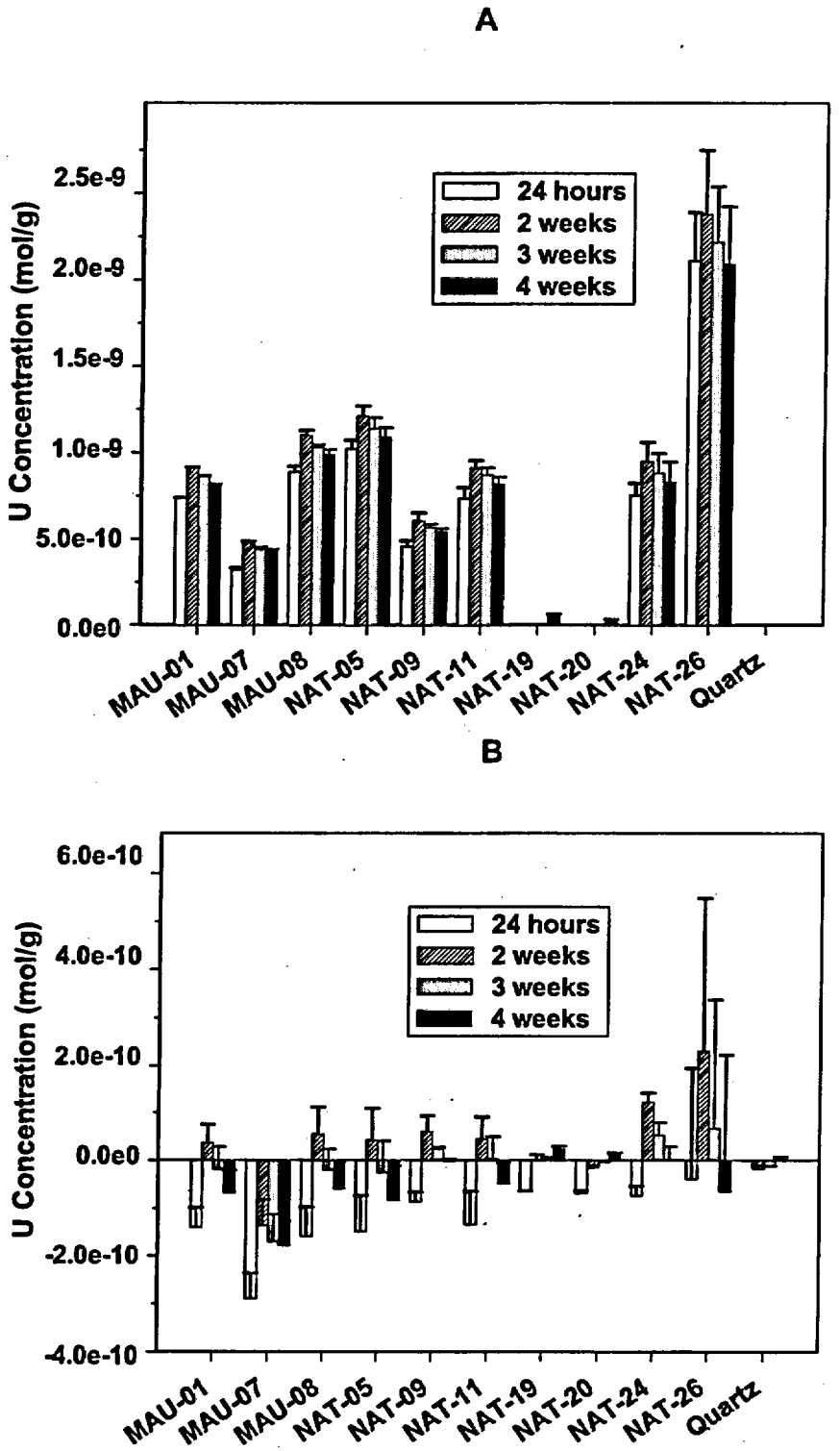

Figure 2.9. Calculated amounts of U(VI) extracted by carbonate solution from quartz samples for various extraction times. The data presented represent the average from two dialysis bags containing quartz that were deployed in each well. Part (A) shows the amount of U(VI) extracted without correction for U(VI) in the water entrained with the quartz samples. Part (B) illustrates the same data after the correction is applied.

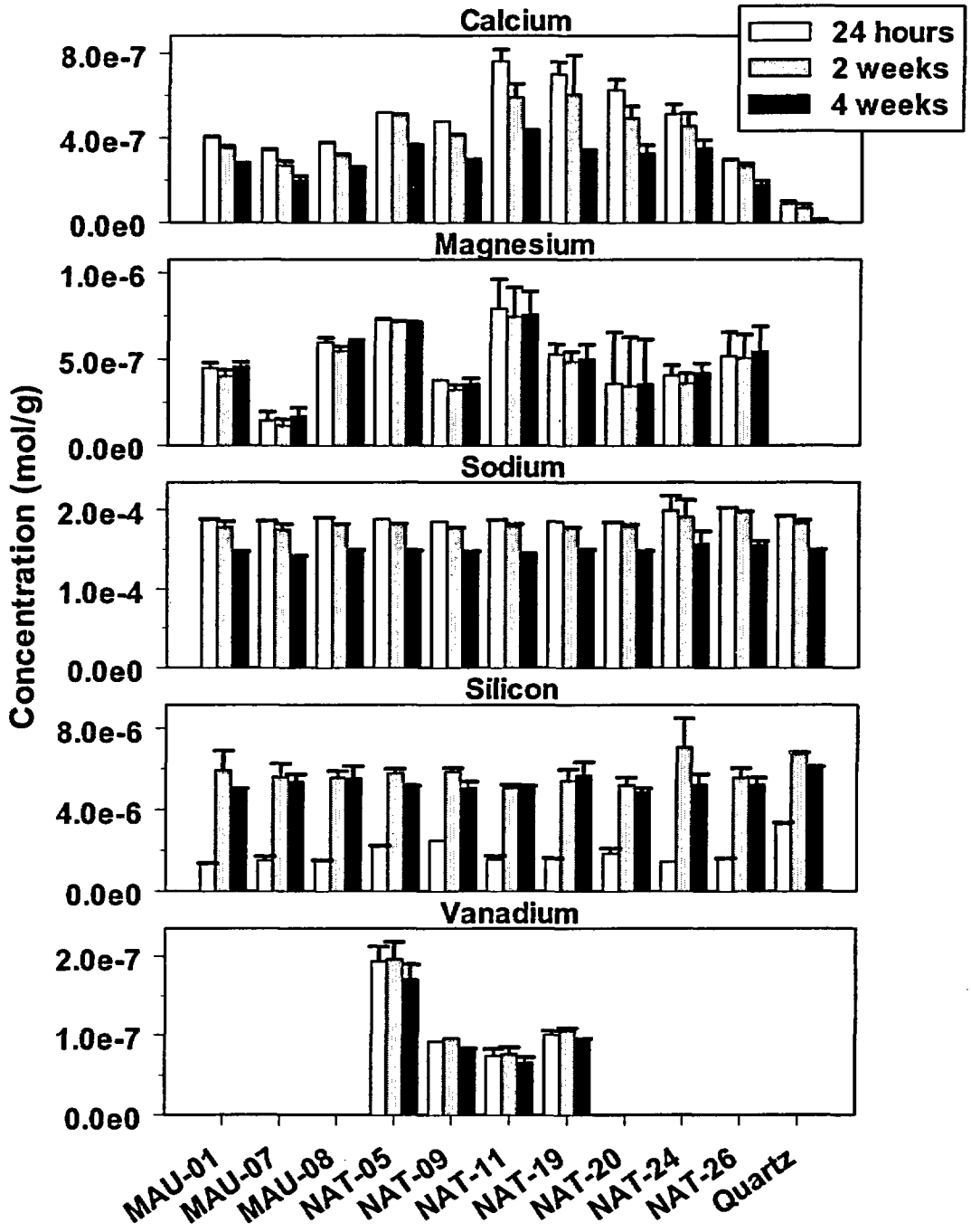

Figure 2.10. Concentrations of various elements (Ca, Mg, Na, Si, V) in carbonate extraction solutions of quartz at various time during the extraction. The data are not corrected for the amounts present in entrained water, except for V. The data presented represent the average from two dialysis bags containing quartz that were deployed in each well. Data below the detection limit for V ($1x10^{-8}$ mol/g) and Mg ($5x10^{-9}$ mol/g) are not plotted. Sample labeled 'Quartz' shows data for extractions without field deployment.

2.6.2 Nitric Acid Extraction Results

Although the amount of U(VI) extracted from the quartz samples by the carbonate solution was not measurable within experimental error, a small amount of extracted U(VI) was measured in hot, concentrated nitric acid extractions (Fig. 2.11). Some V was also extracted by nitric acid, although the amount extracted by carbonate solution accounted for the bulk of the total V recovered.

2.6.3 Predictions with Quartz Surface Complexation Model

As described above, adsorbed U(VI) on the quartz samples could not be determined within the experimental errors of the method. Nonetheless, model-predicted adsorbed U(VI) concentrations and K_d values were calculated from the calibrated SCM recently reported for quartz by Fox et al. (2006). The quartz model-predicted K_d values ranged from 0.053 to 0.13. The predicted quantities of U(VI) adsorbed ranged from 4.0E-12 to 3.5E-10 moles U(VI)/g quartz for all wells other than NAT-26, and a value of 9.8E-10 for well NAT-26. Comparison of these values with the estimates of adsorbed U(VI) in Figure 2.9B show that the model-predicted values of U(VI) adsorbed fall within the experimental errors of the measurements. Thus, the failure to measure adsorbed U(VI) with quartz should be interpreted as a limitation of the field method rather than a problem with the SCM.

2.7 In-situ Hematite Field Measurements

2.7.1 Carbonate Extraction Results

Carbonate-extracted U(VI) for the hematite samples was much higher than any of the other solids investigated in this study (Fig. 2.12). For example, for NAT-26, the well with the highest U(VI) concentrations measured in groundwater, hematite adsorbed 2 orders of magnitude more U(VI) than did kaolinite per unit weight. The surface area of hematite is 50 m^2/g, much greater than that of kaolinite (8.7 m^2/g). Unlike the other minerals investigated, no Ca or Mg was detected in the carbonate extractions for hematite. Some V and Si were detected, but only in samples from wells NAT-05 and NAT-11 (Fig. 2.12).

2.7.2 Nitric Acid Extraction Results

A comparison of the amount of U(VI) extracted by the carbonate solution and nitric acid extractions is shown in Figure 2.13. Significant amounts of U(VI) were recovered in the nitric acid extraction after the carbonate extraction, indicating that the carbonate extraction did not fully recover U(VI) accumulated on hematite during exposure in the wells.

2.7.3 Comparison with Predictions of Hematite Surface Complexation Model

K_d values for U(VI) adsorption by hematite were then calculated from the estimated adsorbed U(VI) concentration divided by the dissolved U(VI) concentration in the groundwater sampled at the same depth in the well. Model-predicted K_d values were calculated from the SCM shown in Table 2.4, the model parameters are based on preliminary models of unpublished data for carbonate adsorption (M. Kohler, unpublished data) and U(VI) adsorption (R. Reitmeyer, unpublished data) on hematite prepared with the same method used here. The two sets of K_d values are shown in Table 2.5. The measured K_d values ranged from 90 mL/g to 210 mL/g for the hematite deployed in the wells, with K_d values generally increasing with decreasing alkalinity and U(VI) concentration. The hematite model-predicted K_d values ranged from 550 to 3750, approximately 5 to 18 times larger than the measured values. As in the case for kaolinite, the reason for the discrepancy between the measured and model-predicted values is unknown, but it is possible that the SCM overpredicts U(VI) adsorption because of the lack of experimental data at high partial pressures of $CO_2(g)$ in the data used to calibrate the hematite model. Again, as in the case of kaolinite, the measured K_d values for wells MAU-07 and MAU-08 did not seem unusually

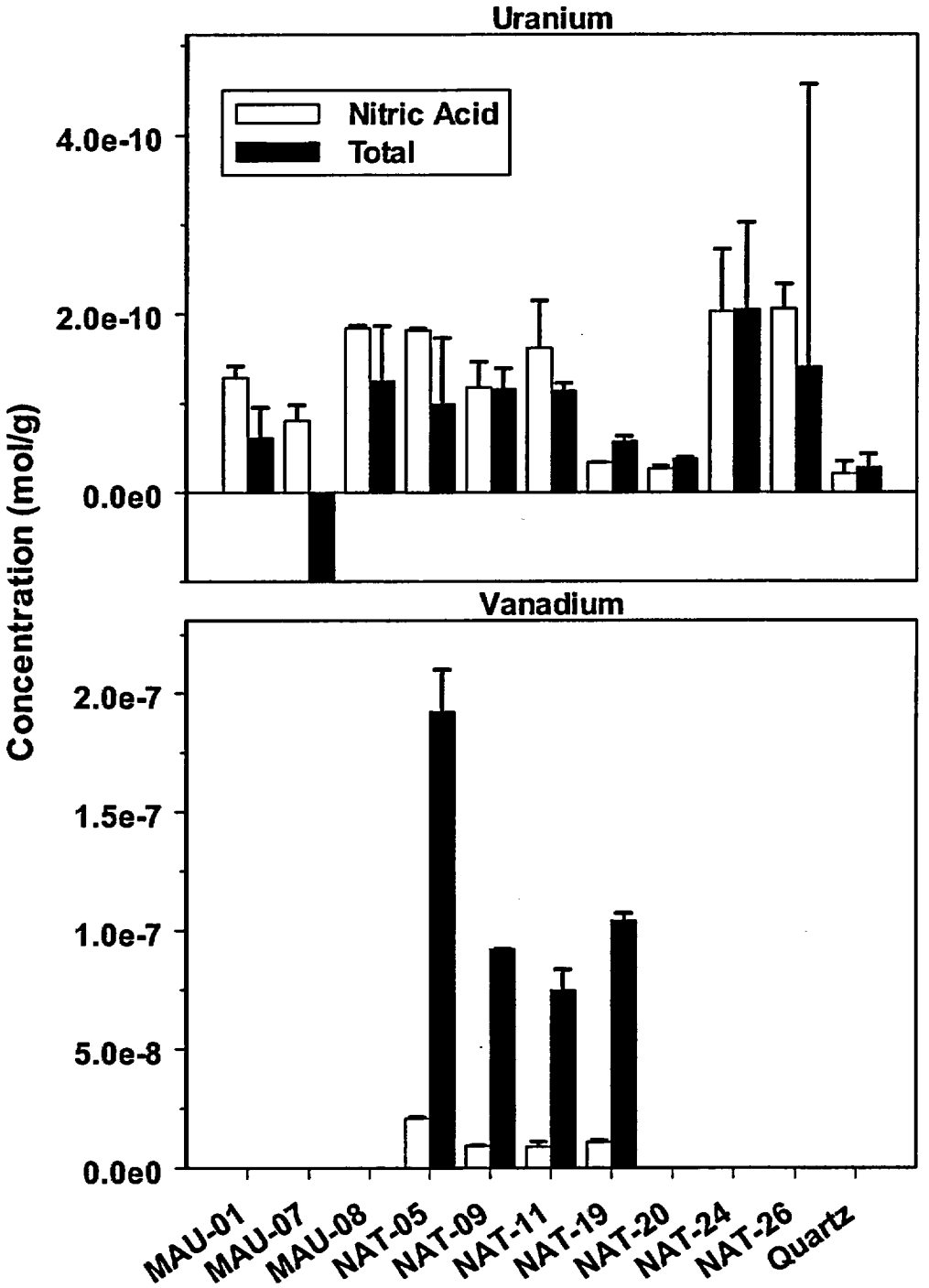

Figure 2.11. Comparison of concentrations of U(VI) and V extracted from quartz by concentrated nitric acid alone versus total extracted (sum of carbonate solution and nitric acid extracts). The total extracted values have been corrected for U(VI) or V present in entrained water during sampling (this caused the total to be lower in some cases than the nitric acid extracted amount). The data presented represent the average from two dialysis bags containing quartz that were deployed in each well. Sample labeled 'Quartz' shows data for extractions without field deployment.

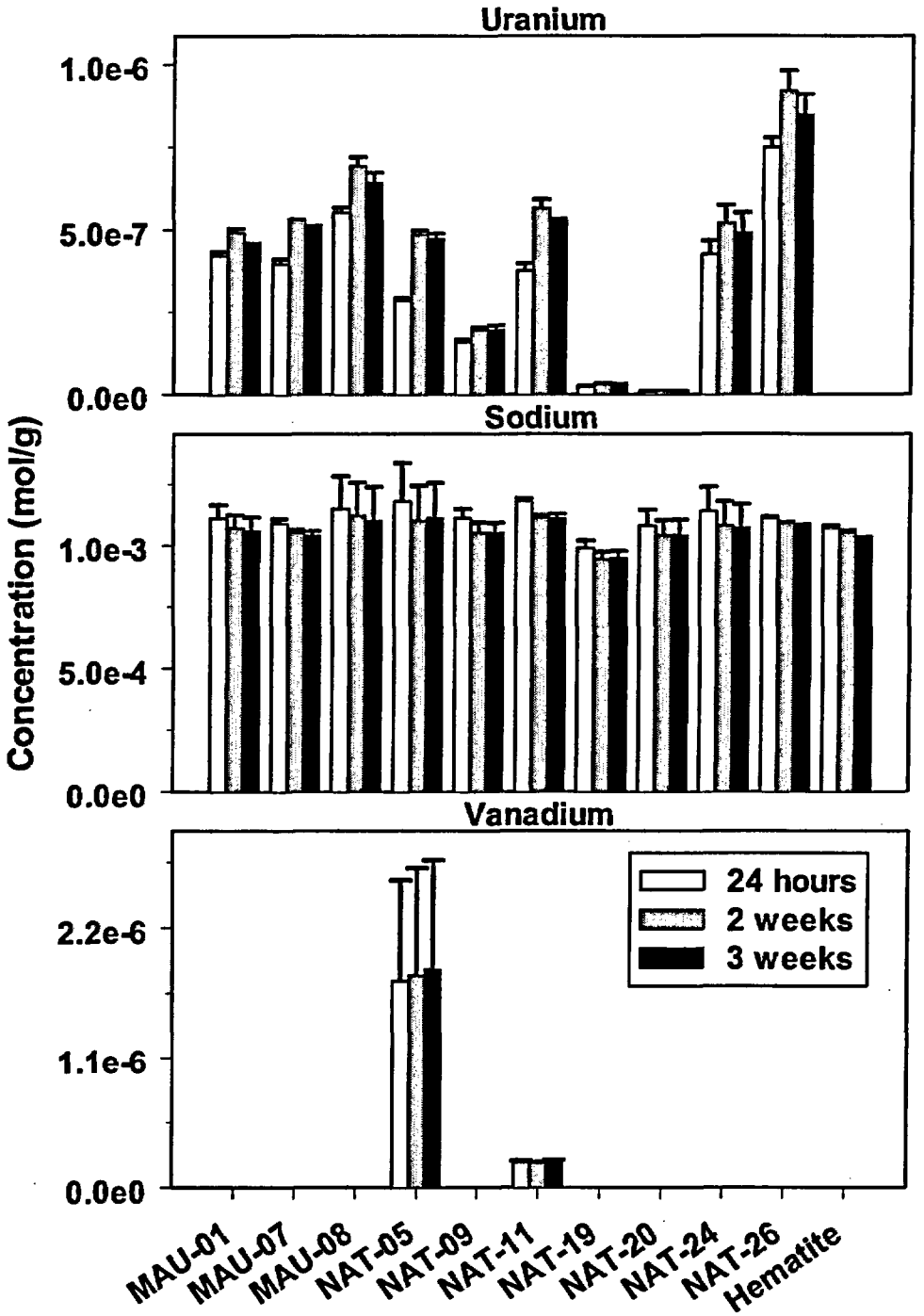

Figure 2.12. Concentrations of various elements at selected times during carbonate solution extracts of hematite after exposure to groundwater for 1 month. For U(VI) and V, data are corrected for the amount of each element present in entrained water when samples were collected. The data presented represent the average from two dialysis bags containing hematite that were deployed in each well. Data that was below the detection limit, including all Ca and Mg values and some V, are not plotted. Sample labeled 'Hematite' shows data for extractions without field deployment.

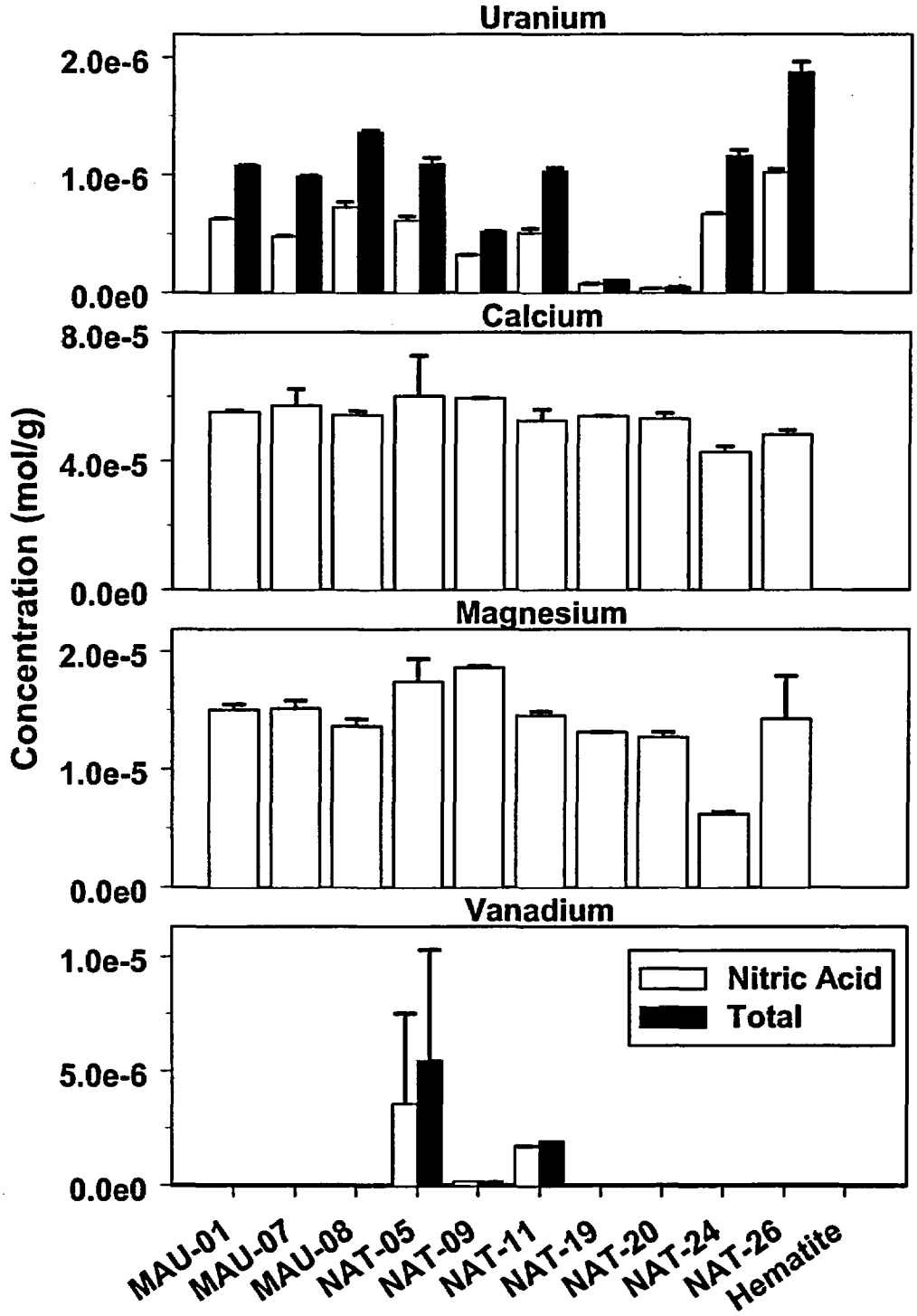

Figure 2.13. Comparison of various elements extracted from hematite by nitric acid alone versus total extracted (sum of carbonate solution and nitric acid extracts) after exposure to groundwater for 1 month. For U(VI) and V, data are corrected for the amount of each element present in entrained water when samples were collected. The data presented represent the average from two dialysis bags containing hematite that were deployed in each well. Data that were below the detection limit for V are not plotted. Sample labeled 'Hematite' shows data for extractions without field deployment.

Table 2.4. Model parameters of the SCM used to predict U(VI) adsorption on hematite deployed in dialysis bags in Naturita groundwater

		Exponents in mass law defining surface species[⊥]						
Model	**Surface species**	a	b	c	d	e	f	**Log K_f (I=0)**
Hematite TLM[⊕] 0.1M $NaNO_3$ U(VI): 10^{-7}–10^{-5}M pH: 4–9 pCO_2: air	SOH_2^+	1	1			1		8.31
	SO^-	1	-1			-1		-11.3
	$SOH_2^+NO_3^-$	1	1			1	-1	9.36
	SO^-Na^+	1	-1			-1	1	-10.4
	$(SOH_2^+)_2CO_3$	2		1		2	-2	10.1
	$(SO_{CO3\text{-}strong}H_2^+)_2CO_3$	2		1		2	-2	12.5
	$(SO_{CO3\text{-}strong})_2CO_3$	2		1		0.82	-0.82	10.2
	$(SOH)_2UO_2CO_3$	2	-2	1	1			2.34
	$(SOH)_2UO_2(CO_3)_2^{2-}$	2	-4	2	1	0	-2	-7.65
	$(SOH_{UO2\text{-}strong})_2UO_2CO_3$	2	-2	1	1			8.95

[⊥]Mass law for formation of the surface species is: [Surface species] = $K_f[SOH]^a(H^+)^b(H_2CO_3)^c(UO_2^{2+})^d\exp\{(-F/RT)(e\Psi_o+f\Psi_\beta)\}$. Coefficients for Na^+ and NO_3^- not shown.

[⊕] Model based on unpublished data of M. Kohler for carbonate adsorption and R. Reitmeyer for U(VI) adsorption. TLM = triple layer model; C_1 = 0.97 Farads/m^2, C_2 = 0.2 Farads/m^2, surface area of hematite (43 m^2/g in carbonate study; 46.1 m^2/g in U(VI) adsorption study; 50 m^2/g in dialysis bag study; weak site density = 33.8 μmoles/m^2; strong carbonate site density = 2.69 μmoles/m^2; strong U(VI) site density = 0.0677 μmoles/m^2; U(VI) surface species form bidentate bonds that consume two surface sites in mass balance and have an exponent of two in the mass law. Acidity and ion-pair electrolyte constants assumed to have the same values for all surface site types.

Table 2.5. Comparison of measured and model-predicted U(VI) K_d values for hematite samples in contact with Naturita groundwater

Well	Measured K_d (mL/g)	Model-Predicted K_d (mL/g)
MAU-01	152	610
MAU-07	191	920
MAU-08	163	1020
NAT-05	125	1010
NAT-09	90	550
NAT-11	188	1070
NAT-19	210	3750
NAT-20	189	3460
NAT-24	210	3120
NAT-26	128	700

larger than other wells, suggesting that U(IV) precipitation onto the samples was likely insignificant.

2.8 In-Situ Clinoptilolite Field Measurements

2.8.1 Carbonate and Formate Extraction Results

Clinoptilolite was first extracted with carbonate solution in the same manner as the other mineral samples. However, clinoptilolite has a very high capacity for ion exchange (Pabalan, 1994), and the sample adsorbed a large amount of calcium. During the carbonate extractions, the pH dropped repeatedly and was readjusted to 9.4 several times throughout the 3-week extraction period. Ca and Mg concentrations were initially high in the carbonate extraction, and dropped by an order of magnitude by 3 weeks (Fig. 2.14). As shown in Table 2.6, the alkalinity of the carbonate extractions measured after 3 weeks was significantly lower than the initial alkalinity of 20 meq/L for all samples. The unexposed clinoptilolite is shown for comparison. These observations suggest that in the field, clinoptilolite adsorbed Ca and Mg, which was subsequently released in the carbonate solution extraction and precipitated as Ca and Mg carbonate phases. Some U(VI) may have co-precipitated with these phases. For this reason, the clinoptilolite samples were extracted with 0.1 M sodium formate at pH 3.5 after the carbonate extraction, to dissolve any precipitated carbonates. Sodium acetate at pH 5 is often used to dissolve carbonates with minimal disturbance of other minerals. However, at pH 5, U(VI) adsorption is strong (Pabalan et al., 1998), and readsorption onto clinoptilolite would have occurred. In contrast, the sodium formate extraction solution is buffered at pH 3.5 at which negligible U(VI) sorption occurs.

The sum of U(VI) dissolved in both the carbonate solution and formate buffer extractions is presented in Figure 2.15. The total amount of U(VI) extracted from clinoptilolite in most of the wells is close to or less than that present in the original clinoptilolite sample prior to groundwater exposure (Fig. 2.15, sample labeled as "Clinoptilolite"). Only samples recovered from MAU-07 and MAU-08, and perhaps MAU-01, contained more U(VI) than was present in the unexposed mineral.

Table 2.6. Alkalinities measured in carbonate solutions after 3 weeks of extraction of clinoptilolite. Two replicate samples (C1 and C2) for each well are shown.

Well	Alkalinity (meq/L)	
	C1	C2
MAU-01	4.48	4.72
MAU-07	4.48	4.66
MAU-08	6.43	7.50
NAT-05	5.89	5.23
NAT-09	5.02	4.60
NAT-11	4.70	4.93
NAT-19	3.30	4.19
NAT-20	2.47	2.49
NAT-24	3.85	3.73
Clinoptilolite	20.47	20.61

2.8.2 Nitric Acid Extraction Results

The nitric acid extractions recovered a greater amount of U(VI) from the clinoptilolite samples than the sum of carbonate solution and formate buffer extractions. However, the amount of U(VI) extracted by nitric acid was approximately equal to the amount present in the unexposed material, as shown in Figure 2.15. In fact, there appeared to be slightly more U(VI) present in the unexposed clinoptilolite, indicating that a small amount of U(VI) may have been released by the mineral during exposure to the groundwater.

The estimated K_d values for U(VI) sorption on clinoptilolite are shown in Table 2.7. Experimental measurements of U(VI) sorption on clinoptilolite have been made in systems equilibrated with air (Pabalan et al., 1998), but no surface complexation model has yet been published for these data. As in the cases of kaolinite and hematite, the measured K_d values for wells MAU-07 and MAU-08 did not seem unusually larger than other wells, suggesting that

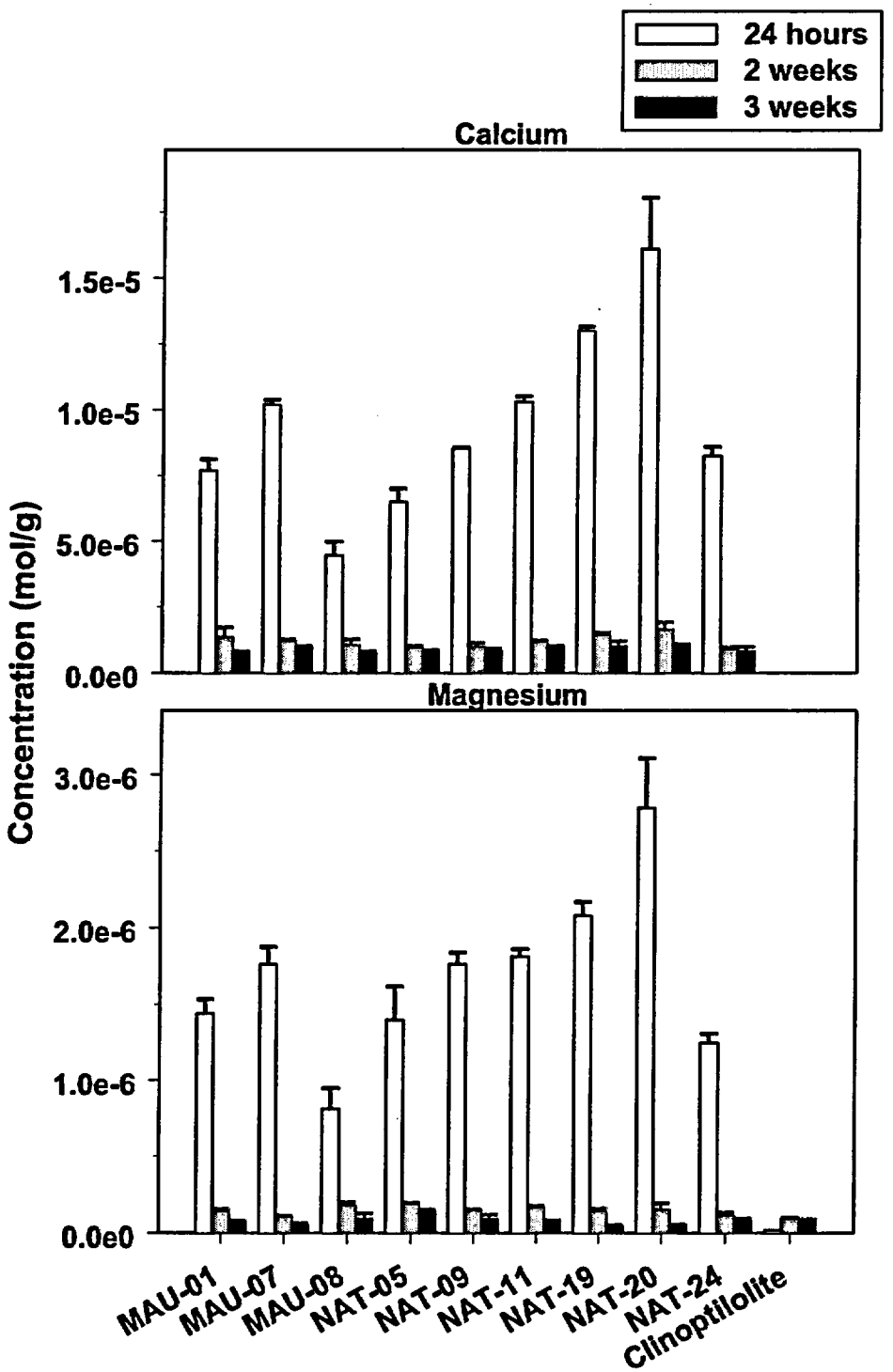

Figure 2.14. Ca and Mg in carbonate solution extractions of clinoptilolite at various times. Data are not corrected for the amount of Ca or Mg present in entrained water during sampling. The data presented represent the average from two dialysis bags containing clinoptilolite that were deployed in each well. Sample labeled 'Clinoptilolite' shows data for extractions without field deployment.

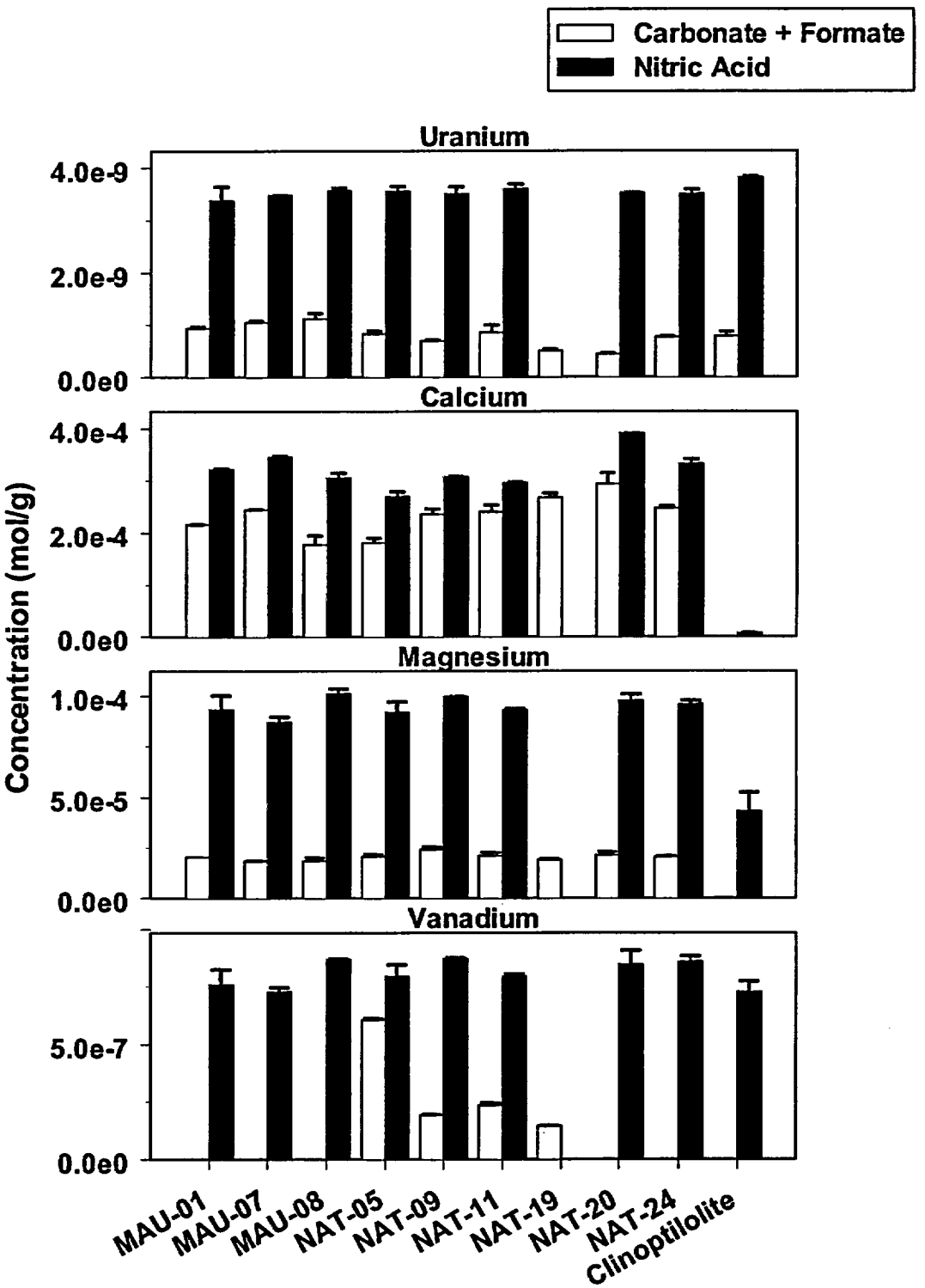

Figure 2.15. Comparison of various elements extracted from clinoptilolite by the sum of the carbonate solution and formate buffer extractions and the nitric acid extraction. The nitric acid sample for well NAT-19 is missing. The data presented is the average of two replicate clinoptilolite dialysis bags sampled from each well. Data below the detection limit is not plotted (i.e. for vanadium). Sample labeled 'Clinoptilolite' shows data for extractions without field deployment.

U(IV) precipitation onto the samples was likely insignificant.

Table 2.7. Measured U(VI) K_d values for clinoptilolite samples in contact with Naturita groundwater

Well	Measured K_d (mL/g)
MAU-01	1.09
MAU-07	1.11
MAU-08	1.06
NAT-05	1.16
NAT-09	1.06
NAT-11	1.00
NAT-19	1.68
NAT-20	2.70
NAT-24	0.91

2.9 In-Situ Measurements with Forty-Mile Wash Sediments

2.9.1 Carbonate Extraction Results

U(VI) extracted from 40-Mile Wash sediments by the carbonate solution is shown in Figure 2.16. The most notable thing about these data is the large amount of U(VI) accumulated on samples placed in well MAU-07. The amount of U(VI) present in groundwater was very similar at wells MAU-07, MAU-01 and MAU-08. However, the total U extracted from the FMW solids was much higher for well MAU-07. While MAU-07 is consistently one of the wells with the largest accumulation of U(VI) for all of the solids tested, only with the FMW dialysis bags was the extent of accumulation significantly higher than the other wells (close to ten times higher than any other well). MAU-07 has the highest concentrations of dissolved Fe of any of the wells studied (Tables 2.1 and 2.2), indicating that iron-reducing conditions exist in the aquifer near this well. It seems likely that some U(VI) was reduced to U(IV) in the dialysis bag for the FMW sediment in well MAU-07, although this did not seem to occur for other mineral phases in well MAU-07 (this study) or when uncontaminated Naturita sediments were suspended in wells MAU-03 and MAU-04 (Davis et al., 2006; Curtis et al., 2004). Perhaps there is something unique about the properties of the FMW sediments (e.g., internal porosity) that favors a more reducing environment and U(VI) reduction. High dissolved Fe(II) concentrations were measured consistently above detection (1.35-2.05 mg/L) in well MAU-07 during the study, but none of the other mineral samples exhibited such a large U accumulation, including clinoptilolite, which was deployed in well MAU-07 at the same time as the FMW sample.

For the FMW sediment, there was a fairly large variation in the amount of U(VI) recovered from replicate samples (e.g., MAU-08 and NAT-05 in Fig. 2.16C). For well NAT-05, there was also a large variation in the amount of V recovered. The FMW solid is a composite sample that is much more heterogeneous than any of the single mineral samples studied here, and it is likely that the 1 g sample sizes used in these experiment was not sufficiently large to achieve uniform samples. Calcium concentrations in the carbonate solution extractions dropped over the 3-week period for all of the FMW samples. However, unlike clinoptilolite, the pH was only readjusted once throughout the extraction period. Alkalinities measured at the end of 3 weeks were 16-18 meq/L as shown in Table 2.8, only slightly lower than the starting alkalinity of 20 meq/L. The alkalinity of unexposed FMW material is shown for comparison. It is possible that some U(VI) co-precipitated with carbonates during this extraction. Any co-precipitated U(VI) would be recovered in the nitric acid extraction. We chose not to extract these samples with 0.1M sodium formate buffer because: (1) carbonate precipitation was not very extensive, and (2) the FMW sediments contains naturally occurring carbonates which would be dissolved along with any newly precipitated carbonates.

2.9.2 Nitric Acid Extraction Results

Some U was extracted by the nitric acid extraction (Fig. 2.17), but only exceeded the amount of U extracted from the unexposed material in a couple of cases (MAU-07, perhaps MAU-08). The amount of U extracted by the carbonate solution extraction greatly exceeded

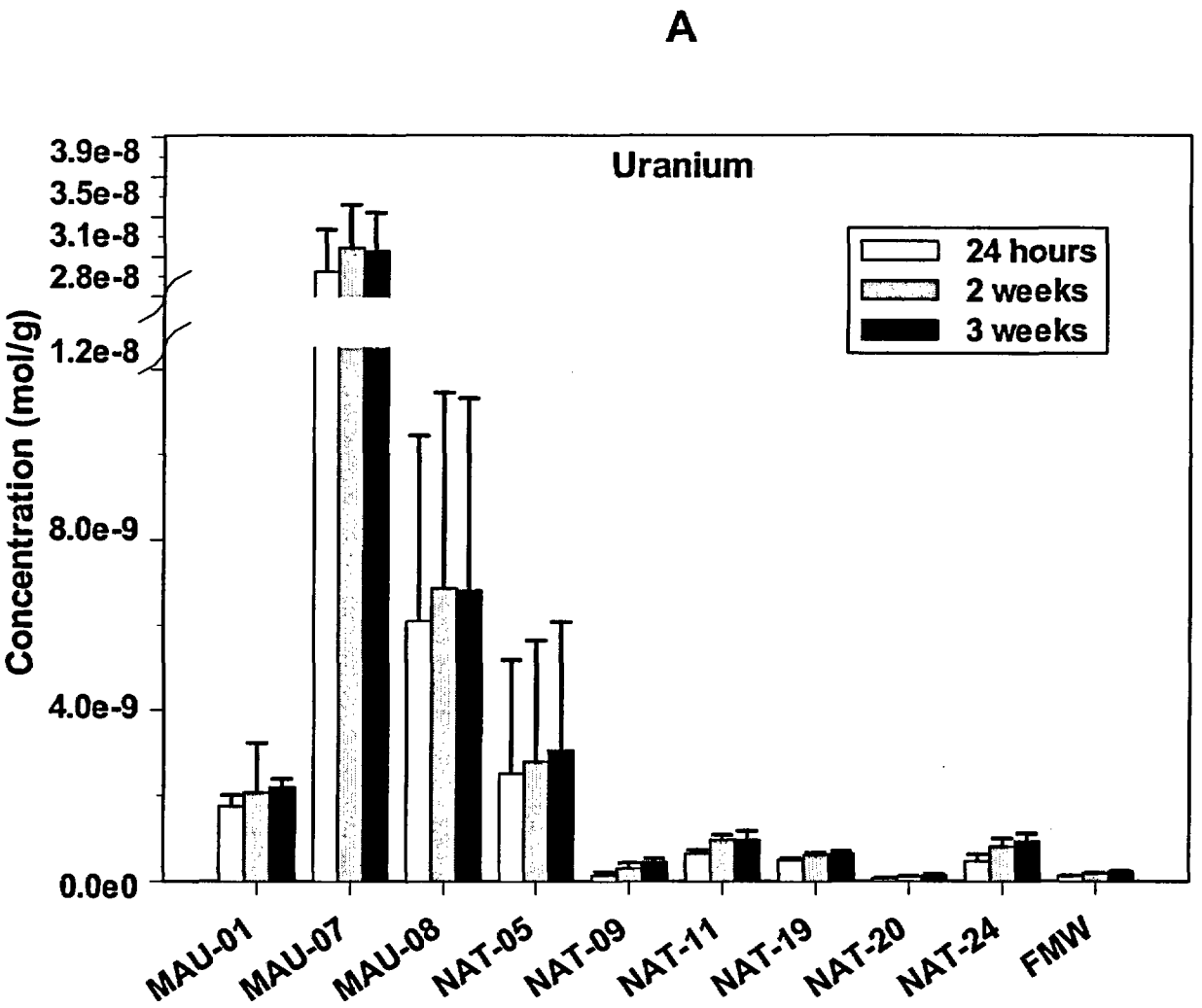

Figure 2.16. The concentrations of various elements dissolved in carbonate solution extracts of 40-Mile Wash sediments. Part (A) shows U, Part (B) shows Ca, Fe, Mg, Na, and V, and Part (C) shows individual replicate samples for U and V. Parts (A) and (B) show the average of two replicate samples. U and V data are corrected for the amount present in entrained water. Data below the detection limit for V are not plotted. Sample labeled 'FMW' shows data for extractions of the 40-Mile Wash sediment composite without field deployment.

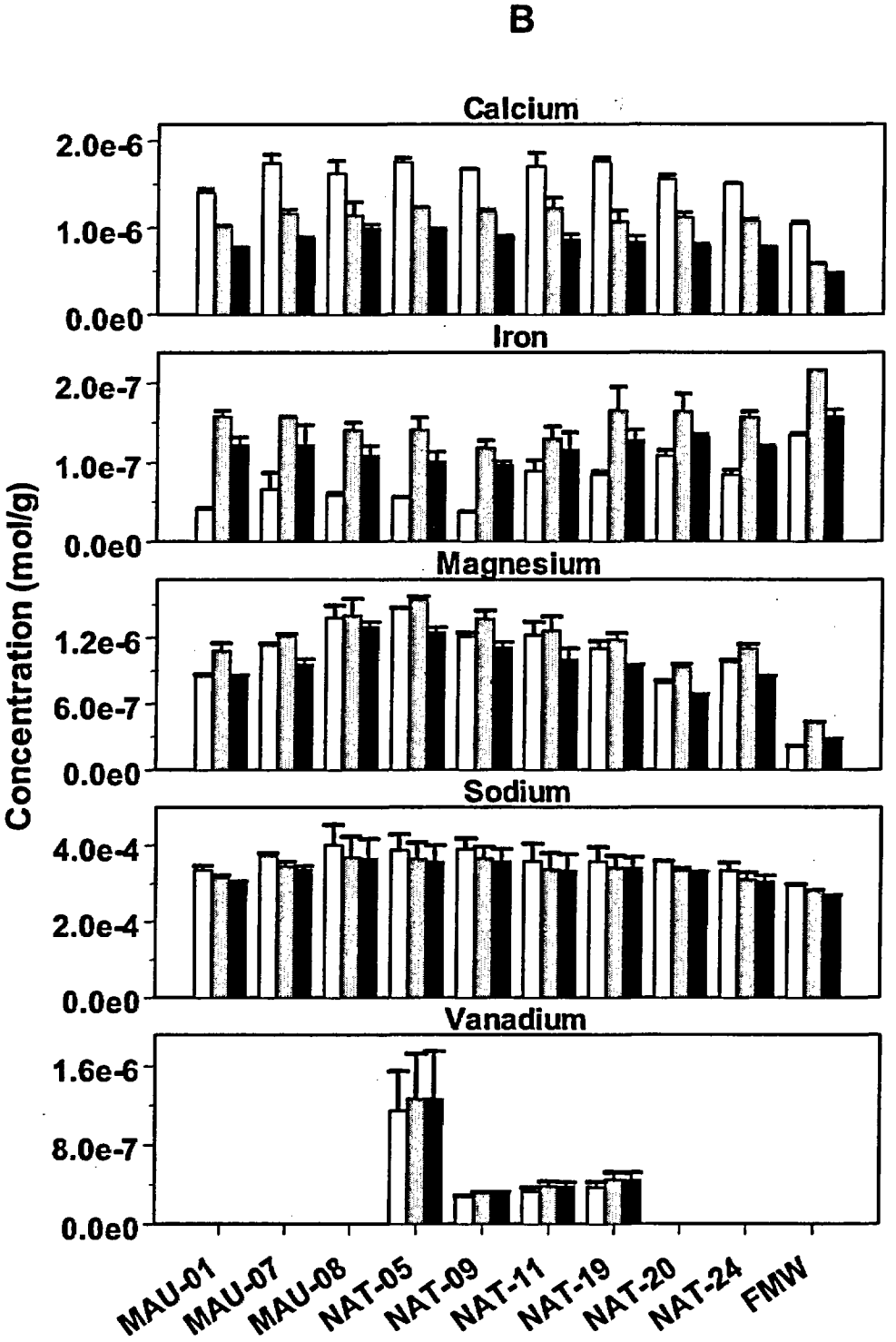

Figure 2.16 (continued). The concentrations of various elements dissolved in carbonate solution extracts of 40-Mile Wash sediments. Part (A) shows U, Part (B) shows Ca, Fe, Mg, Na, and V, and Part (C) shows individual replicate samples for U and V. Parts (A) and (B) show the average of two replicate samples. U and V data are corrected for the amount present in entrained water. Data below the detection limit for V are not plotted. Sample labeled 'FMW' shows data for extractions of the 40-Mile Wash sediment composite without field deployment.

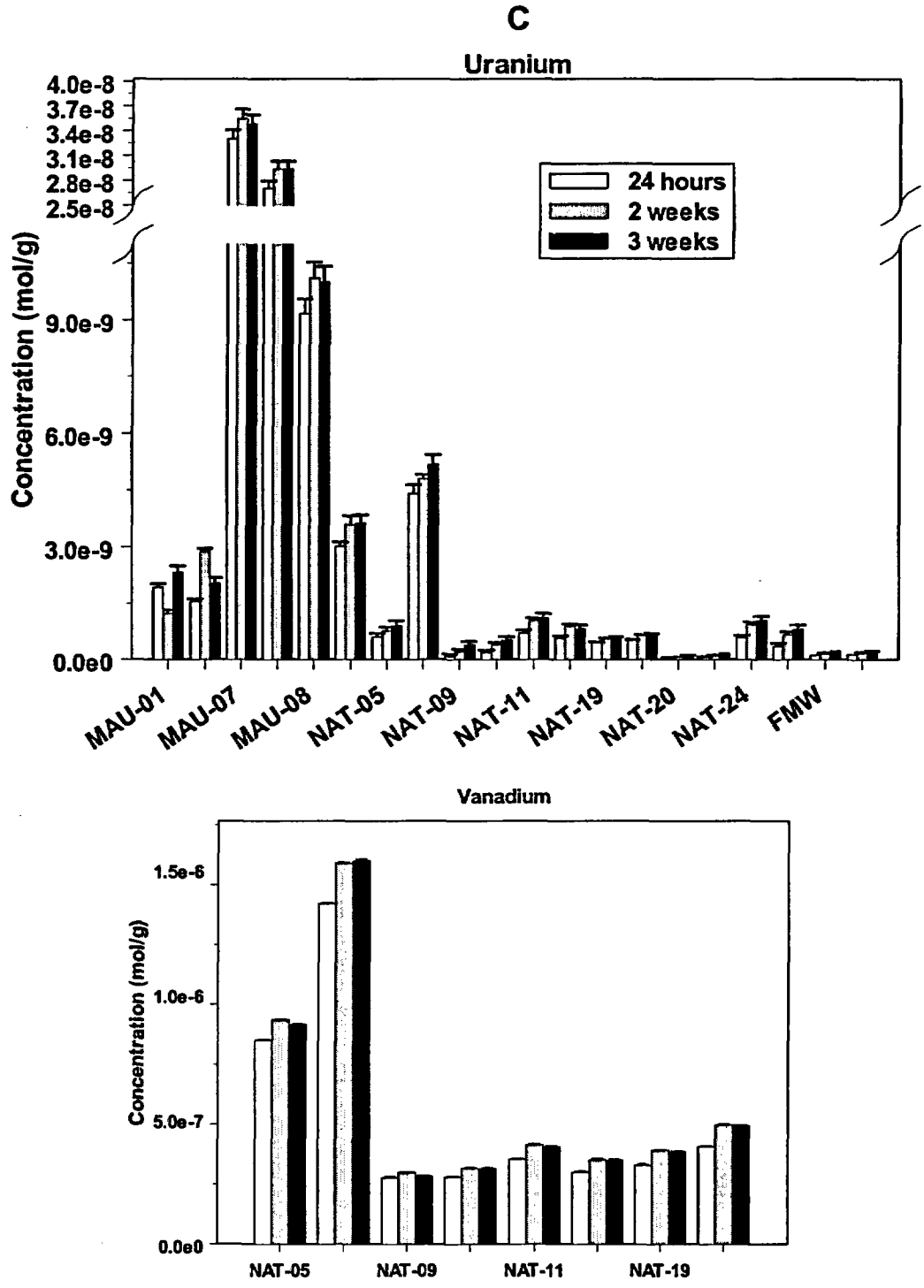

Figure 2.16 (continued). The concentrations of various elements dissolved in carbonate solution extracts of 40-Mile Wash sediments. Part (A) shows U, Part (B) shows Ca, Fe, Mg, Na, and V, and Part (C) shows individual replicate samples for U and V. Parts (A) and (B) show the average of two replicate samples. U and V data are corrected for the amount present in entrained water. Data below the detection limit for V are not plotted. Sample labeled 'FMW' shows data for extractions of the 40-Mile Wash sediment composite without field deployment.

that extracted by nitric acid for the sample collected from well MAU-07.

Table 2.8. Alkalinities measured in carbonate solution extractions of replicate (F1 and F2) 40-Mile Wash sediment samples deployed in Naturita wells after 3 weeks of extraction

Well	Alkalinity (meq/L)	
	F1	F2
MAU-01	15.64	16.27
MAU-07	16.10	16.68
MAU-08	17.59	17.09
NAT-05	17.94	17.37
NAT-09	17.13	16.48
NAT-11	16.28	16.28
NAT-19	16.45	16.14
NAT-20	15.72	16.02
NAT-24	16.24	16.03
FMW	15.48	15.62

The estimated K_d values for U(VI) sorption on clinoptilolite are shown in Table 2.9.
A surface complexation model for U(VI) sorption on 40-Mile Wash sediments has not yet been published, but measurements are currently being made in the laboratory and a model will be available in a future NUREG report.

Table 2.9. Measured U(VI) K_d values for 40-Mile Wash sediment samples in contact with Naturita groundwater

Well	Measured K_d value (mL/g)
MAU-01	0.80
MAU-07	12.0
MAU-08	1.91
NAT-05	0.84
NAT-09	0.22
NAT-11	0.33
NAT-19	4.09
NAT-20	2.57
NAT-24	0.37

2.10 Conclusions

The in-situ adsorption measurements were conducted as further tests of the method of measuring K_d values with dialysis bags suspended in boreholes and as a measure of the applicability of surface complexation models to the field environment. A similar approach was successful in a previous application with uncontaminated Naturita sediments (Curtis et al., 2004), although the grain sizes were much larger, allowing the use of mesh bags rather than dialysis tubing. However, the results presented here suggest that either: a) the method or experimental approach need improvement, and/or b) the surface complexation models for kaolinite and hematite did not work well when applied to the aqueous chemical conditions in the Naturita aquifer. In particular, the ability of the kaolinite and hematite surface complexation models to predict U(VI) adsorption under conditions of high bicarbonate concentration is not well known. The quartz surface complexation model presented here was calibrated with data at high bicarbonate concentrations. However, the ability of this model to predict U(VI) adsorption could not be determined because of several factors, including the very low surface area of the quartz sample and the experimental error of the dialysis bag method related to the entrained water collected with the sample. Improvements to the method and the deployment of larger sample sizes in the well could solve some of these problems. Larger samples would allow a sampling of water within the dialysis bag for aqueous chemical conditions. The use of a centrifuge in the field might be required to improve solid/liquid phase separation at the time of sampling, which would reduce the correction required for entrained water in the sample.

In-situ K_d values for U(VI) adsorption on samples of clinoptilolite and a 40-Mile Wash sediment composite were also made, but these values could not be compared with model-predicted values because of the lack of published models for these samples at present.

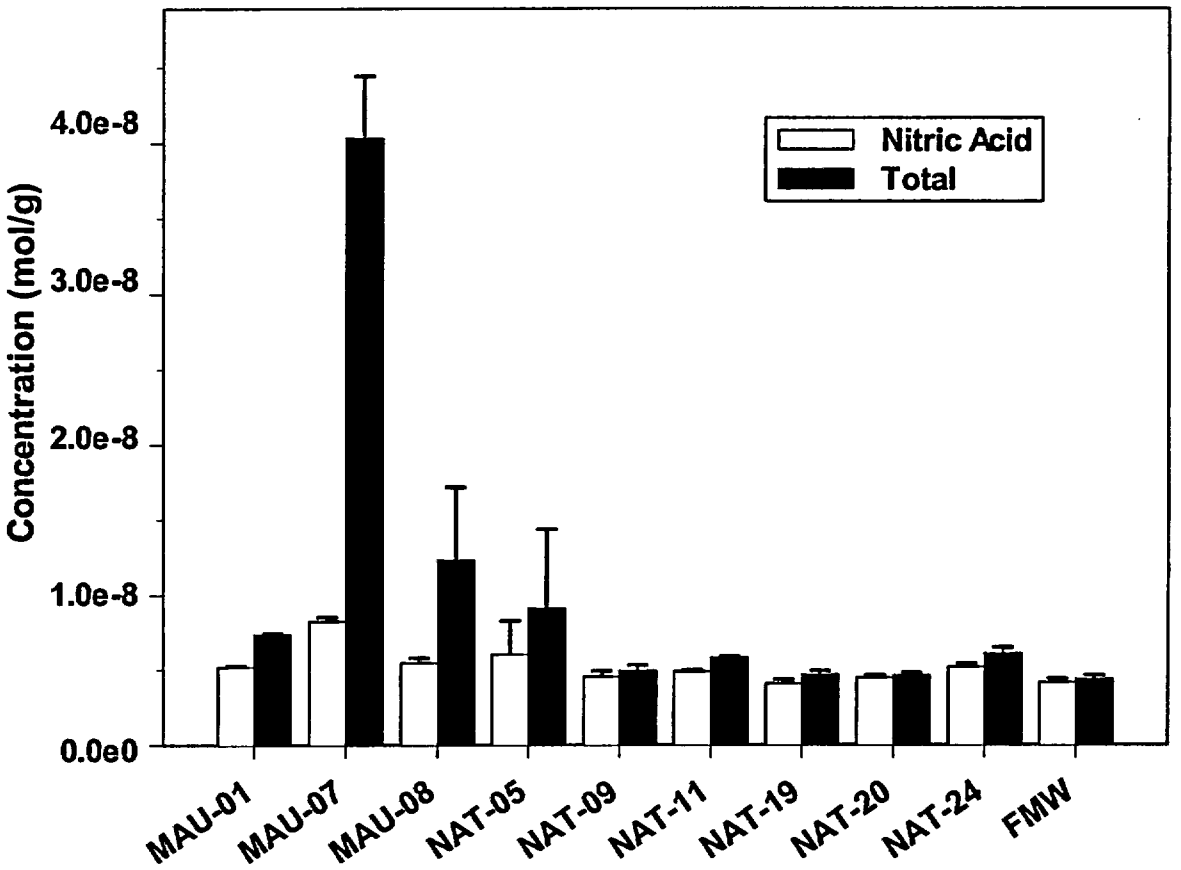

Figure 2.17. Comparison of U extracted from 40-Mile Wash sediments by nitric acid alone and total U extracted by the sum of the carbonate solution and nitric acid extractions. Nitric acid data for a couple of samples are missing (NAT-09 and NAT-19). The data presented is the average of two replicate FMW sample dialysis bags sampled from each well. Sample labeled 'FMW' shows data for extractions of the 40-Mile Wash sediment composite without field deployment.

3 REACTIVE TRANSPORT MODELING APPROACHES FOR *IN-SITU* TRACER TESTS

3.1 Introduction

Previous work (Davis and Curtis, 2003; Curtis et al., 2006) demonstrated that the reactive transport of U(VI) at the Naturita site could be simulated with a model that used a semi-mechanistic SCM to describe U(VI) adsorption to the aquifer sediments. While these results are encouraging, the simulations do not provide a rigorous test of the SCM because the good match between the observed and simulated U(VI) concentrations was achieved by model calibration. Specifically, the concentrations of U(VI) and alkalinity in recharge water that had leached through the mill yard and the tailings pile were varied to optimize the fit to the observed data. The composition and spatial and temporal distribution of this contaminated recharge were not measured and consequently significant uncertainty must be attributed to the U(VI) source and therefore to the transport simulation results. The semi-mechanistic model gave good predictions of U(VI) K_d values measured under variable chemical conditions for both contaminated sediments (Kohler et al., 2004) and for NABS samples that were suspended in 17 different monitoring wells (Curtis et al., 2004). These studies involved equilibration times that ranged from days to years and therefore may not be applicable to the dynamic conditions present in an aquifer. Therefore, small-scale tracer tests are a more rigorous approach for evaluating the applicability of the semi-mechanistic SCM developed for Naturita aquifer background sediments (NABS).

3.1.1 Background

Two types of experiments were conducted to evaluate the applicability of the semi-mechanistic SCM to describe U(VI) adsorption and desorption under field. Both single well push-pull tests (Section 4) and multi-well, small-scale migration tests (Section 5) were conducted to evaluate the effect of variable geochemical conditions on the reactive transport of U(VI). The tracer tests were conducted in the shallow alluvial aquifer downgradient from the former uranium mill and the tailings disposal area. The U(VI) concentration in the groundwater at the tracer test site was approximately 4 μM, the alkalinity was 7.5 meq/L and the pH was approximately 7.1. Previous studies at the site demonstrated the U(VI) concentration was most sensitive to the alkalinity and least sensitive to the pH values relative to the range of measured values. Uranium migration tests were conducted on a scale of 1-3 m and considered variable U(VI) concentration and alkalinity, and included Br as an inert tracer. The objectives of these tests were to evaluate field methods for determining and evaluating adsorption reaction constants for use in reactive transport simulations.

3.1.2 Uranium(VI) Adsorption

In the absence of separate U phases, adsorption is probably the most significant factor that reduces U(VI) mobility in groundwater. Batch adsorption experiments were conducted using Naturita aquifer background sediments (NABS) that were collected from a gravel pit located upgradient of well DOE547 (Davis et al., 2004b). The batch experimental conditions encompassed the range of geochemical conditions observed in the field and a semi-mechanistic SCM was fit to the adsorption data using the geochemical optimization program FITEQL (Herbelin and Westall, 1999). The SCM consists of 6 reactions and 3 different site-types that are listed as Model 1 in Table 3.1. The three site-types are described as very strong (>SSOH), strong (>SOH), and weak (>WOH) sites, corresponding to their relative U(VI) binding strength (Table 3.1). Multiple site-types are commonly used in formulating SCMs and approximating the nonlinear isotherms commonly observed for cation adsorption on well-characterized metal oxides (Dzombak and Morel, 1990). Postulating multiple site-types was also important for simulating peak tailing in laboratory columns packed with quartz (Kohler

Table 3.1 NABS Surface Complexation Model [1]

Reaction	Symbol[2]	Log K	k_f
Model 1: Reactions in terms of the UO_2^{+2} species			
$>SSOH + UO_2^{2+} = >SSOUO_2^+ + H^+$	K_{SS}	6.80	$3x10^{14}$
$>SOH + UO_2^{2+} = >SOUO_2^+ + H^+$	K_S	5.82	$4x10^{13}$
$>WOH + UO_2^{2+} = >WOUO_2^+ + H^+$	K_W	2.57	$2x10^{10}$
$>SSOH + UO_2^{2+} + H_2O = >SSOUO_2OH + 2H^+$	K_{SSOH}	-0.67	$5x10^{14}$
$>SOH + UO_2^{2+} + H_2O = >SOUO_2OH + 2H^+$	K_{SOH}	-2.08	$4x10^{13}$
$>WOH + UO_2^{2+} + H_2O = >WOUO_2OH + 2H^+$	K_{WOH}	-5.32	$2x10^{10}$
Model 2: Reactions in terms of the $Ca_2UO_2(CO_3)_3$ species			
$>SSOH + Ca_2UO_2(CO_3)_3 + 2H^+ = >SSOUO_2^+ + 3HCO_3^- + 2Ca^{2+}$		7.23	$1.8x10^{22}$
$>SOH + Ca_2UO_2(CO_3)_3 + 2H^+ = >SOUO_2^+ + 3HCO_3^- + 2Ca^{2+}$		6.25	$9.0x10^{21}$
$>WOH + Ca_2UO_2(CO_3)_3 + 2H^+ = >WOUO_2^+ + 3HCO_3^- + 2Ca^{2+}$		3.01	$1.8x10^{18}$
$>SSOH + Ca_2UO_2(CO_3)_3 + H^+ + H_2O = >SSOUO_2OH + 3HCO_3^- + 2Ca^{2+}$		-0.23	$6.0x10^{14}$
$>SOH + Ca_2UO_2(CO_3)_3 + H^+ + H_2O = >SOUO_2OH + 3HCO_3^- + 2Ca^{2+}$		-1.65	$4.0x10^{13}$
$>WOH + Ca_2UO_2(CO_3)_3 + H^+ + H_2O = >WOUO_2OH + 3HCO_3^- + 2Ca^{2+}$		-4.88	$1.8x10^{09}$

et al., 1996). Davis et al. (2004b) illustrated that observed and modeled K_D values at constant pH and alkalinity decreased by a factor of approximately 3 as U(VI) concentration increased from 0.03 μM to 10 μM indicating that the adsorption isotherm is moderately nonlinear. The semi-mechanistic SCM does not include an electrical double layer term and assumes that the adsorption occurs by U(VI) binding to generic sites that represent average surface chemical properties of the sediment.

3.1.3 Push-Pull Tracer Tests

A push-pull test (also known as a single-well injection-withdrawal test) involves the injection ("push") of a test solution into an aquifer followed by the extraction ("pull") of the test solution/groundwater mixture from the same location (Hall et al., 1991; Leap and Kaplan, 1988; Istok et al., 1997). The push and pull phases of the test may be separated by a "drift" phase where the test solution migrates with the native groundwater and provides time to allow reactions of interest to occur. The tests may be performed in existing monitoring wells or multi-level samplers and therefore could be applicable at many sites. The injected test solution usually consists of groundwater with a non-reactive tracer added to account for dilution, and the test solution can contain one or more other solutes of interest. During the injection phase, the test solution is injected into the aquifer where it flows away from the injection well as a roughly cylindrical tracer cloud in an ideal case. During the extraction phase, flow is reversed and the

concentrations of tracer, reactive solutes, and possible reaction products are measured as a function of time at the same well. Push-pull tests have been conducted to evaluate the physical properties of an aquifer including the porosity, dispersivity, advection velocity and the extent of mass transfer between mobile and immobile zones. Push-pull tests have also been conducted to evaluate *in-situ* reactions related to a variety of processes including estimating biodegradation rates, ion exchange reactions, and partitioning of tracers between aqueous and non-aqueous phases.

3.1.4 Objectives

The purpose of this section is to develop a strategy for modeling the reactive transport that occurs during the *in situ* push-pull tracer tests. These simulations, coupled with sensitivity analyses, are critical for discriminating between competing processes that affect U(VI) concentration such as adsorption, dilution and reduction.

3.2 Reactive Transport Modeling Approaches for Push-Pull Tests

Although push-pull tests have been conducted to investigate a wide variety of subsurface processes including advection, dispersion, degradation and sorption, the application of a general reactive transport model to push-pull tests has generally lagged behind the experimental studies. Part of this difference probably results because push-pull tests have often been used to investigate physical processes such advection and dispersion (Hall et al., 1991; Leap and Kaplan, 1988). Most push-pull studies involving reactive processes have focused on kinetically controlled reactions (Istok et al., 1997, Reinhard et al, 1997; Haggerty et al., 1998; Schroth et al, 1998). Push-pull tests have also been conducted to evaluate the reductive immobilization of U by reducing U(VI) to U(IV) (Senko et al., 1998). Only a few push-pull studies have considered adsorption (Istok et al., 1999; Schroth et al, 2001). One previous study on adsorption of DOWAX, a commercially available surfactant, simulated adsorption using a Langmuir isotherm and found that the effect of adsorption was overpredicted, possibly because of rate-limited adsorption (Istok et al., 1999). None of the previous studies have used multicomponent reactive transport modeling to help understand the processes controlling adsorption that is sensitive to variable chemical conditions.

Push-pull tests in most field settings require at least a two-dimensional (e.g., Schroth et al., 2001) and perhaps a three-dimensional solution. This arises because during the injection and withdrawal phases of the experiment, the transport occurs radially outward from or toward the groundwater well in response to the pumping stress. However, during the drift phase of the experiment, transport may occur primarily in one direction in response to the natural gradient. In aquifers where the vertical hydraulic conductivity is significantly smaller that the longitudinal or transverse hydraulic conductivity, it might be possible to approximate the aquifer as a single two-dimensional layer. Conversely, if the vertical hydraulic conductivity is comparable in magnitude to the longitudinal or transverse hydraulic conductivity, or if there are significant heterogeneities in the hydraulic conductivity, three-dimensional simulations may be required.

Although push-pull tests have the advantage that the tests are conducted *in situ*, the tests have the disadvantage that the flow system and transport velocities are highly perturbed during the both the push and pull (but not drift) phases of the experiment. Specifically, during both the push and pull phases of the test, the flow field is dominated by radial transport and consequently the groundwater velocities with the radial distance squared if the flow is predominantly cylindrical or even with the radial distance cubed if the flow is predominantly spherical. Moreover, the local equilibrium assumption may not be valid in radial flow (Valocchi, 1986). Consider, for example, a typical study described discussed in chapter 4 that involved injection of $0.04m^3$ (40L) into a well with a 1m-screened interval at a uniform rate of $0.08\ m^3/hr$. If it assumed that the adsorption reaction can be described by a linear isotherm having a half life

of 24 hours, then the dimensionless parameter that can be considered to equal the rate of adsorption relative to the rate of advection has a value of 400 at a distance of 1m from the well. Valocchi (1986) found that for such a value of the dimensionless parameter, the local equilibrium assumption would probably introduce significant errors into a simulation result. Although it is difficult to extrapolate these results for a linearly sorbing solute reacting with an infinite supply of adsorption sites to the case of U(VI) adsorption where the adsorption is nonlinear and constrained by a finite number of sites, the results nevertheless raise questions about the validity of the local equilibrium approximation for U(VI).

3.2.1 Alternative Conceptual Models For Simulating Push-Pull Tests

The primary goal of this project is to evaluate if semi-mechanistic SCM models can be used to described U(VI) adsorption and desorption under variable geochemical conditions. Owing to the complexity of the geochemical and hydrological systems, this evaluation inevitable involves the comparison between observations and numerical model simulations. The simple approach of assuming local equilibrium assumption is an obvious starting point for these numerical simulations. Other approaches considered include a kinetics approach, a mass transfer approach and a hybrid approach that ignores adsorption-desorption reactions during the push and pull phases of the experiments.

3.2.1.1 Local Equilibrium

The local equilibrium approach was used previously to simulate U(VI) transport at the Naturita site (Curtis et al., 2006). This approach assumes that the characteristic times of adsorption reactions are fast relative to the characteristic times for reaction. This assumption makes it possible to ignore the many possible causes for departure from equilibrium such as kinetic limitations of sorption-desorption, diffusion within aggregates or mass transfer between zones of different hydraulic properties.

3.2.1.2 Kinetically Controlled Adsorption

An alternative to the local equilibrium approach is to assume that the adsorption reactions are kinetically controlled. Adsorption of U(VI) by the NABS sample in batch adsorption studies required approximately 3 days to reach equilibrium (Davis et al., 2004b). Transport simulations with kinetically controlled adsorption reactions were conducted to evaluate if this adsorption time scale could produce significant deviations from local equilibrium in the field scale simulations (Davis and Curtis, 2003). Although the kinetic effects were found to be negligible for the plume scale simulations, kinetically limited sorption could be important in the small-scale push-pull tests where the flow field is highly perturbed.

An empirical approach to simulate the effect of slow kinetics is to use 'mass action kinetics' which relates the rate of the reaction to the reaction stoichiometry. For example, the adsorption reaction can be written as:

$$UO_2^{+2} + > WOH + H_2O \underset{k_r}{\overset{k_f}{\rightleftarrows}} > WOUOOH + 2H^+ \qquad (3\text{-}1)$$

where k_f and k_r are rate constants. The rate of formation of adsorbed U(VI) is:

$$\frac{\partial(> WOUOOH)}{\partial t} = k_f(> WOUOOH)(H^+)^2 - k_r(> WOH)(UO_2^{+2}) \quad (3\text{-}2)$$

In order to maintain consistency with the NABS SCM, the rate constants were related to the equilibrium constant (K_{EQ}) by:

$$K_{EQ} = \frac{k_f}{k_r} \quad (3\text{-}3)$$

Alternatively, the adsorption reaction in terms of the abundant aqueous $Ca_2UO_2(CO_3)_3$ is:

$$Ca_2UO_2(CO_3)^0_{3(aq)} + > WOH + H^+ + H_2O \underset{k'_r}{\overset{k'_f}{\rightleftarrows}} > WOUO_2OH + 3HCO_3^- + 2Ca^{2+} \quad (3\text{-}4)$$

A complete set of rate expressions using UO_2^{+2} ion as the reactant in the adsorption reactions is referred to as Model 1 and a complete set of rate expressions using the $Ca_2UO_2(CO_3)_3^0{}_{(aq)}$ ion as the reactant is referred to as Model 2 and these are summarized in Table 3.1. The two stoichiometric formulations listed in Table 3.1 were used because the two kinetic models are affected differently by variable chemical conditions.

The rate constants in Table 3.1 were estimated from batch data collected at pH 7.9 and at atmospheric partial pressure of CO_2 (Davis et al., 2004b). The two calibrated batch adsorption models are illustrated in Figures 3.1a and 3.1b for batch data collected at 0.09 and 9.5 μM U(VI). For both initial concentrations the model simulations reach a stable concentration after approximately 50 to 70 hr, in agreement with the adsorption data. The simulated U(VI) concentrations are slightly smaller than the observations for both cases because the NABS SCM does not exactly fit the adsorption data for the particular experimental conditions of the kinetic experiments.

3.2.1.3 Slow Mobile-Immobile Exchange

Flow velocities in many aquifers are often nonuniform with water flowing rapidly in some zones of the aquifer, slow and other zones and even stagnant in other zones of the aquifer. This distribution of velocities can result from the heterogeneity in hydraulic conductivity or from stagnant zones that occur within particle grains. When the mass transfer between regions of high velocity and regions low velocity or stagnant zones is slow compared to the rate of advection, the system is in physical nonequilibrium. The simplest approach to simulating this nonequilibrium is to assume that any slowly moving water is stagant and that the mass transfer between the mobile and immobile zones is described by a simple first order mass transfer process:

$$\frac{\partial C}{\partial t} = k_{La}(C_{im} - C_m) \quad (3\text{-}5)$$

where k_{La} is a first order mass transfer coefficient, C_m is the dissolved concentration in the mobile phase, and C_{im} is the dissolved concentration in the immobile phase. Equation 3-5 inherently assumes that no gradients exist in either the mobile or immobile zones. Equation 3-5 is perhaps the simplest approach for simulating physical nonequilibrium transport in porous medium. More complex approaches treat transport in the immobile zone as a diffusive process by explicitly simulating spatial gradients. Alternatively, the multirate mass transfer approach treats the more general case represented by equation 3-5, where multiple

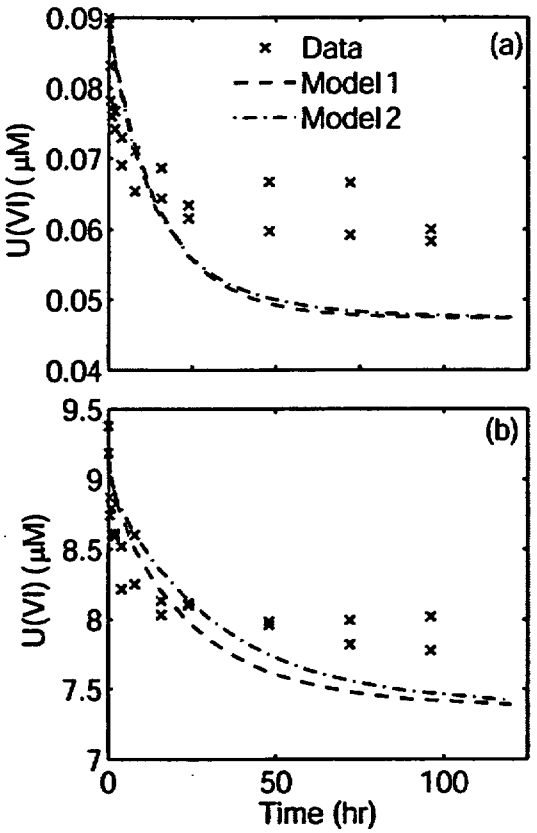

Figure 3.1. Kinetic data and model for U(VI) adsorption in laboratory batch experiments.

immobile zones exist and the mass transfer coefficient is represented by a distribution rather than a single value (Haggerty and Gorelick, 1995).

3.2.1.4 Instantaneous Injection

A hybrid approach for simulating a push-pull test is to assume that no adsorption reactions occur during the push or pull phases of the experiment. In this approach, it is assumed that all of the adsorption reactions and mass transfer processes are so slow that during the push and pull phases of the simulations the adsorption reactions can be ignored and U(VI), like all other species, is transported conservatively during the injection and withdrawal phases of the experiment. However, during the drift phase of the simulation, the adsorption reactions are assumed to be equilibrium controlled even if the duration of the drift phase is arbitrarily small but greater than zero. To implement this approach, three separate simulations are conducted for the push, drift and pull phases. In the push phase of the experiment, the simulation is conducted assuming that the concentration of adsorption sites is zero. This yields a spatial distribution of all dissolved solutes including U(VI) which is in effect linearly related to the concentration of a nonreactive tracer. With the exception of U(VI), these distributions are used as initial conditions for the total aqueous concentrations for the drift phase. For the case of U(VI), the simulated *dissolved* U(VI) concentration at the end of the injection phase is added adsorbed U(VI) computed from the NABS SCM and the background conditions in the aquifer to define the *total* (aqueous plus adsorbed) U(VI) concentration. Consequently, when the drift phase of the test is initiated, the simulation distributes the total U(VI) between the dissolved and adsorbed phases. During the drift phase of the experiment, U(VI) transport is controlled by local equilibrium processes. The simulated aqueous concentrations at the end of the drift phase are used as the initial conditions for a third simulation, which represents the pull phase of the tracer test. These last simulations are conduced with no adsorption reactions.

3.3 Model Scenarios

The behavior of U(VI) was simulated for each of the conceptual models described above for several geochemical scenarios. Two dimension simulations were conducted in a hypothetical aquifer that was 8m long and 4m wide as depicted in Figure 3.2. No flow boundaries were assumed along the long axis of the aquifer and constant head boundaries were assumed along the short axis of the aquifer. The heads at the constant head boundaries were computed from the average gradient of 0.001, which is typical of the Naturita aquifer near well NAT25, where the tracer tests described in Section 4 were conducted. Other values used in the simulations are listed in Table 3.2; each is representative of the tracer test site near well NAT25.

Most of the simulations were conducted by assuming that the aquifer could be approximated as a 2-dimensional areal aquifer with constant thickness. In general, the simulated aquifer was constructed to be representative of the general conditions near well NAT25. Most of the tests described in chapter 4 involved injecting 0.035 to 0.040 m^3 of groundwater into the test well; therefore the injected volume was assumed to equal 0.036 m^3 in all simulations. The thickness of the aquifer was assumed to equal only 0.3m even though the saturated thickness near well NAT25 is approximately 2m. This thin layer was assumed because the tracer tests described in Chapter 4 were conducted in wells with a 0.15 screen length. In addition, most of the tracer tests described in Section 5 showed distinct vertical gradients, suggesting that the vertical spreading was small and thus supporting the 2D approximation. Moreover, separate simulations that used a 3D approach for describing the push-pull test results, witha vertical hydraulic conductivity that was 10 percent of the horizontal hydraulic conductivity, showed only small differences when compared to the 2D simulations.

Figure 3.2 illustrates the most significant features of the simulated aquifer. The width of the aquifer was assumed to be 4m. This width was selected because it is approximately 10 times than the diameter of a cylinder that would enclose the 0.04m^3 injection for the assumed porosity of 0.3 and aquifer thickness of 0.3m. The length of the aquifer was twice the width (8m) and the injection well was located 2.6m from the upgradient boundary. No flow boundary conditions were assumed along the sides of the aquifer and constant head boundary conditions were assumed on the upgradient and downgradient boundaries.

One of the challenges in conducting the simulations described below was that during the push and pull phases of the simulated tests, the flow in the aquifer was predominantly radial but during the drift phase of the test, the flow was predominantly longitudinal. These two different flow regimes naturally suggest a radial grid and a Cartesian grid respectively but this was not feasible for a single simulation. For simplicity, a uniform Cartesian grid was used in all of the simulations. However, the timestep used in the simulations was varied to insure that the Courant number ($Cr=v\Delta t/\Delta x$) was equal to 0.8 for push, drift and pull phases of the simulation.

The base case properties used in simulations are listed in Table 3.2. The simulations, however, assumed that the aquifer was confined because this assumption made it easier to conduct the simulations because it avoided the tendency of the simulations to produce dry cells during the pull phase of cases involving low hydraulic conductivities.

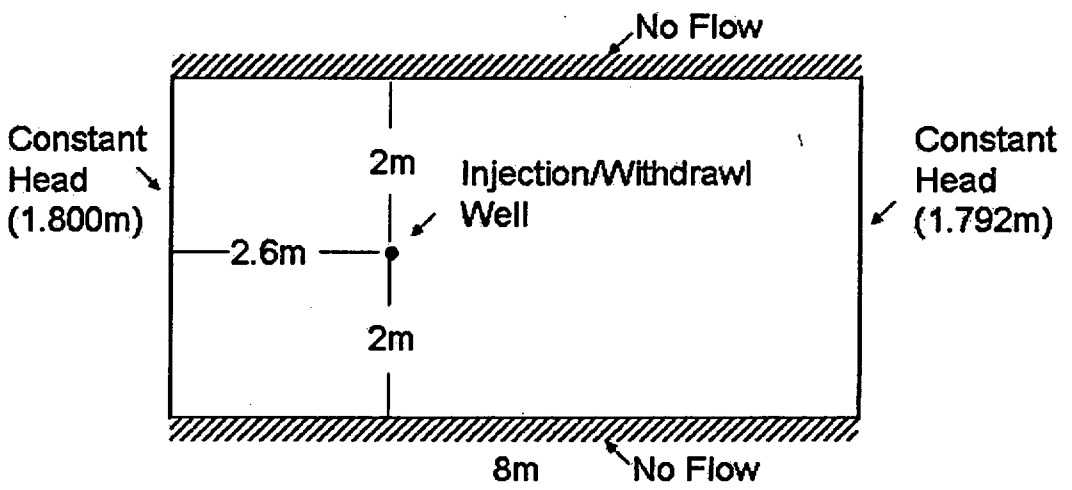

Figure 3.2. Model domain for hypothetical tracer test simulations.

Table 3-2. Properties of Hypothetical Aquifer

Property	Value
Hydraulic Conductivity	60 m/d
Thickness	0.3m
Porosity	0.3 (m^3/m^3)
Longitudinal Dispersivity	0.05m
Transverse Dispersivity	0.01m
Anisotropy Ratio	1.0
Δx	0.1m
Δy	0.1m

The initial conditions used in the modeling scenarios were typical of the groundwater at well NAT25 and are listed in Table 3.3. These example simulations considered three hypothetical geochemical scenarios defined primarily by the alkalinity and the U(VI) concentration of the injectate. The simulations also assumed that the aquifer was in equilibrium with respect to calcite and that the background ionic strength was determined by measured values of SO_4^{-2} and Cl^- together with the assumption that the Na^+ concentration was constrained by charge balance considerations. The aquifer sediments in the simulations were assumed to have a specific surface area of $4.2 m^2/g$ and the site density was assumed to equal 2.31 sites/nm^2. These values, together with an assumed porosity of 0.3 gave a total adsorption site concentration of 4.75×10^{-2} sites per liter of groundwater.

The model simulations used a uniform hydraulic conductivity and uniform distribution of adsorption sites in all cases. While there are abundant reports that demonstrate the heterogeneous nature of hydraulic conductivity, the simple homogeneous approach was selected for these hypothetical simulations because, as is demonstrated below, the simulated U(VI) transport in some cases is complex just because of geochemical considerations. If the simulations had included realistic estimates of hydraulic conductivity it would have been difficult to understand the extent to which the U(VI) simulations were controlled by complex geochemistry or complex hydrogeology.

3.4 Push-Pull Reactive Transport Modeling Results

Simulations were conducted for each of the four conceptual models for reactive transport described in Section 3.2 (e.g., the local equilibrium approach, the kinetically controlled approach, the first order mass transfer approach and the instantaneous injection approach). For each conceptual model, simulations were conducted for the cases where the injectate had either high or low alkalinity but otherwise nearly constant geochemical conditions or for the case where the injectate was typical of uncontaminated groundwater. Each simulation considered an injection volume of $0.036 m^3$ that was injected at a uniform rate of 0.06 m^3/hr, consistent with a total injection time of 0.6 hr. The plume resulting from the injection was allowed to migrate under the influence of a natural gradient for 15 hr and then the solution was extracted from the aquifer at a rate of 0.06 m^3/hr.

Table 3.3. Geochemical Composition of the Initial Groundwater Conditions And Injectate Used in the Hypothetical Simulations

Groundwater Description	U(VI) (μM)	Alkalinity (meq/L)	pH (-)	SO_4^{-2} (mM)	Cl^- (mM)	$Ca^{+2\dagger}$ (mM)	$Na^{+\neg}$ (mM)
Initial Conditions	4.0	7.5	7.1	9.0	3.4	0.4	20.6
High Alkalinity	4	22.5	7.1	9.0	3.4	1.3	18.8
Low Alkalinity	4	2.5	7.1	9.0	3.4	3.3	13.8
Uncontaminated	0.01	2.5	7.1	3.7	0.3	3.3	1.1

† Calculated from calcite equilibrium and selected alkalinity and pH

¬ Calculated from charge balance

3.4.1 Local Equilibrium Simulations

Figure 3.3 shows the simulated Br, alkalinity, $U(VI)_{AQU}$ and $U(VI)_{ADS}$ spatial distributions at five times corresponding to: (1) 0.6 hr, corresponding to the end of the injection, (2) 6 hr after the end of the injection, (3) 15.6 hr, corresponding to the end of the drift phase of the simulation, (4) 16.2 hr, corresponding to the time required to extract one injection volume (0.036 m^3) from the aquifer, and (5) 17.4 hr, corresponding to the time required to extract two injection volumes (0.072 m^3) from the aquifer. The Br plumes in Figure 3.3 illustrate that for the selected conditions, the idealistic ellipsoidal plume migrates downgradient so that at the end of the drift phase, the upstream boundary of the plume is located at the injection well. During the extraction (from 15.6 to 17.4 hr), the center of mass of the Br plume is roughly stationary and a significant amount of Br remains in the aquifer even though 2 injection volumes had been extracted during the pull phase of the test. This indicates that the water pumped from the well is a mixture of injectate and background water entering the injection well from upgradient locations. The simulated alkalinity behaves nearly identically to the simulated Br because there are no important reactive processes affecting transport of HCO_3^-, the major constituent of alkalinity for the simulation conditions. The simulated $U(VI)_{AQU}$ plume exhibits distinctly different simulation results when compared the either Br or alkalinity. At the end of the injection the concentration at the injection well is 4 μM, which equals both the initial concentration and the injected concentration. However, a halo of high dissolved concentration U(VI) develops around the injection well because the high alkalinity of the injectate leaches adsorbed U(VI) from the sediment surfaces. The time between 0.6 and 15.6 hr corresponds to the drift phase of the simulated push-pull test and during this time period the Br and alkalinity behave nearly identically. Both plumes migrate under the influence of the natural gradient such that at the end of the drift phase the upgradient extent of each plume coincides approximately with the location of the injection well. The nearly symmetric dissolved U(VI) plume present at the end of the injection transforms into an asymmetric plume with the highest concentrations located downgradient of the injection well at the end of the drift period. The geochemical changes at the injection well are more easily seen from a profile taken through the injection well along the mean direction of the groundwater flow. Figure 3.4a shows five alkalinity profiles at the same times shown in Figure 3.3; at the end of the injection, approximately midway through the drift phase, at the end of the drift phase, and at two times during the pull phase of the simulation. After 0.6 hr, the alkalinity has an approximately Gaussian shape that migrates downgradient during the drift phase that ends after 15.6 hr, such that the peak concentration is approximately 0.8 m downgradient of the injection well. During the pull phase of the simulation, the upgradient portion of the alkalinity plume is nearly completely extracted by 16.2 hr, but a significant portion of the alkalinity remains in the groundwater after one injection volume has been extracted. This remaining alkalinity in the aquifer implies that a significant portion of the water pumped during the first 0.6 hr of the pull phase was derived from background water.

The dissolved U(VI) concentrations shown in Figure 3.4b illustrate that the U(VI) concentration at the injection well at the end of the push phase (0.6 hr) nearly equals equals 4 μM, which is equivalent to the concentration in the injectate. Both upgradient and downgradient of the injection well the U(VI) concentration reaches peak concentrations of 9.4 μM because the high alkalinity of the injectate leaches adsorbed U(VI) from the sediment as shown in Figure 3.4c. During the drift phase of the simulation the U(VI) migrates downgradient, but the adsorption processes vary spatially and temporally as shown in Figure 3.4d. Dissolved U(VI) upgradient of the injection well readsorbs (Figure 3.4c) to the sediment surfaces because the alkalinity plume migrates downgradient nearly conservatively, whereas the U(VI) has a K_d value ranging between 0.3 to 0.8 mL/g (Figure 3.4d), corresponding to retardation factors ranging from 1.8 to 5.8. Conversely, downgradient of the injection well the excess

alkalinity causes further desorption (Figure 3.4c). Together, the readsorption of U(VI) upgradient of the injection well and desorption downgradient causes the asymmetric U(VI) plume shown in Figures 3.3 and 3.4.
The simulation results presented in Figure 3.5 show the alkalinity, uranium, and K_d profile for the case where the hydraulic conductivity was decreased by a factor of 10 relative to the simulations presented in Figure 3.4. In this scenario, each of the profiles is nearly symmetric at each of the simulation times illustrated because the groundwater velocity is only 0.02 m/d.

In a push-pull test, the most relevant experimentally observable values are the concentrations in the water pumped from the aquifer during the pull phases of the experiment. These concentrations, which are traditionally presented as concentrations versus volume extracted normalized to the volume injected, are illustrated in Figure 3.6 for the two cases where different hydraulic conductivity values of 6 and 60 m/d were used. The bromide concentrations in Figure 3.6a show that tailing was more significant in the case where the hydraulic conductivity equaled 60 m/d. This tailing is caused by the mixing of uncontaminated upgradient water with contaminated downgradient water in the model cell containing the well. The bromide in the low hydraulic conductivity simulation initially decreases rapidly, but nevertheless still has a tail of small concentrations that extends to more that 8 extraction volumes. The simulated alkalinity values in Figure 3.6b show behavior that is nearly identical to that for bromide because, as noted above, alkalinity is not significantly impacted by reactions.

The concentration histories for U(VI) at the extraction well show significant differences depending on the hydraulic conductivity. For the case where the hydraulic conductivity was only 6 m/d, the U(VI) concentration in the extracted groundwater was initially 5.1 μM, which slowly declined to 4 μM over the course of the 8 extraction volumes. In contrast, for the case where the hydraulic conductivity was 60 m/d, the U(VI) concentration was practically constant throughout the extraction phase of the simulation. This is particularly surprising given that the Figures 3.3 and 3.4 show that the peak simulated U(VI) concentrations were 2.2 times larger than the background concentrations. The nearly constant concentrations in this latter case are probably the result of multiple interacting processes, including U(VI) and alkalinity transport and speciation, along with the effects of advection and dispersion.

Figure 3.7 illustrates similar results for push-pull simulations simulated using the local equilibrium assumption and variable alkalinity values. The simulations for the low alkalinity case show that the U(VI) concentration was very nearly constant at the injection well even though the U(VI) in parts of the simulation were decreased by a factor of 2.2. The U(VI) in the simulation where the background water was used as the injectate show a gradual increase over the first 4 extraction volumes. However, almost all of this increase can be attributed to simple mixing between the injectate and the native groundwater, indicating that the effect of reactions on the U(VI) was small. Taken together, the simulations shown in Figures 3.6 and 3.7 suggest that the U(VI) concentration measured in the extracted groundwater may be relatively insensitive to several model variables including the injected alkalinity. This insensitivity could result from the inherent reversibility of the thermodynamic equilibrium, coupled with the reversible nature of the flow simulations; the primary irreversible process was dispersion, which was chosen to be relatively small in the selected simulations.

3.4.2 Nonequilibrium Simulations

As described above, the simplified analysis for a linearly sorbing solute suggested that the local equilibrium assumption may be a poor assumption for the push and pull phases of a push-pull test. Therefore, simulations were conducted using three additional conceptual models that include rate-limited sorption. Results using these approaches are described below.

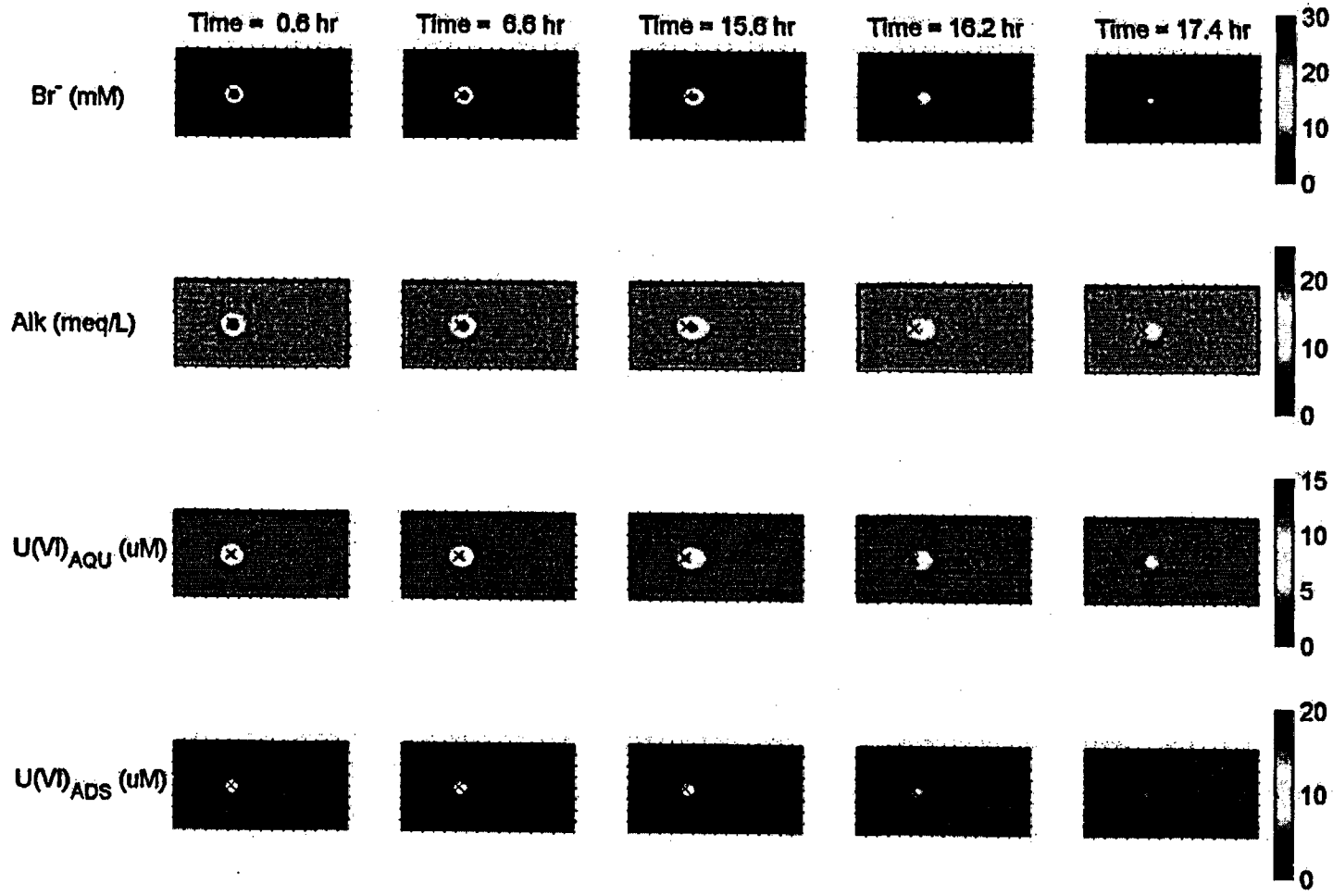

Figure 3.3. Temporal evolution of bromide, alkalinity, total dissolved U(VI) ($U(VI)_{AQU}$), and total adsorbed U(VI) ($U(VI)_{ADS}$)

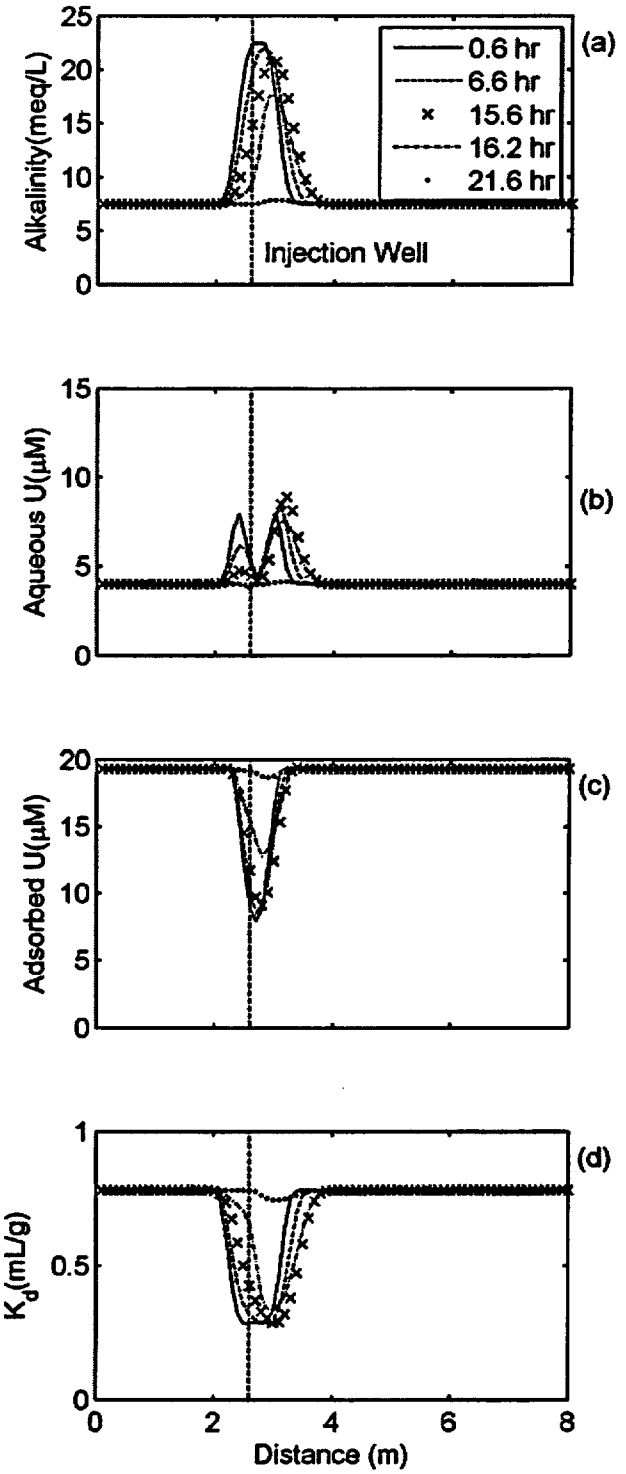

Figure 3.4. Simulated profiles of (a) alkalinity, (b) aqueous U(VI), (c) adsorbed U(VI) and (d) K_d values for a hydraulic conductivity of 60 m/d.

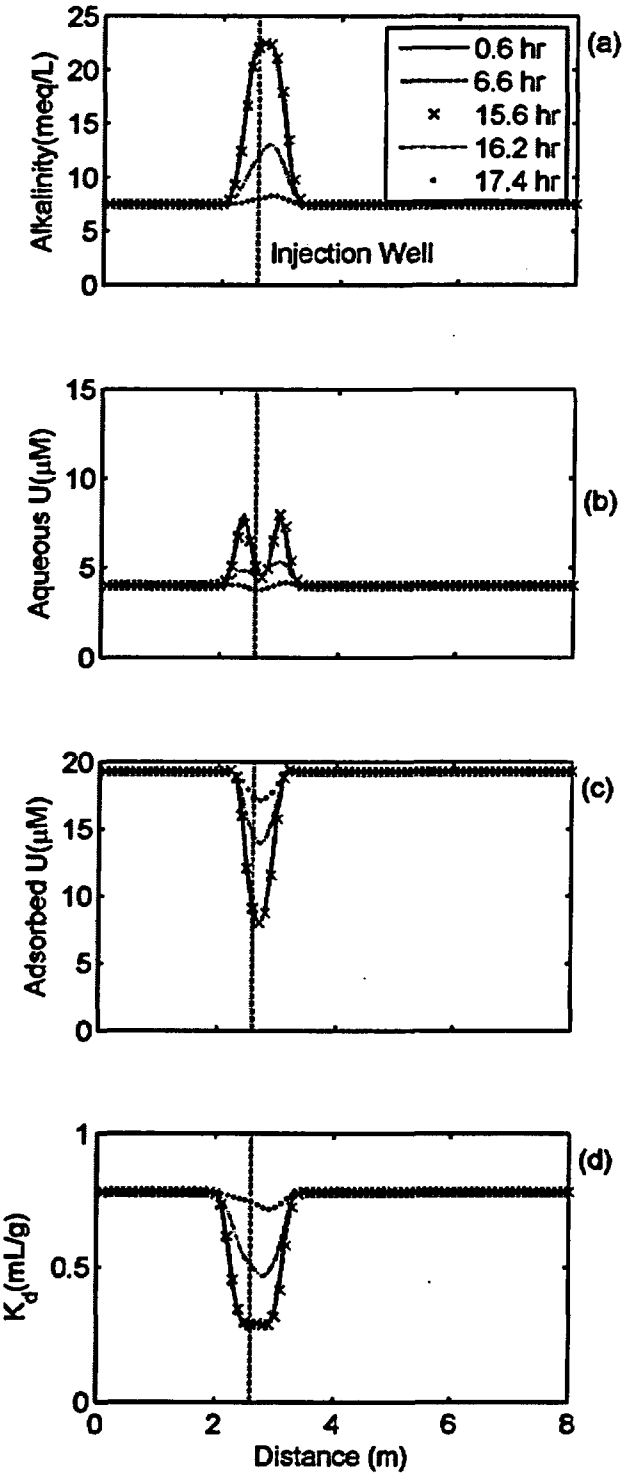

Figure 3.5. Simulated profiles of (a) alkalinity, (b) aqueous U(VI), (c) adsorbed U(VI) and (d) K_d values for a hydraulic conductivity of 6 m/d.

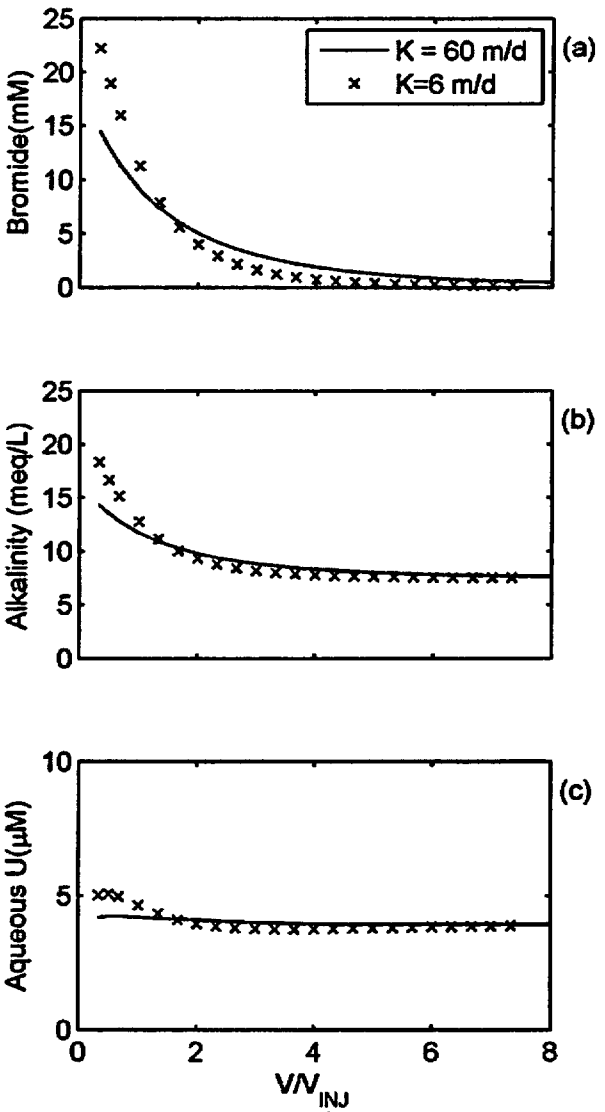

Figure 3.6. Simulated concentration histories for (a) bromide, (b) alkalinity, (c) aqueous U(VI) at the push-pull injection-extraction well.

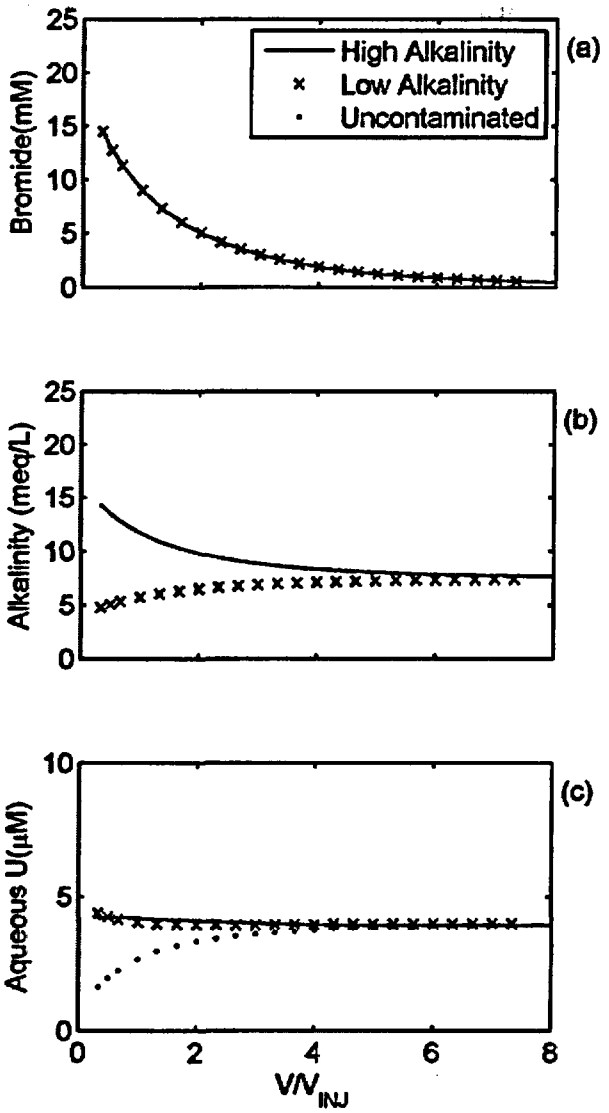

Figure 3.7. Simulated concentration histories for (a) bromide, (b) alkalinity, (c) aqueous U(VI) at the push-pull injection-extraction well for the high alkalinity, low alkalinity and uncontaminated injection scenarios.

3.4.2.1 Kinetically Controlled Adsorption

Simulations using the chemical kinetics approach to simulate adsorption previously showed that at the plume scale, there was no significant difference between the kinetic simulation and the local equilibrium simulation (Davis and Curtis, 2003). At smaller scales, however, kinetic limitations are more likely to be significant.

Figure 3.8 shows the simulation results obtained using kinetic model 1 (see Table 3-1) for Br, alkalinity, dissolved U(VI) and adsorbed U(VI) at five times corresponding the end of the push phase, during and at the end of the drift phase and during the pull phase of the simulation. The Br and alkalinity are nearly identical to Figure 3.3, but the U(VI) species show some differences. The halo of high U(V) at the end of the push phase (0.6hr) was less distinct for the kinetically controlled simulation as is the peak that forms at the

leading edge of the plume at the end of the drift phase (15.6 hr). This is shown in additional detail in Figure 3.9, which, when compared with the local equilibrium simulation in Figure 3.4, shows that each of the profiles in Figure 3.10 is generally more diffuse than the local equilibrium simulation. Such results are typical of kinetically controlled simulations.

The simulated concentration histories for the kinetic model are shown in Figure 3.10 for the case where the injectate had a high alkalinity of 22.5 meq/L and a U(VI) concentration of 4 μM. Simulations are illustrated for Model 1, Model 2, and also Model 1 with each of the rate constants decreased by a factor of 10. This adjustment to the rate constant was made for both the forward and backward rate constants so that the adsorption equilibrium would not change. The two kinetic simulations for Model 1 and Model 2 were generally quite close to the simulation results based on the local equilibrium assumption. In contrast, the kinetic simulation that used Model 1 with each rate constants reduced by a factor of 10 showed significantly different results. In this case, the dissolved U(VI) increased to 5 μM and then gradually decreased to background conditions. Apparently, this results because the U(V) desorption remains relatively fast, possibly because of the high alkalinity, but the rate of readsorption is kinetically slow.

3.4.2.2 First Order Mass Transfer Simulation Results

The simulation using the simple first order mass transfer model were conducted using mass transfer coefficients ranging from 10^{-1} and 10^{-5} hr^{-1}. Values of 10^{-1} gave simulation results that were nearly identical to those for the local equilibrium simulation. Concentration profiles obtained using a mass transfer constant equal to 10^{-2} hr^{-1} are shown in Figure 3.11. The results are quite similar to the simulation results obtained using the kinetic model. The concentration histories for these conditions are shown in Figure 3.12. The simulated U(VI) concentration is nearly independent of time; similar results were also observed for the mass transfer coefficient equal to 10^{-3} hr^{-1} as well as for values of 10^{-4} hr^{-1} or 10^{-5} hr^{-1}. In general, none of the simulations reproduced the typical observations described in Section 4, where significant increases in U(VI) concentration were observed in cases where the alkalinity of the injectate was increased.

3.4.2.3 Instantaneous Source

The instantaneous source approach is the third nonequilibrium approach used to simulate the push-pull test. In this approach, however, no kinetically controlled process is explicitly included in the simulation. Instead, the approach assumes complete disequilibrium during the push and pull phases of the simulation.

Figure 3.13 shows simulated profiles for the case of the injection of the high alkalinity water. The simulated alkalinity in Figure 3.13 is essentially identical to that simulated for the local equilibrium case. The simulated U(VI) concentration, however, is significantly different for the these two cases. For the instantaneous source method, the U(VI) concentration is nearly linearly related to the alkalinity after 0.6hr because no adsorption is allowed during the injection. Consequently, the halo of high U(VI) concentration that forms in the local equilibrium case did not form when adsorption was not included. During the drift phase of the simulation, the aqueous U(VI) increased and adsorbed U(VI) decreased because adsorption reactions were allowed to equilibrate. Relative to the local equilibrium case, there are higher U(VI) concentrations near the injection well for the instantaneous source.

The higher concentrations near the injection well yield initially higher concentrations during the pull phase of the simulation as show in Figure 3.14. Specifically, the simulated U(VI) at the extraction well starts at 8 μM and then decreases to background

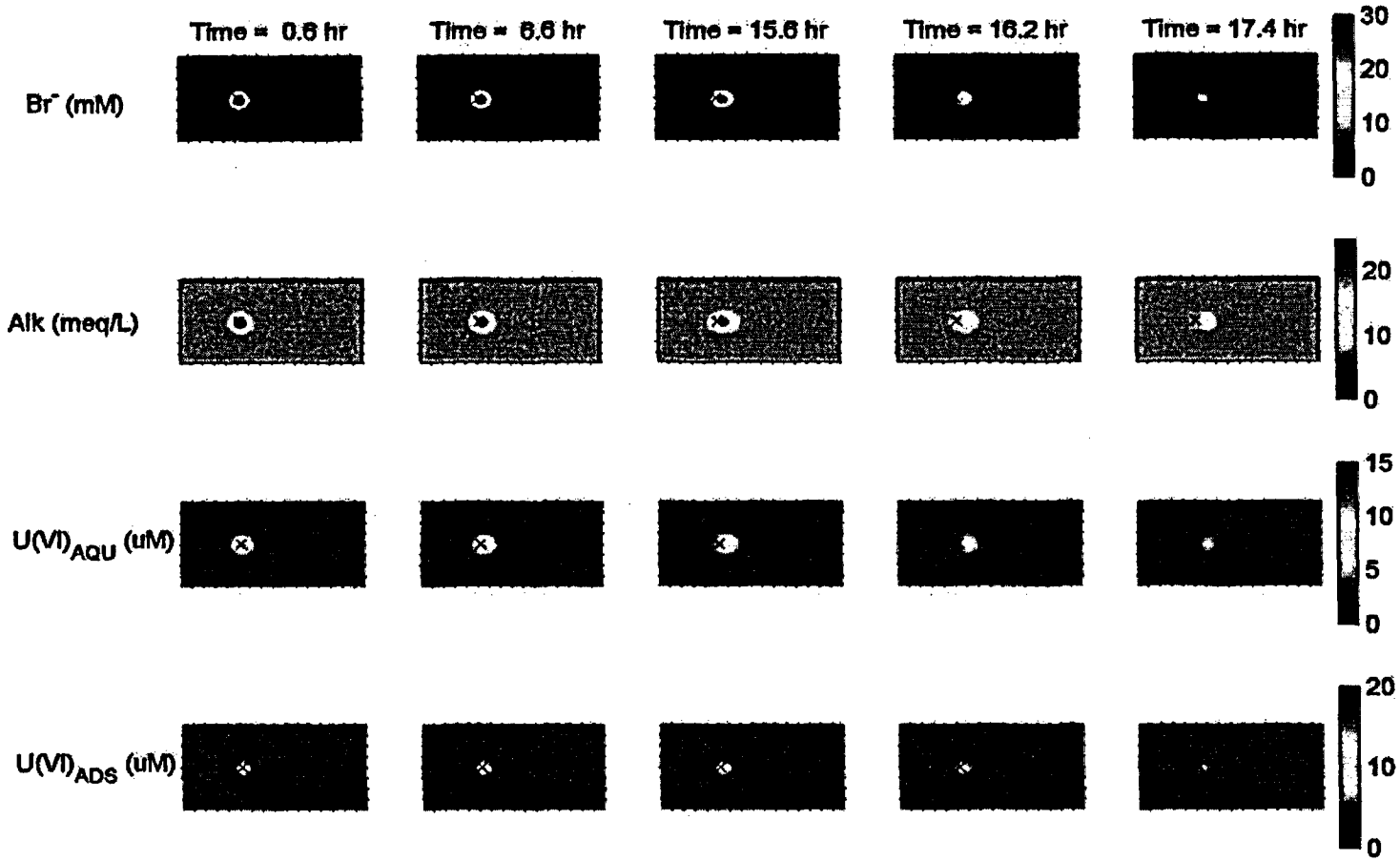

Figure 3.8. Temporal evolution of bromide, alkalinity, total dissolved U(VI), [shown as $U(VI)_{AQU}$], and total adsorbed U(VI) [shown as $(U(VI)_{ADS}$] for kinetically controlled simulations using Model 1.

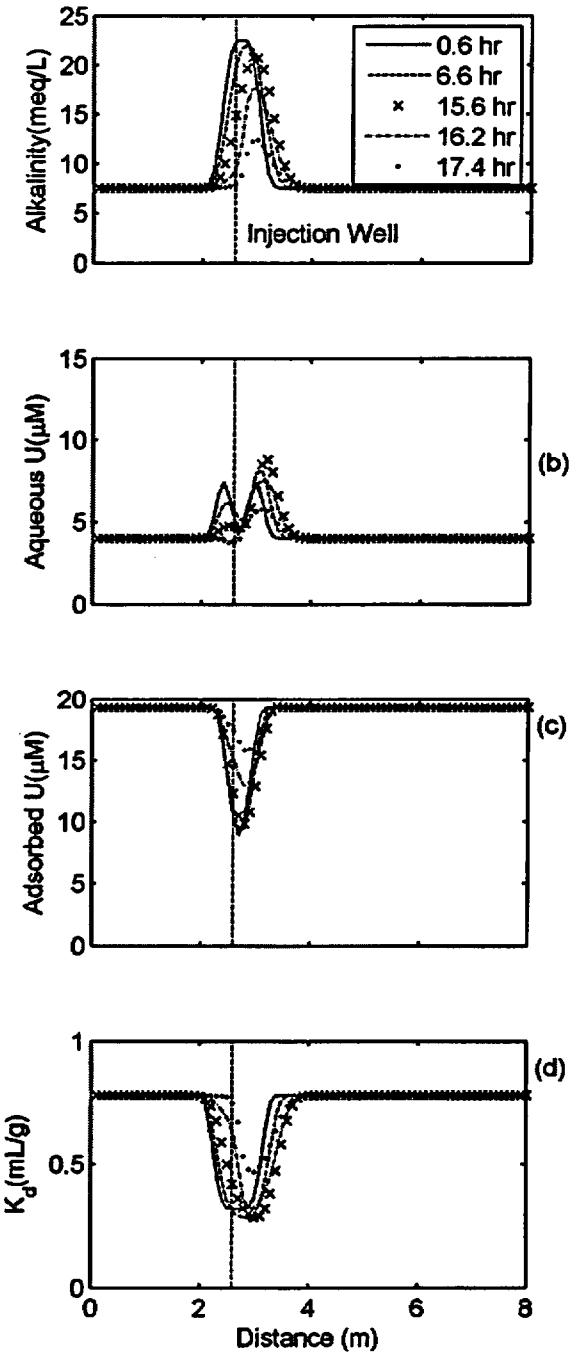

Figure 3.9. Simulated profiles of (a) alkalinity, (b) aqueous U(VI), (c) adsorbed U(VI) and (d) K_d values for kinetically controlled adsorption and Model 1.

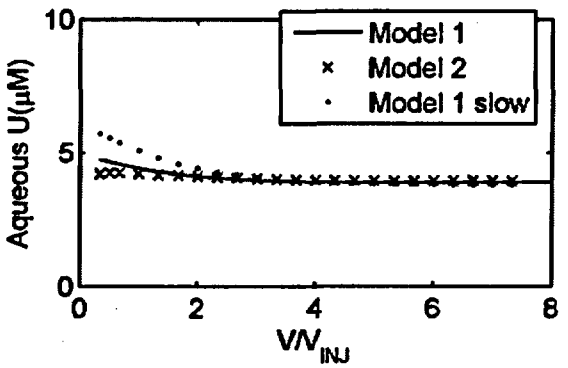

Figure 3.10. Simulated concentration histories for aqueous U(VI) at the push-pull injection-extraction well the kinetically controlled simulations using model 1, model 2 and model 1 with decreased forward and backward rate constants.

concentrations after approximately 5 injection volumes. This simulated behavior is quite similar to that simulated for the slow kinetics case in Figure 3.10. Figure 3.14 also shows the simulated concentration histories for the case when the injection water had low alkalinity or low alkalinity plus low U(VI) concentration. In both cases, the U(VI) concentrations were approximately 1μM, and this concentration gradually increased to background concentrations after approximately 5 injection volumes.

3.5 Conclusions

Each of the local equilibrium simulations showed that calculated U(VI) concentrations at the extraction well were relatively constant. This result was obtained even though the simulations showed that there were significant geochemical changes in the aquifer. The relatively small changes simulated for the equilibrium case show that push-pull tests are probably not effective experiments for evaluating semi-mechanistic surface complexation model parameters. However, push-pull tests may be very useful for studying rates of sorption and desorption in aquifers.

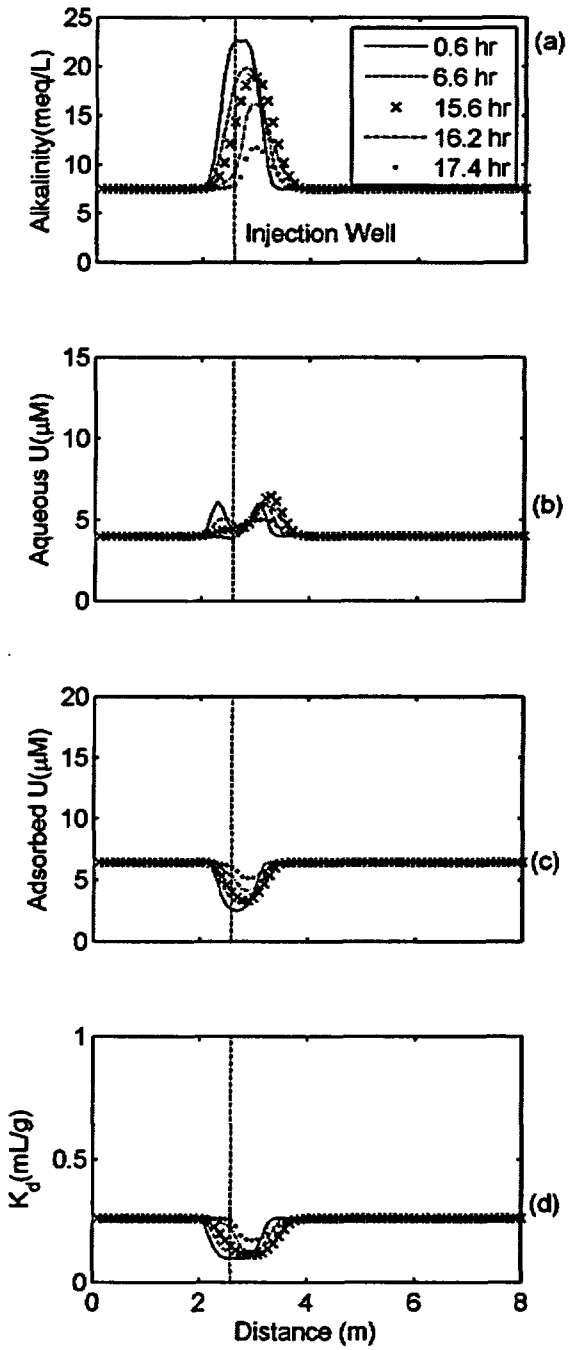

Figure 3.11. Simulated profiles of (a) alkalinity, (b) aqueous U(VI), (c) adsorbed U(VI) and (d) K_d values for the first order mass transfer model.

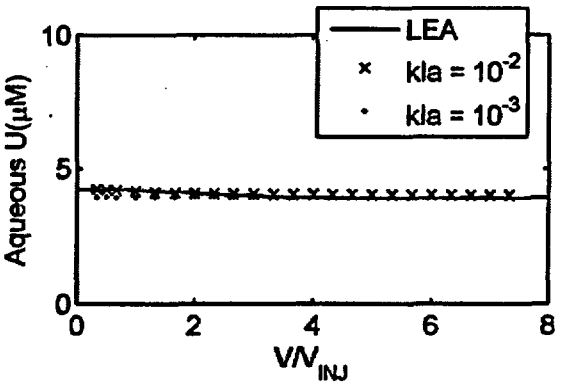

Figure 3.12. Simulated concentration histories for aqueous U(VI) at the push-pull injection-extraction well for mass transfer coefficients equal to 10^{-3} and 10^{-2} hr.

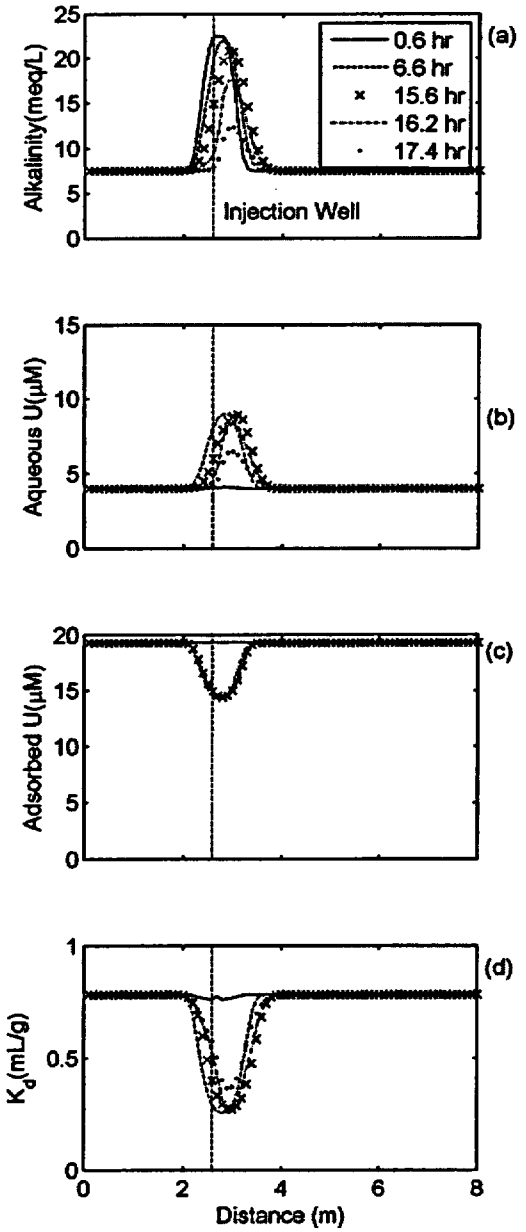

Figure 3.13. Simulated profiles of (a) alkalinity, (b) aqueous U(VI), (c) adsorbed U(VI) and (d) K_d values for the disequilibrium-equilibrium case.

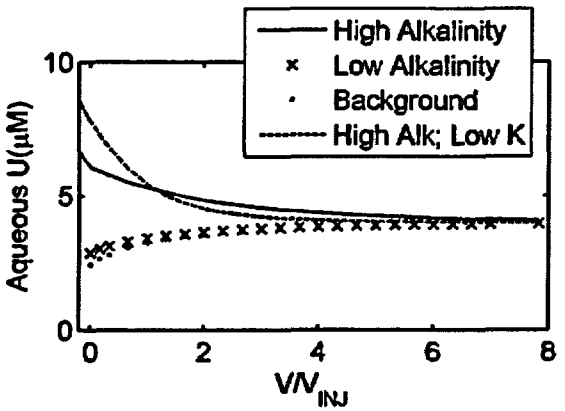

Figure 3.14. Simulated concentration histories for aqueous U(VI) at the push-pull injection-extraction well for injection waters having high alkalinity, low alkalinity, uncontaminated water with a hydraulic conductivity of 60 m/d and high alkalinity injection with a hydraulic conductivity of 6 m/d.

4 OBSERVATIONS AND MODELING OF U(VI) TRANSPORT IN PUSH-PULL TRACER TESTS

4.1 Introduction

Simulations of reactive transport processes in groundwater often require many parameters as model inputs. These parameters include hydrologic parameters that describe flow and transport as well as reaction parameters that describe the chemical reaction network. While hydrologic parameters are often determined from field tests such as pump tests, slug tests, or tracer tests coupled with model calibration, there is less agreement on how chemical reaction parameters should be determined. For chemical reaction processes, parameter values could be based on a variety of sources including tabulated thermodynamic data, laboratory experiments using site-specific materials, or field-determined values.

The appropriate method used to obtain reaction parameters may depend on the type of the chemical reaction being modeled. For example, tabulated equilibrium constants may be adequate for simulating aqueous complexation reactions and some solubility constraints (Grenthe et al., 1992, Allison et al., 1991, Smith and Martell, 1976). For adsorption reactions, laboratory experiments using site-specific materials have been used to develop surface complexation models (SCM) that describe the reaction stoichiometry and apparent stability constants (Davis et al., 2004b; Stollenwerk, 1998; Davis et al., 1998; Davis and Curtis, 2003). Although the SCM approach has been applied in the laboratory, these models have generally not been independently tested in the field. This study compares hexavalent uranium (U(VI)) adsorption calculated from an SCM developed from laboratory batch experiments (Davis et al., 2004b) with adsorption measured under *in situ* conditions at a field site.

In oxic environments, the most stable valence of uranium is U(VI), which forms moderately soluble solid phases (Guillaumont et al., 2003). Thus, at concentrations less than approximately 20 μM, the mobility of U(VI) can be controlled by adsorption reactions at circumneutral pH values (Davis and Curtis, 2003). Adsorption of U(VI) to minerals surfaces in oxic waters is sensitive to pH and carbonate activity and therefore to the partial pressure of CO_2 (P_{CO2}). This sensitivity arises primarily because of changes in aqueous speciation, and perhaps surface speciation. Adsorption is generally small at low pH values where the dominant species is the UO_2^{2+} cation. Adsorption increases with increasing pH usually in the pH range of 4 to 6 and U(VI) hydrolysis species in solution become increasingly dominant (Davis et al., 2002; Hsi and Langmuir, 1985; Waite et al., 1994; Pabalan et al., 1998). In the alkaline region, U(VI) is strongly adsorbed in the absence of dissolved CO_2 (Hsi and Langmuir, 1985; Prikryl et al., 2001), but in the presence of dissolved CO_2, the formation of aqueous U(VI)-carbonato and Ca-U(VI)-carbonato complexes can cause adsorption to be negligible (Davis et al., 2004b; Hsi and Langmuir, 1985; Waite et al., 1994).

A semi-mechanistic SCM for U(VI), developed for the Naturita aquifer background sediments (NABS, Davis et al., 2004b), was found to predict U(VI) adsorption within a factor of approximately 3 by contaminated sediments at the site (Kohler et al, 2004) and by NABS samples that were contacted *in situ* with contaminated groundwater (Curtis et al., 2004). The SCM was also successfully used in plume scale simulations that were fit to historical U(VI) observation at the Naturita mill site (Curtis et al., 2006). However, because these simulations were calibrated to the observed data, the simulations were not a rigorous evaluation of the performance of the SCM under conditions of transient reactive transport.

The objective of the research presented in this section was to evaluate the semi-mechanistic SCM approach in push-pull tests. Push-pull tracer experiments were conducted at the NAT25 experimental test field. The tests

considered both variable alkalinity and U(VI) concentration, as these variables were found to be most significant in controlling U(VI) transport at the Naturita site (Curtis et al., 2006). These data are compared with reactive transport simulations using the semi-mechanistic SCM developed for the Naturita aquifer background solids.

4.2 Methods and Materials

4.2.1 Site Description

Infrastructure for small-scale tracer tests was developed at the Naturita site at a location that was downgradient of the highest U(VI) concentrations and in a relatively uniform sandy portion of the alluvial aquifer near well, NAT25 (Figure 4.1). The groundwater at this location had an average alkalinity of 8.5 meq/L, an average U(VI) concentration of 4 μM (950 ppb), and the pH was approximately 7.1. The groundwater near well NAT25 is nearly saturated with respect of calcite (-0.3<SI<0.4).

Eleven wells were installed downgradient of NAT25 and these wells were constructed using a variety of methods that changed over time. Wells 25B, 25C, 25F and 25G were installed as stainless steel drive points with a 15 cm screened interval that was connected to a 1.25 cm polyethylene tube with a hose barb. All of the materials installed below the water table were constructed from either stainless steel or polyethylene. Wells 25A, 25D and 25E were multilevel wells constructed from 0.75 cm polypropylene tubing housed in a 2.5 cm PVC well casing. The end of the tubing protruded from the well casing and was covered with a stainless steel screen. Wells 25K, 25L 25M, 25N, 25O, and 25P were multilevel 1.25 cm PVC wells with a 15 cm slotted interval. These wells had custom fabricated permanent packers that isolated the two separate screened intervals, which were separated vertically by 30cm.

4.2.2 Tracer Test Descriptions

The push-pull tests were conducted by pumping groundwater from the alluvial aquifer at the Naturita site into 10 gallon containers, adding bromide (as KBr or NaBr) as a conservative tracer and then, in some instances, either increasing or decreasing the alkalinity of the pumped groundwater prior to siphoning the groundwater sample back into the aquifer. Varying geochemical conditions were used in the tracer tests, especially the alkalinity or U(VI) concentration, and the conditions for the tests are summarized in Table 4.1. The alkalinity in the tests varied by approximately a factor of 8, while the U(VI) concentration varied by a factor of 100. The first two push-pull tests (PPT) were conducted in September 2001. PPT3 through PPT7 were conducted in July and August 2005, and the remaining tests were conducted in October and November 2005.

Several tests used water that had a low U(VI) concentration. In these experiments, water from well DOE547, which is upgradient of the former ore mill, was collected and transported to the NAT25 field test site. Other experiments used water that was pumped from the same vertical level of the well in which the push-pull test was conducted.

In some experiments, the alkalinity of the injectate was decreased by adding concentrated HCl while purging the containers with N_2 gas. The N_2 gas was used to remove CO_2 from solution in order to increase pH without further changing the alkalinity. The HCl was added slowly while the containers were continuously purged with N_2, such that the pH of the groundwater did not drop below 6. After the alkalinity was decreased to approximately 3.9 meq/L, the pH was adjusted to the final value of 7.1 by N_2 purging.

The alkalinity of the injectate was increased in some experiments by adding $NaHCO_3$ and Na_2CO_3. The pH of the containers was first decreased to approximately 6.0 by purging with 10% CO_2 in N_2. The $NaHCO_3/Na_2CO_3$ was then added slowly so that the pH remained below 7.3. Once the desired amount of $NaHCO_3/Na_2CO_3$ was added, the pH was decreased to the ambient pH by purging the containers with the N_2/CO_2 gas mixture. This method was used to reduce the

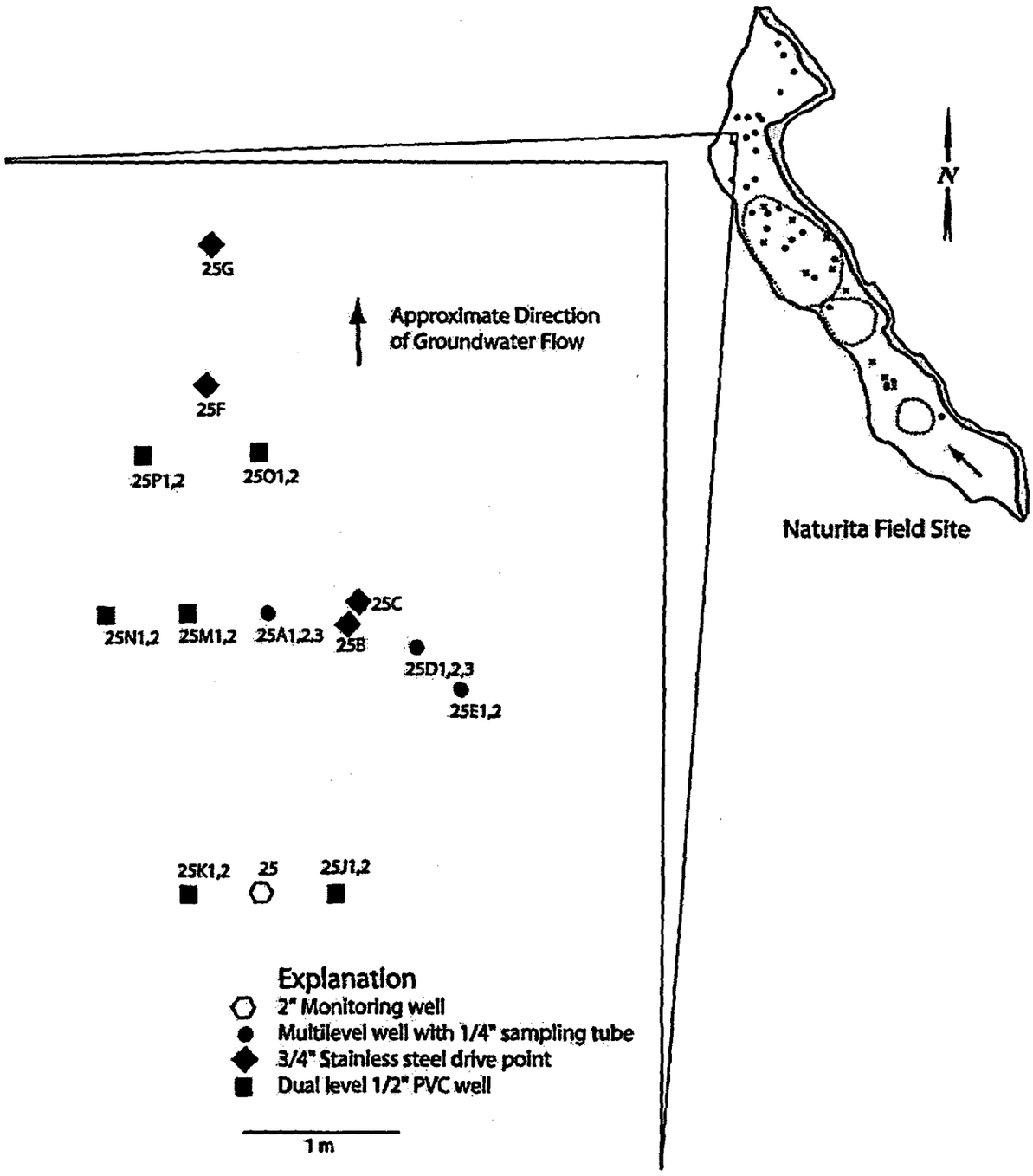

Figure 4.1. Map of the small-scale tracer test site developed near well NAT25. The numbers after the well designations indicate the different sampling levels, with 1 being the deepest screened interval.

Table 4.1. Composition of Injectate Solutions and Groundwater in Push-Pull Tests

			Injection Water			Test Site water		
	Injected Volume (L)	Drift (hr)	pH	U(VI) (μM)	Alkalinity (meq/L)	pH	U(VI) (μM)	Alkalinity (meq/L)
PPT1	36.7	14.7	7.04	0.03	3.85	7.17	3.50	8.43
PPT2	35.6	15.6	7.18	0.03	7.62	7.26	3.69	8.42
PPT3	38.0	0.5	7.08	0.08	10.95	7.05	3.52	8.35
PPT4	36.5	12.8	7.11	3.32	15.17	7.12	3.36	7.69
PPT5	35.1	13.7	7.09	0.08	9.34	7.09	3.43	7.71
PPT6	44.3	13.6	7.10	3.40	3.88	7.07	3.47	7.99
PPT7	34.8	13.4	7.17	0.08	3.20	7.13	3.47	7.84
PPT8	36.6	15.4	7.11	4.65	6.04	7.07	4.57	8.40
PPT9	35.3	0.4	7.05	4.58	24.00	7.07	4.57	8.30
PPT10	30.3	2.1	7.03	4.81	8.30	7.03	4.74	8.30
PPT11	30.0	2.5	7.14	4.76	8.30	7.08	4.94	8.30
PPT12	37.4	15.4	7.11	4.62	21.80	7.05	4.92	7.93

chances of co-precipitating U(VI) in carbonate phases, which might have been significant if $NaHCO_3/Na_2CO_3$ was added rapidly to the containers. Finally, an experiment was conducted with a reduced Ca concentration. For test PPT12, Ca was precipitated by adding 28.7 grams of Na_2CO_3 to approximately 53 liters of groundwater. The precipitated calcite was allowed to settle overnight and then the supernatant was filtered with a high capacity 0.45 μm filter and placed in a second container. The alkalinity of the filtrate was increased by adding 31.9 grams of $NaHCO_3$ and the pH (8.1 after filtration) was adjusted to 7.1 by bubbling CO_2 gas into the water as described above.

4.2.3 Groundwater Sampling and Analysis

Groundwater was collected using a peristaltic pump and filtered with a 0.45 μm Millex HV filter (Millipore). Samples were diluted as necessary and analyzed for dissolved U(VI) (by kinetic phosphorescence analysis) and for selected other elements by ICP-AES. Water samples collected for alkalinity were titrated with sulfuric acid using the Gran titration method. Bromide samples were analyzed using a Lachat flow-injection analyzer. The surface area was measured on triplicate samples using the BET-N_2 gas adsorption method with a Micrometrics Flowsorb 2000 instrument.

4.3 Results

4.3.1 Observed Concentration Histories

Figure 4.2 shows the results for PPT1, which was conducted by injecting 36.7 liters of background water that had a low alkalinity and low U(VI) concentration into well 25F, after 21.1 g of KBr was added to the water. After a drift phase that lasted 14.7 hr, the groundwater was pumped from the injection well with a peristaltic pump at a constant rate of 49.9 L/hr. The first Br sample had a concentration that was only 62 percent of the injected concentration. Thereafter, the Br concentrations decreased slowly as a result of mixing in the aquifer. Even though only 36.7 liters of water were injected into the aquifer, Br concentration was still significant after 160 L had been pumped from the injection well. At the end of the experiment, 88.5 percent of the injected Br had been extracted from the sampling well. The alkalinity of the first sample taken was 5.7 meq/L, which was between the alkalinity of the injectate (3.85 meq/L) and that of the initial groundwater (8.43 meq/L). If the sample alkalinity was a result of simple linear mixing of the injectate and groundwater, the expected alkalinity value would be 6.6 meq/L, which is relatively close to the observed value of 5.7 meq/L. The U(VI) concentration of the groundwater slowly increased from approximately 2.2 to 3.6 μM,

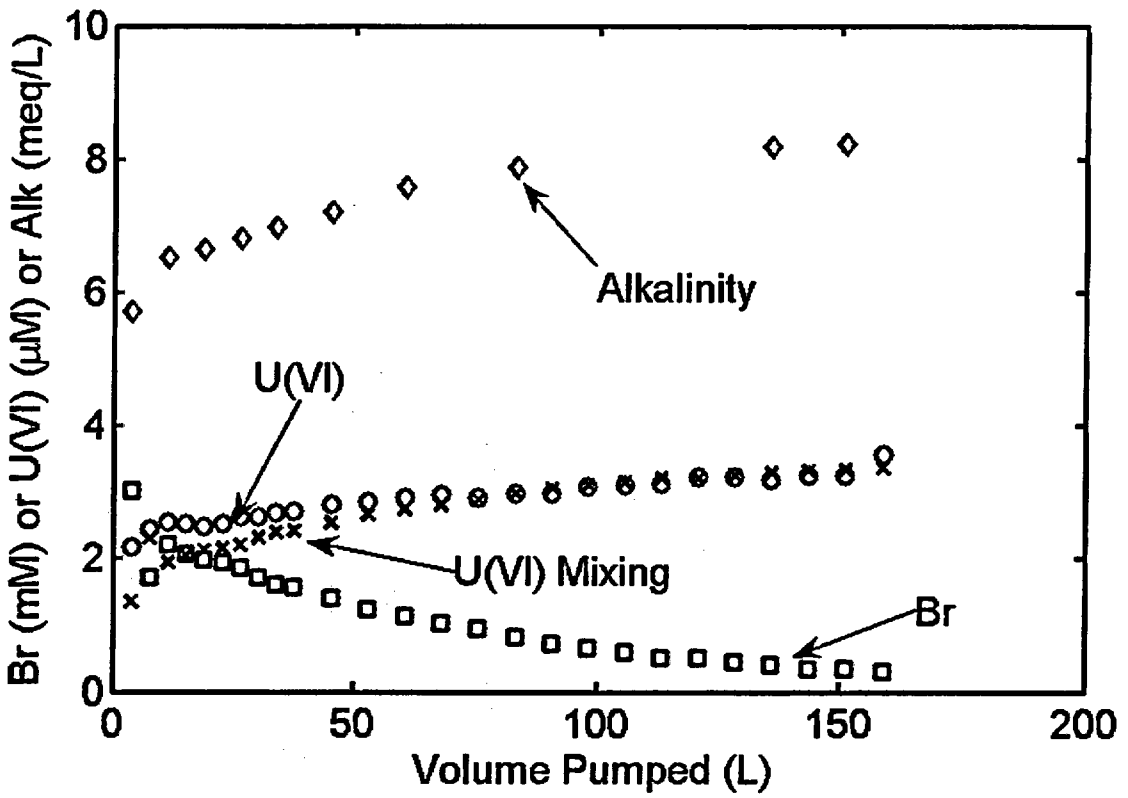

Figure 4.2. Concentration histories observed in push-pull tracer test 1 (PPT1).

and this generally followed a trend that was opposite that of the Br tracer. Figure 4.2 also shows the results expected for U(VI) concentration computed from a simple mixing calculation using the Br concentration observations. The observed U(VI) concentrations were larger than the concentration calculated from mixing in the first 70 liters of water pumped from the well, suggesting that there was a small amount of U(VI) desorption that contributed to the observed values.

The extent of U(VI) desorption into uncontaminated groundwater was further investigated in four additional experiments that had different drift times and different alkalinity values in the injectate. Figure 4.3a illustrates the results for PPT3, which had a drift period of only 0.5 hr. In this experiment, the Br concentration remained at a constant value of 4.6 mM for the first 30 L of groundwater extraction, which was equal to the injected Br concentration, suggesting that there was negligible mixing between the injectate and the groundwater. The U(VI) concentration in the first sample taken 0.5 hr after the injection was approximately 2.2 μM, which must be attributed to U(VI) desorption given the negligible mixing indicated by the Br observations (see dashed line). The U(VI) concentration gradually increased in the groundwater after 25 L of pumpage, and this increase can be attributed to mixing between native groundwater and the groundwater that had 2.2 μM resulting from U(VI) desorption during the first 0.5 hr.

Figures 4.3b and 4.3c illustrate the results for U(VI) desorption into uncontaminated groundwater that had alkalinity values of 7.62 and 9.34 meq/L, respectively. The U(VI) concentrations versus volume pumped in Figure 4.3b was similar to that in Figure 4.3a. Since PPT2 and PPT3 had drift times of 15.6 hr and 0.5 hr, respectively, the results suggest that U(VI) desorption did not continue significantly

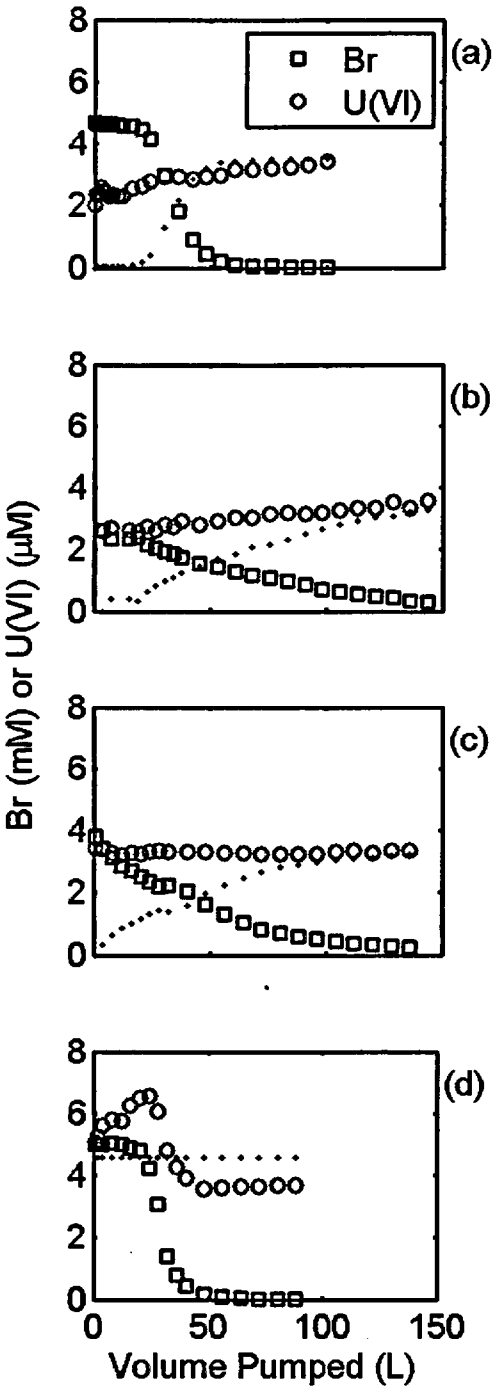

Figure 4.3. Concentrations of U(VI) and Br tracer in push-pull tracer tests conducted with uncontaminated groundwater for various drift periods and injected alkalinities: (a) PPT3, (b) PPT2, (c) PPT5, and (d) PPT9. The dashed line represents U(VI) concentrations expected from the mixing of injected and native groundwater, based on the concentrations of Br tracer.

with increasing drift time. In PPT5, which had a slightly elevated alkalinity in the injectate, the U(VI) concentration was nearly constant for the duration of the experiment (Fig. 4.3c).

Figure 4.3d illustrates the desorption of U(VI) in an experiment that had a drift time of only 0.4 hr, with an increased alkalinity of 24 meq/L. Unlike the previous test results shown in Figure 4-3, the injectate had a U(VI) concentration of 4.6 μM, which equaled that of the ambient groundwater. The U(VI) concentration of the groundwater that was pumped from the injection well (after a drift time of 0.4 hr) increased as the first 35 L of water was pumped from the well. After 35 L were pumped, the Br and U(VI) concentrations decreased sharply, as nearly all of the injectate was recovered. The Br decreased to background concentrations, whereas the U(VI) decreased to approximately 90 percent of the initial and background U(VI) concentrations of 4.6 μM. The U(VI) concentration remained nearly constant at this slightly depressed concentration for the duration of the experiment. As discussed in detail in Section 5, this decrease in U(VI) concentration is probably caused by U(VI) adsorption that occurs as native groundwater encounters sediments that had been leached with the high alkalinity injected water.

The effect of alkalinity was examined further in experiments with contaminated groundwater that was treated to either increase the alkalinity to 15.2 meq/L or decrease the alkalinity to 6.0 meq/L (Fig. 4.4). When the alkalinity was increased by a factor of two in the injectate, the U(VI) concentration in the first sample pumped from the well had also increased by a factor of 2 (compared to the injectate concentration). After the first sample, the alkalinity and Br and U(VI) concentrations gradually decreased to the initial values in the aquifer.

When the alkalinity was decreased by 50%, the U(VI) concentration increased slightly in the first 10 liters pumped from the well, after which the concentration was nearly constant. The increase in U(VI) concentration was also observed in a duplicate experiment (results not shown). The reasons for the observed increase in U(VI) concentrations in these tests are not

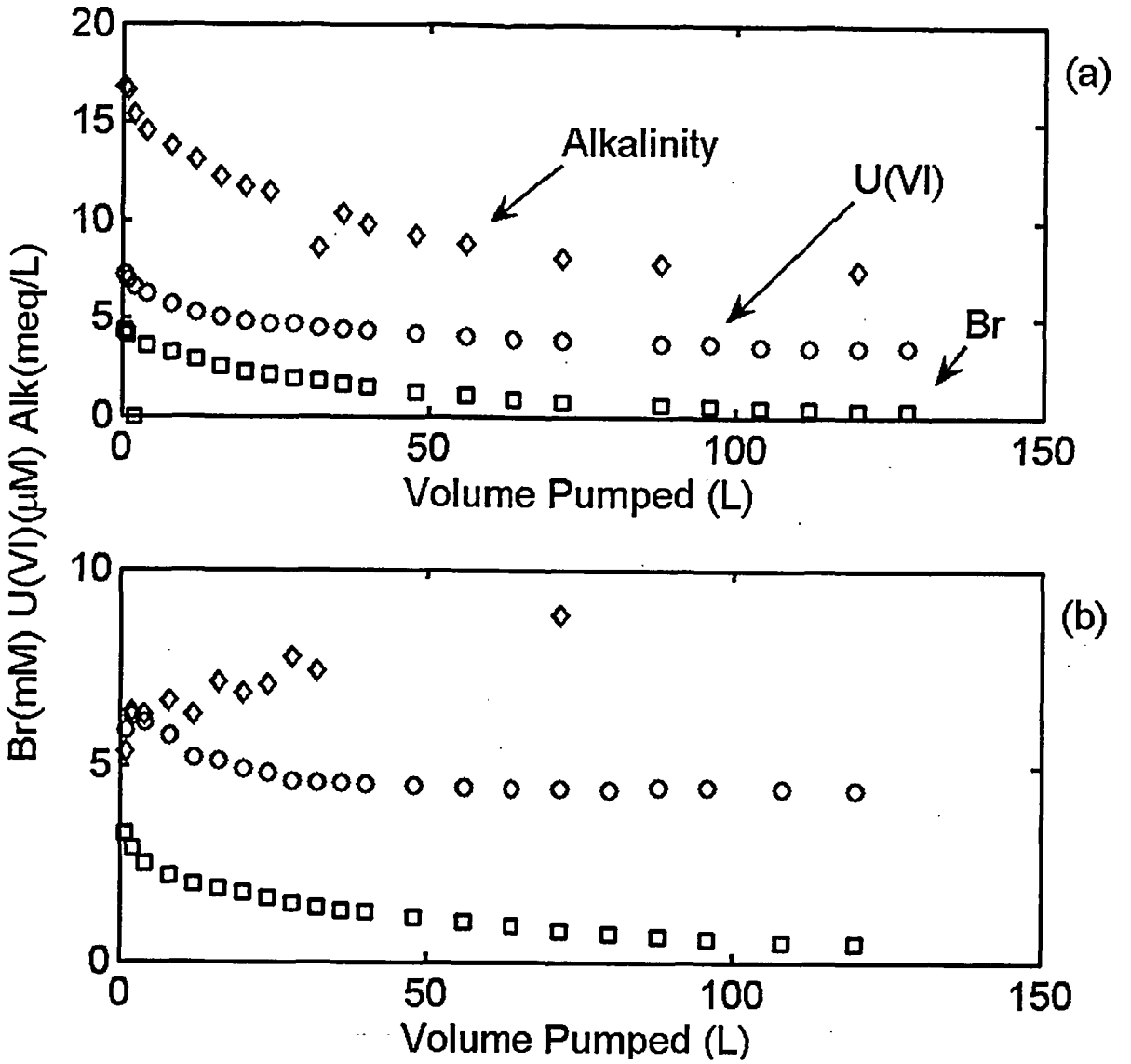

Figure 4.4. Concentration histories for U(VI), Br tracer, and alkalinities in PPT4 and PPT8. Results show U(VI) desorption into contaminated groundwater that was treated to (a) increase the alkalinity or (b) decrease the alkalinity.

known. The decrease in alkalinity was expected to cause some U(VI) present in the injectate to be adsorbed in a region close to the well, leading to a decrease in local U(VI) concentrations.

Figure 4.5 shows the U(VI) and Ca concentrations observed in two experiments that compared the effects of adding Br as either NaBr or KBr. The U(VI) concentration and alkalinity values were identical in the injectate and the groundwater in both experiments. For the KBr experiment, the U(VI) concentration increased 4.3 to 5.5 μM and, at the same time, the Ca concentration increased slightly from 4.3 to 4.8 mM. In contrast, the U(VI) and the Ca concentrations were essentially constant in the case with NaBr added to the injectate. These results suggest that the addition of K causes ion exchange with Ca on clay surfaces, and that the liberated Ca increases the formation of dissolved Ca-U(VI)-CO_3 complexes. The Na has only a small effect on Ca concentration, probably

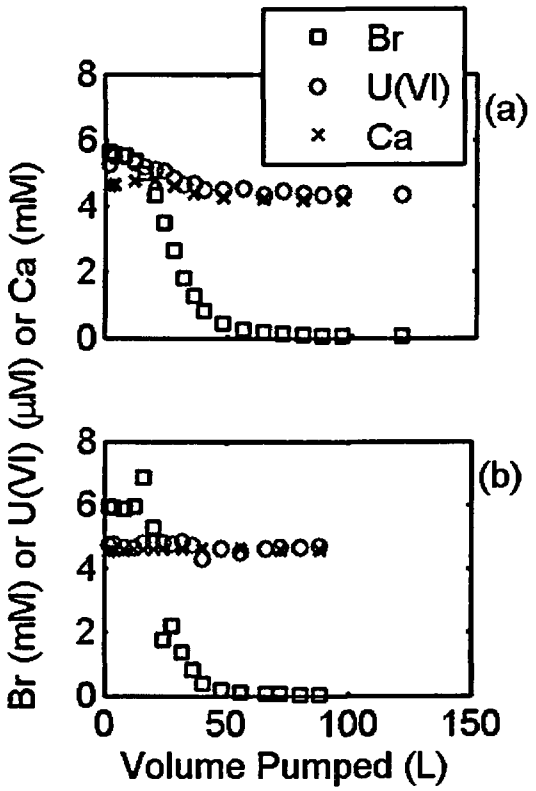

Figure 4.5. Changes in U(VI) concentration resulting from the addition of Br as either (a) KBr or (b) NaBr.

because the background Na concentration is not changed significantly by the injection (approximately 20 mM in native groundwater and 24 mM in the injectate). In contrast, the K concentration is 0.3 mM in the native groundwater and 4.3 mM in the injectate.

The effect of Ca on U(VI) partitioning in the groundwater was further investigated in PPT12, in which dissolved Ca was removed from the injectate by precipitating calcite (as described in methods). The results show that the U(VI) concentration initially was 90 percent of the ambient value, even though the alkalinity had been increased to 22 meq/L (Fig. 4.6). For comparison, the U(VI) concentration in PPT4 increased by a factor of 2.1 when the alkalinity was increased to only 15.2 meq/L. Thus, U(VI) adsorption is apparently affected by both the dissolved Ca concentration and alkalinity in these experiments. Fox et al. (2006) found that dissolved Ca concentrations impact U(VI) adsorption on quartz by changing aqueous U(VI) speciation.

4.3.2 Nonreactive Transport Calibration

The Br concentrations observed in the push-pull tests were fit to a two-dimensional nonreactive flow and transport model. The model domain and discretization were described in Section 3. The purpose of the calibration was to account for the observed behavior of Br tracer, so that the reactive transport of U(VI) could be predicted using the semi-mechanistic SCM (Table 3.1, Model 1). The observed Br concentrations were calibrated by varying the hydraulic conductivity and the longitudinal dispersivity within the aquifer. Mobile-immobile zones were not considered because the mass transfer parameter could not be calibrated from the observed data Br data when the longitudinal dispersivity was also used a calibration parameter. The final calibrated model simulations for four selected cases are shown in Figure 4.7 and the model parameters are summarized in Table 4.2.

4.3.3 Reactive Transport Simulations

The applicability of the semi-mechanistic SCM (Table 3.1, Model 1) was assessed by comparing reactive transport simulations with the observed data. The groundwater velocity, dispersivity and mass transfer coefficient for exchange between the mobile and immobile porosity and the duration of the hypothetical injection were obtained by calibrating a one-dimensional nonreactive transport model to the observed Br breakthrough curves. The reactive transport of U(VI) was then predicted using the calibrated nonreactive transport model parameters together with the semi-mechanistic SCM. The concentration of adsorption sites used in the model was $1.92 \cdot 10^{-6}$ sites/m^2 (Davis et al., 2004b) and was calculated from the measured surface area (4.0 m^2/g) of a core sample collected near well NAT25 (see Section 5.3.1). The total porosity of the aquifer was assumed to equal 0.4. The model simulations were conducted using the model RATEQ (Curtis, 2005). Simulations were conducted using the

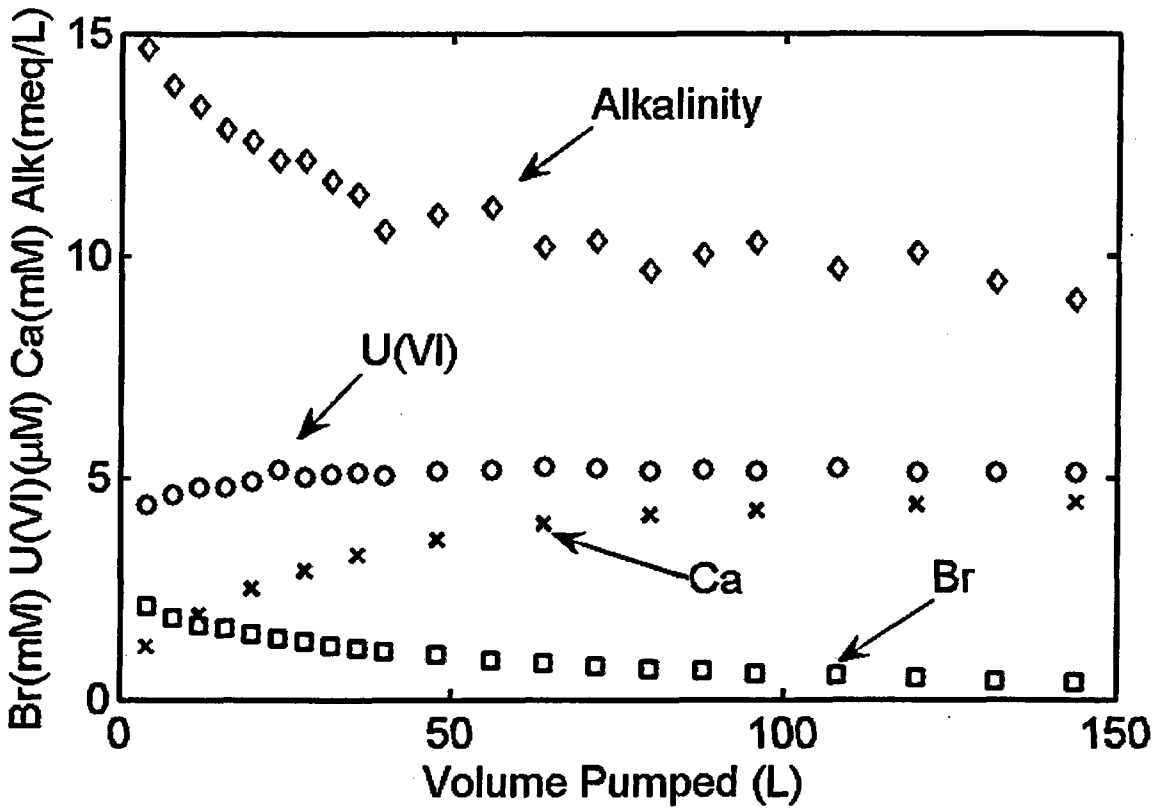

Figure 4.6. Concentration histories observed in push-pull tracer test 12, which had an injectate with a low dissolved Ca concentration and an increased alkalinity.

Table 4.2 Summary of Flow and Transport Parameters Determined by Model Calibration

	Drift (hr)	Well	Hydraulic Conductivity (m/hr)	Longitudinal Dispersivity (m)
PPT1	14.7	25F	0.98	0.047
PPT4	12.8	25O1	1.00	0.073
PPT8	15.4	25O1	2.26	0.004
PPT12	2.5	25K1	0.71	0.30

local equilibrium approach, the kinetics approach and the instantaneous source approach as described in Section 3.

Each of the three approaches gave simulated alkalinity values that were nearly identical, and therefore, only the results obtained using the local equilibrium approach are shown in Figure 4.7. In each of the four cases considered, the simulations gave good predictions of the observed alkalinity. However, the alkalinity in these experiments was behaving nearly as a nonreactive solute, which was determined by comparing the normalized concentrations of alkalinity and Br tracer (results not shown). The three modeling approaches also gave nearly the same U(VI) simulation results, although the models did not predict the observed changes in several cases. A fair prediction for U(VI) concentration history was achieved for PPT1 (Fig. 4.7a), but most of the change in U(VI) concentration can be attributed to mixing of the injectate and the groundwater, and not to reactive processes. In the remaining three cases (Figs. 4.7b-4.7d), all of the predictions for U(VI) concentrations underpredicted the observed data.

4.4 Conclusions

The experimental observations illustrate that increases in alkalinity can desorb U(VI) that has been present in the Naturita aquifer for several decades. In addition, U(VI) desorption was relatively fast; push-pull tracer tests that had contact times of as little as 0.5 hr had U(VI) concentrations that increased from an initial concentration of 0.05 μM in the injected water to 2 μM in sampled groundwater. Higher concentrations, up to 17 μM, were observed in some experiments where the alkalinity was increased. However, in one experiment where the alkalinity was increased and the Ca concentration was decreased, the U(VI) concentration was nearly constant.

The push-pull test results were not useful for evaluating adsorption model parameters for the purpose of reactive transport. This limitation results from the nearly reversible nature of the reactive transport simulations when applied to cases where sorption processes are probed by manipulating the groundwater alkalinity. In addition, the velocity and or dispersive processes at this site were sufficiently large that the geochemical effects were dampened by dilution in many of the experiments. It is possible that push-pull tests would be more successful in environments where the groundwater velocity is small.

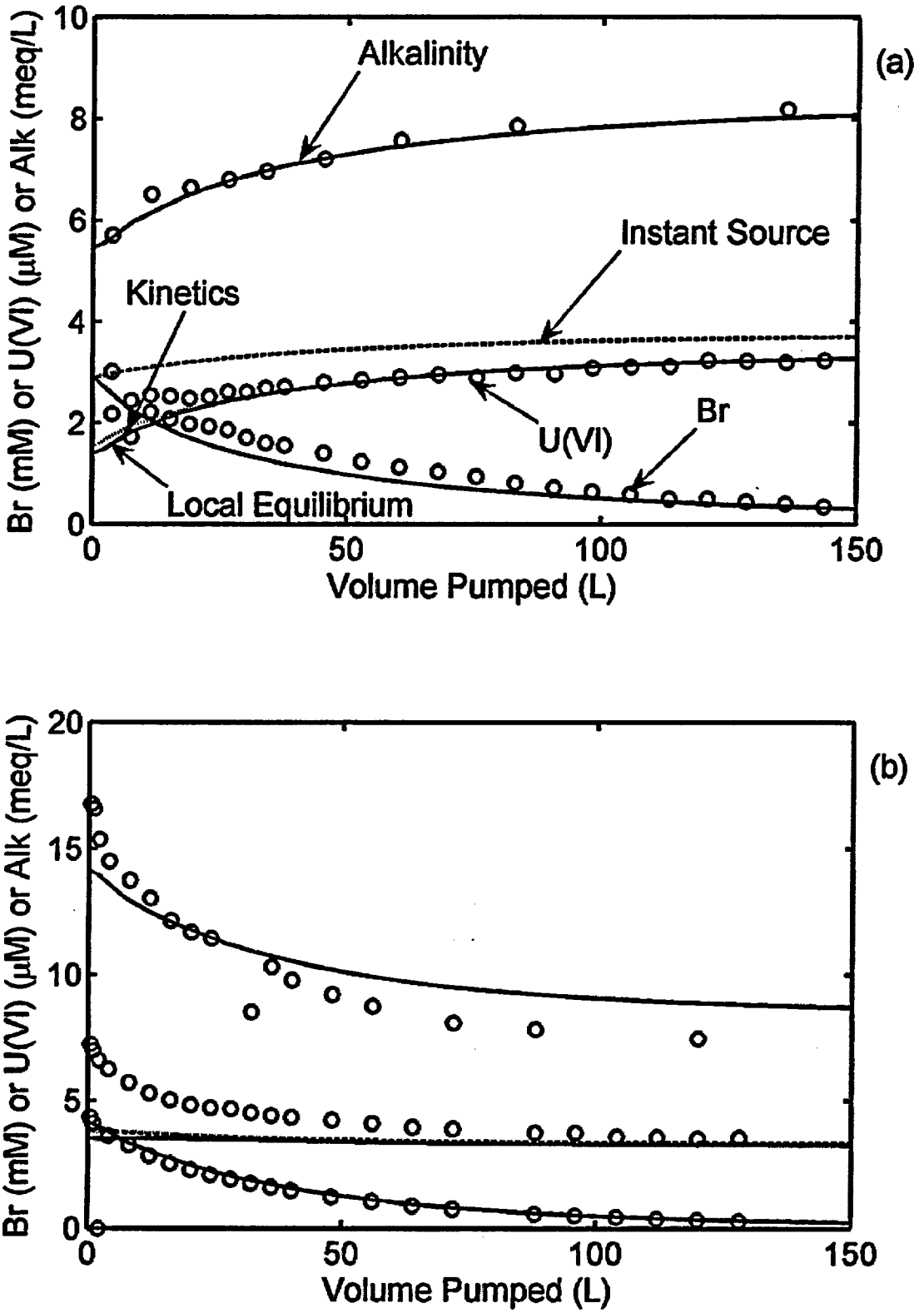

Figure 4.7. Comparison of observed concentration of Br, U(VI) and alkalinity with model simulations for: (a) PPT1 and (b) PPT4.

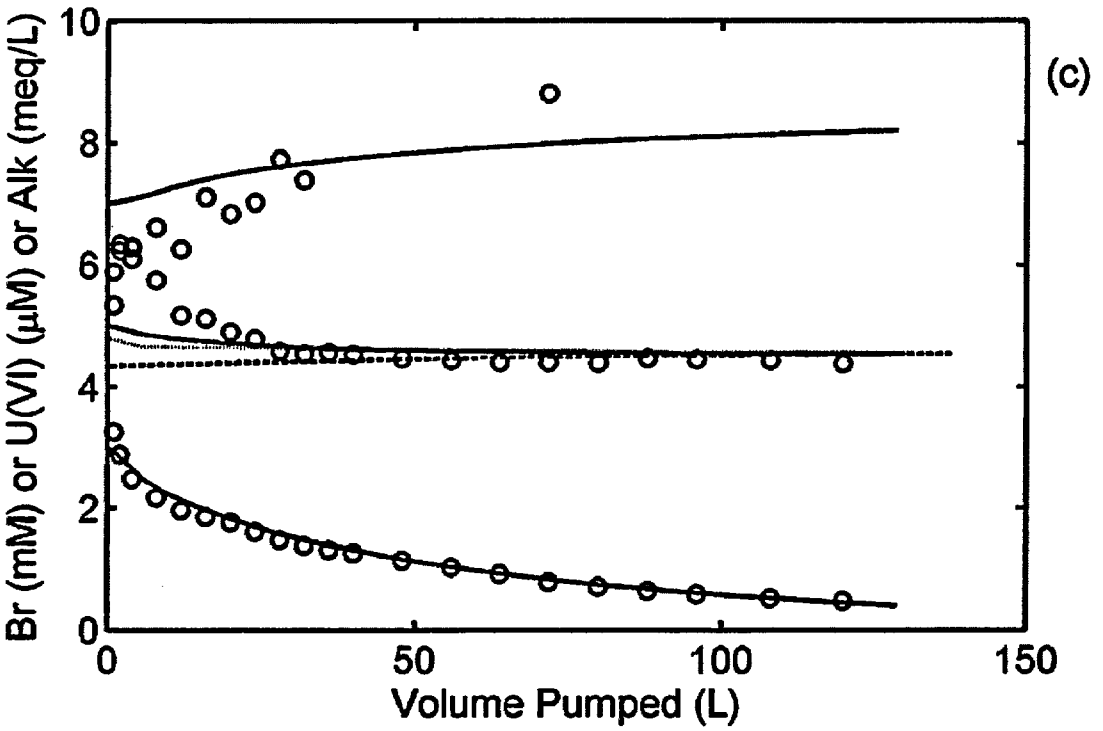

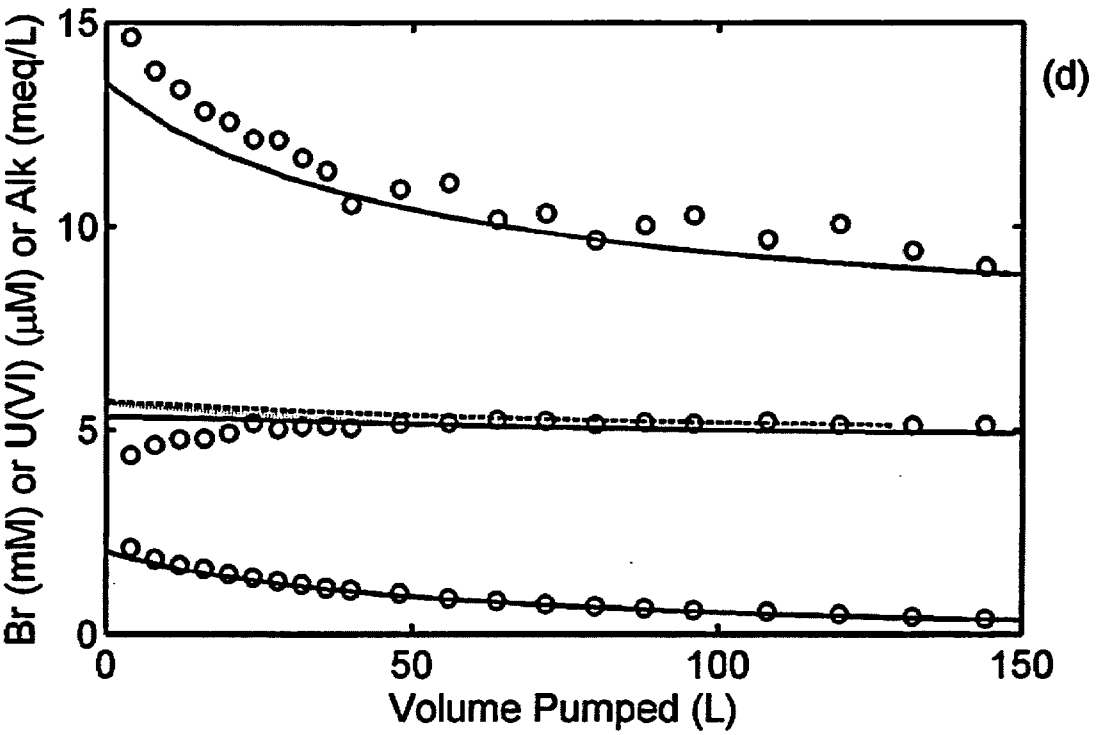

Figure 4.7 (cont). Comparison of observed concentrations of Br, U(VI) and alkalinity with model simulations for (c) PPT8 and (d) PPT12.

5 OBSERVATIONS AND MODELING OF U(VI) TRANSPORT IN SMALL-SCALE MIGRATION TRACER TESTS

5.1 Introduction

Uranium (U) contamination of soils and groundwaters occurs at mining and mill sites and is also an important contaminant at many U.S. Department of Energy sites resulting from the storage, disposal, and processing of nuclear materials (Riley et al., 1992; Crowley and Ahearne, 2002). Under oxidizing conditions, uranium is predominantly present as U(VI), which can be quite mobile in aquifers (Davis and Curtis, 2003; Curtis et al., 2006). The mobility of U in water-rock systems is controlled both by precipitation reactions and by sorption reactions with mineral surfaces. Furthermore, the extent of U(VI) adsorption and mobility in aquifers with circumneutral to alkaline pH values is controlled by the formation of both uranium-carbonato species (e.g., $UO_2(CO_3)_2^{-2}$ and $UO_2(CO_3)_3^{-4}$) and, in calcium rich environments, by aqueous ternary calcium-uranium-carbonato species (e.g., $CaUO_2(CO_3)_3^{2-}$ and $Ca_2UO_2(CO_3)_3^{0}$). Even in environments where U precipitates are present, adsorption processes can be important controls on the small, but significant, concentrations that linger after a precipitate dissolves. Thus, a detailed understanding of aqueous speciation and sorption is necessary for accurate risk assessments to be performed at uranium-contaminated sites.

Numerous investigations of U(VI) sorption by natural soils and sediments have been described in the literature (Duff and Amrhein, 1996; Turner et al., 1996; Barnett et al., 2000, 2002; Zheng et al., 2003; Davis et al., 2004b, Dong et al., 2005, Lui et al., 2005, Qafoku et al, 2005, Wang et al, 2005a, Wang et al, 2005b). In some cases, U(VI) adsorption was well described by surface complexation models (Davis et al., 2004b), but only a few studies have evaluated the SCM performance under field conditions. A semi-mechanistic U(VI) SCM developed for the Naturita aquifer background sediments (Davis et al., 2004b) was found to predict U(VI) adsorption within a factor of approximately 3 by contaminated sediments at the site (Kohler et al, 2004) and by NABS samples that were contacted *in-situ* with contaminated groundwater (Curtis et al., 2004). The SCM was also successfully used in plume scale simulations that were fit to historical U(VI) observation at the Naturita mill site (Curtis et al., 2006). However, because these latter results were calibrated to the observed data, the simulations were not a rigorous evaluation of the performance of the SCM under conditions of transient reactive transport.

Small-scale natural gradient migration tests are directly applicable approaches for evaluating the semi-mechanistic SCM approach for modeling adsorption reactions in reactive transport simulations of subsurface geochemical behavior. In this approach, a known volume of water is injected into an aquifer and the aquifer is sampled at downgradient wells to obtain a description of the geochemical changes in the aquifer. The sampling can be conducted either at a single location over a period of time to provide a temporal description (e.g., a breakthrough curve) of the reactive transport processes, or the sampling can be conducted over a dense sampling network to obtain a spatial description of the geochemical conditions at a single time. The temporal approach (breakthrough curves) has the advantage that a dense observation network is not required.

Small-scale migration tests have several advantages when compared with the push-pull tests described in Chapter 4. First, after the relatively short injection period, the reactive transport processes occur under the influence of the natural hydraulic gradient. Therefore, the tests are conducted at groundwater flow velocities representative of the aquifer of interest. In addition, the natural gradient tests usually sample a larger volume of the aquifer, and therefore are less likely to be influenced by very small-scale heterogeneities. Like the push-pull tests, small-scale migration tests are *in-situ*

tests and are influenced by the natural distribution of hydraulic conductivity, abundance of sorption sites, and geochemical conditions, such as the redox environment, all of which can be difficult to reproduce in the laboratory. Small-scale migration tests, however, do have a number of limitations. First, in many aquifers it can be difficult to accurately assess the direction of groundwater flow at the small-scale because of heterogeneities in hydraulic conductivity. This creates a significant probability that an injected tracer will not be detected unless a dense monitoring network is used. Second, small migrations tests can require a significant effort to monitor the spatial and temporal changes that may occur over several months, in order to fully resolve the complex geochemical response to an injected plume.

The objectives of the work described in this section were to evaluate the semi-mechanistic SCM approach in small-scale migration tests. In the work described below, breakthrough curves were recorded at several wells that were located between 1.8 and 2.3 m downgradient of the injection wells at the NAT25 experimental tracer test site. The tests considered both variable alkalinity values and U(VI) concentration, as these variables were found to be most significant in controlling U(VI) transport at the Naturita site (Curtis et al., 2006). These data are compared with reactive transport simulations using the semi-mechanistic SCM developed for the Naturita aquifer background solids (NABS).

5.2 Methods and Materials

5.2.1 Site Description

Infrastructure for small-scale tracer tests was developed at the Naturita site at a location downgradient of the highest U(VI) concentrations and in a relatively uniform sandy portion of the alluvial aquifer near NAT25 (Figure 5.1). The groundwater has an average alkalinity equal to 8.5 meq/L, an average U(VI) concentration of 4 μM (950 ppb), and the pH was approximately 7.1. The groundwater sampled from well NAT25 is nearly saturated with respect to calcite (-0.3<SI<0.4).

Eleven wells were installed downgradient of well NAT25, and these wells were constructed using a variety of methods that changed over time. Wells 25B, 25C, 25F and 25G are stainless steel drive points with a 15 cm screened interval that are connected to a 1.25cm polyethylene tube with a hose barb. All of the materials installed below the water table are constructed from either stainless steel or polyethylene. Wells 25A, 25D and 25E are multilevel wells constructed from 0.75cm polypropylene tubing housed in a 2.5 cm PVC well casing. The end of the tubing protrudes from the well casing and is covered with a stainless steel screen. Wells 25M, 25N, 25O and 25P are multi-level 1.25cm PVC wells with a 15 cm slotted interval. These wells have custom-fabricated permanent packers that isolate the two separate screened intervals, which are separated vertically by 30 cm. Finally, wells 25K and 25L are identical to 25M-P except that these wells were used as injection wells.

5.2.2 Sediment Collection

A core was collected approximately 0.5 m west of well NAT25P1 in August 2005. The core was collected by hand augering 3.9 m to the water table, and then driving a 1.5" PVC pipe fitted with a 'core catcher' into the saturated zone of the aquifer. The core could only be driven to a total depth of 4.6 m, which was approximately 8 cm above the center of the lower screened interval at well NAT25P. The core was removed from the auger hole, and cut into 8 cm segments. The top 0.3 m of the core was missing, probably because some to the sediments fell out of the core when it was removed from the auger hole, given the streaking observed on the inside of the core liner.

The sediments collected from the core were primarily Fe and Al oxyhydroxide coated quartz (90-95%), with minor amounts of K-feldspar and ferromagnetic minerals. Carbonate minerals were present in the sediments.

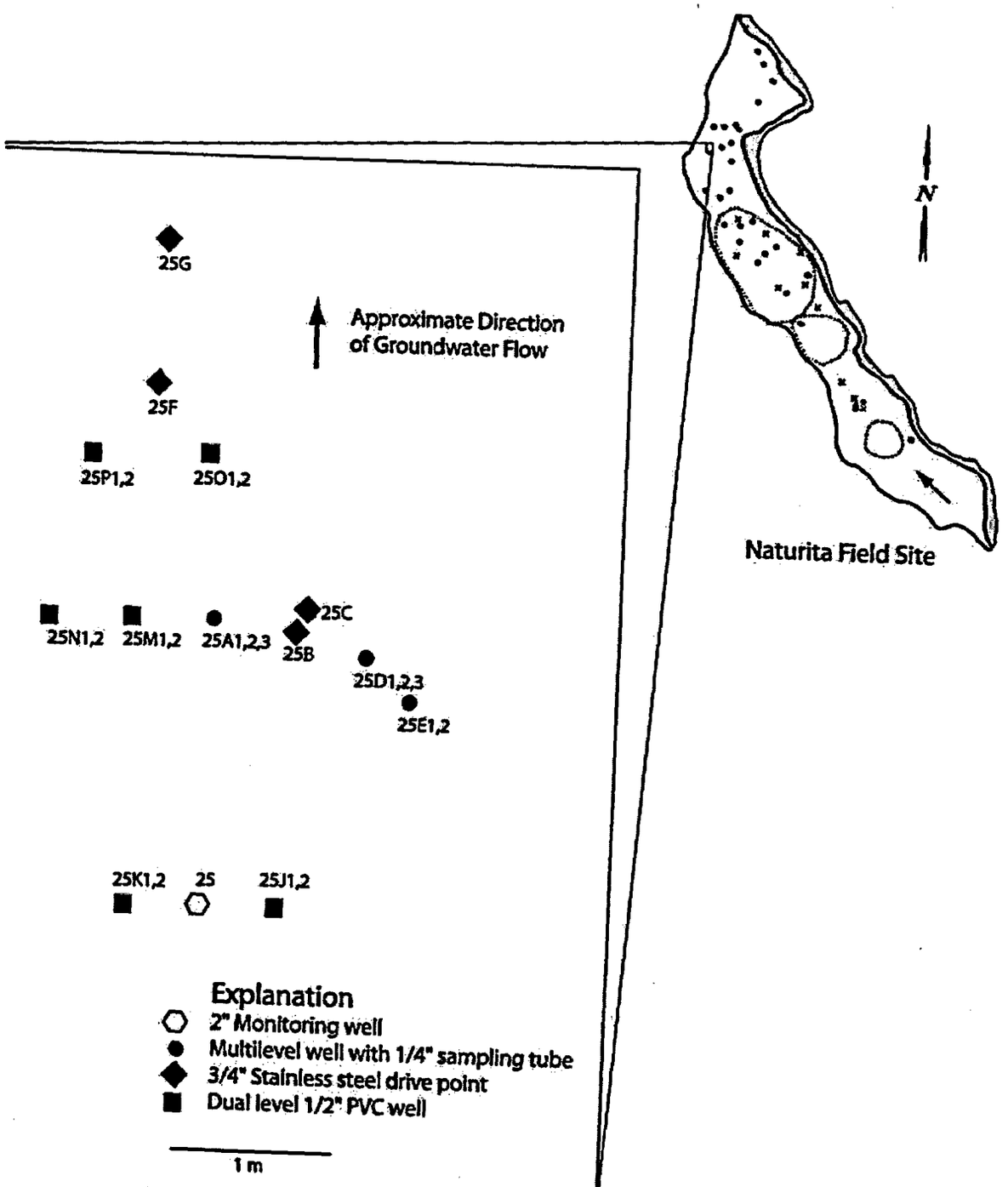

Figure 5.1. Map of the small-scale tracer test site developed near NAT25. The numbers after the well designations indicate the different sampling levels with 1 being the deepest screened interval.

5.2.3 Uranium(VI) Adsorption

The purpose of the small-scale migration tests described in this section was to compare field observations of transient U(VI) transport with reactive transport simulations that used the equilibrium surface complexation model previously developed in the laboratory to simulate adsorption reactions. Batch adsorption experiments were conducted using uncontaminated Naturita aquifer background sediments (NABS) that were collected from a gravel pit located upgradient of well DOE547 (Davis et al., 2004b). The batch experimental conditions encompassed the range of geochemical conditions observed in the U(VI) plume at the Naturita site, with alkalinities that ranged from 4 to 12 meq/L (Davis and Curtis, 2003). However, the alkalinities in the field experiments described below were as high as 24 meq/L, and consequently, use of the NABS SCM for the migration tests requires a modest extrapolation. A semi-mechanistic SCM was fit to the adsorption data using the geochemical optimization program FITEQL (Herbelin and Westall, 1999). The SCM consists of 6 reactions (2 reactions each with 3 different site-types) that are listed as Model 1 in Table 5.1. The three site-types are described as very strong (>SSOH), strong (>SOH), and weak (>WOH) sites, corresponding to their relative U(VI)-binding strength (Table 5.1). Multiple site types are commonly used in formulating SCMs and approximate the nonlinear isotherms commonly observed for cation adsorption on well-characterized metal oxides (Dzombak and Morel, 1990). Postulating multiple site types was also important for simulating peak tailing in laboratory columns packed with quartz (Kohler et al., 1996). Davis et al. (2004b) illustrated that observed and modeled K_d values at constant pH and alkalinity decreased by a factor of approximately 3 as U(VI) concentration increased from 0.03 μM to 10 μM, indicating that the adsorption isotherm is moderately nonlinear. The semi-mechanistic SCM does not include an electrical double layer term and assumes that the adsorption occurs by U(VI) binding to generic sites that represent average surface chemical properties of the sediment.

5.2.4 Tracer Test Descriptions

The small-scale migration tests were conducted by pumping groundwater from the alluvial aquifer at the Naturita site into 30 gallon containers, adding bromide (as KBr) as a conservative tracer and then, in some instances, either increasing or decreasing the alkalinity of the pumped groundwater prior to siphoning it into the aquifer. Three different geochemical conditions were used in the tests, which are summarized in Table 5.2. Alkalinity in the tests was varied by approximately a factor of 12, while the U(VI) concentration was varied by a factor of 100.

The first migration test (MT1) was conducted when only wells 25A-25E were installed in the

Table 5.1 NABS Surface Complexation Model [*Davis et al.*, 2004b] [1]

Reaction	Log K
Model 1: Reactions in terms of the UO_2^{+2} species	
$>SSOH + UO_2^{2+} = >SSOUO_2^{+} + H^{+}$	6.80
$>SOH + UO_2^{2+} = >SOUO_2^{+} + H^{+}$	5.82
$>WOH + UO_2^{2+} = >WOUO_2^{+} + H^{+}$	2.57
$>SSOH + UO_2^{2+} + H_2O = >SSOUO_2OH + 2H^{+}$	-0.67
$>SOH + UO_2^{2+} + H_2O = >SOUO_2OH + 2H^{+}$	-2.08
$>WOH + UO_2^{2+} + H_2O = >WOUO_2OH + 2H^{+}$	-5.32

[1] The total site concentration was 1.92·10-6 sites/g. The fraction of weak sites (>WOH) was 0.9989, the fraction of strong sites (>SOH) was 0.001 and the fraction of very strong sites (>SSOH) was 0.0001.

Table 5.2. Summary of Migration Tests at the NAT25 Small-Scale Tracer Test Site

Test Number	Source Water	Injection Well	Observation Wells	Gallons injected	Br^- (mM)	U(VI) (μM)	Alkalinity (meq/L)
MT1	DOE547	NAT25	NAT25A1	90	6.6	0.04	4.0
MT2	NAT25	NAT25, 25K, 25L	NAT25A3, M1, N1, O1, P1	150	6.7	4.6	2.0
MT3	NAT25	NAT25, 25K, 25L	NAT25A3, D1, M1, N1, O1, P1	150	6.6	4.6	24

aquifer. In this test, water from well DOE547, which is upgradient of the former ore mill location, was collected and transported to the NAT25 site. After the KBr tracer was added to the water, the water was siphoned into the aquifer without any further changes in geochemical conditions.

In test MT2, alkalinity was decreased by adding concentrated HCl while purging the containers holding the groundwater with N_2 gas. The N_2 gas was used to remove CO_2 from solution in order to increase pH without further changing the alkalinity. The HCl was added sufficiently slowly while the containers were continuously purged with N_2 gas such that the pH did not drop below 6. After sufficient acid was added to decrease the alkalinity to 2.0 meq/L, the pH was re-adjusted to the final value of 7.1 by N_2 purging.

In test MT3, the alkalinity of the pumped groundwater was increased by adding $NaHCO_3$ and Na_2CO_3. The pH of the containers was first decreased to approximately 6.0 by purging with 10% CO_2 in N_2. The $NaHCO_3/Na_2CO_3$ was then slowly added so that the pH remained below 7.3. Once all of the $NaHCO_3/Na_2CO_3$ was added, the pH was decreased to the ambient pH by purging the containers with the N_2/CO_2 gas mixture. This method was used to reduce the chances of co-precipitating U(VI) in carbonate mineral phases, which may have been significant if $NaHCO_3$ was rapidly added to the containers.

5.2.5 Groundwater Sampling and Analysis

Groundwater was collected using a peristaltic pump and filtered with a 0.45μm Millex HV filter (Millipore). Samples were diluted as necessary and analyzed for dissolved U(VI) concentration by kinetic phosphorescence analysis and selected other elements (by ICP-AES). Water samples collected for alkalinity were titrated with sulfuric acid using the Gran titration method. Bromide samples were analyzed using a Lachat flow-injection spectrophotometer. The surface area was measured on triplicate samples using the BET-N_2 adsorption method with a Micrometrics Flowsorb 2000 instrument.

5.3 Results

5.3.1 Surface Area

The sediments that were recovered from the core sample were air-dried, and analyzed to determine specific surface area. The results, shown in Figure 5.2, illustrate that the surface area decreased with increasing depth. The depth shown in Figure 5.2 equals the total depth driven into the ground corrected for the 0.3 m of missing core. The measured surface areas suggest that the surface area approaches a nearly constant value near a depth of 4 m, although this trend needs to be verified with samples collected at greater depth. A single sample collected at NAT25B had a specific surface area equal to 5.4 m^2/g (Kohler et al., 2004), although the depth from which this sample was collected is

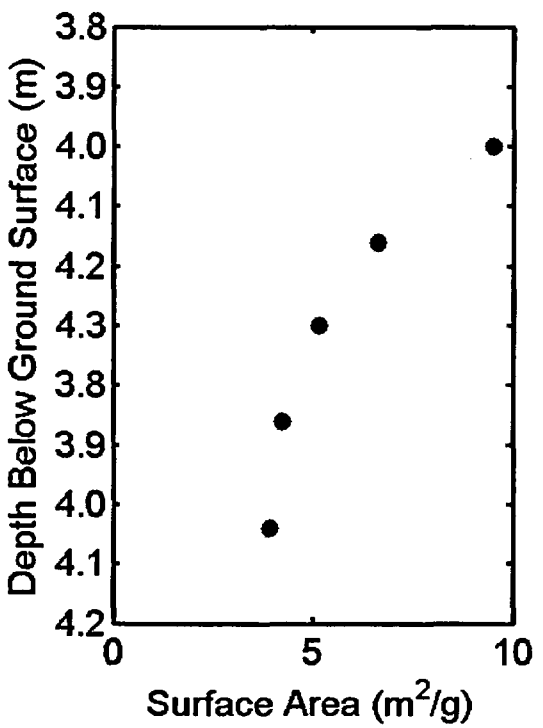

Figure 5.2. Variation of specific surface area with depth.

uncertain because the auger hole collapsed during sampling. For comparison, the surface area of the NABS sample (< 3 mm) was 5.15 m^2/g, and the average surface area of sediments collected in 1998 from auger flights (during monitoring wells installation) was 12.4 m^2/g (Davis et al., 2004b). All of the sediments collected near well NAT25 consisted of fine sand, and it is estimated that only a few percent by weight of these samples were particles greater than 3 mm in diameter. This contrasts markedly with the uncontaminated sediments from which the NABS sample was derived, which had approximately 85 percent of the material exceeding 3 mm in diameter. It is possible, however, that larger materials were excluded from the 3.7 cm core barrel during the sampling of the NAT25 samples.

5.3.2 Uranium(VI) Aqueous Speciation

The groundwater near the NAT25 tracer test site has a U(VI) concentration of approximately 4 μM, an alkalinity of 7.5 meq/L, and a very stable pH value of 7.1. Alkalinity of the groundwater was varied from 2 meq/L to 24 meq/L in the migration tests. Figure 5.3 illustrates that at pH 7.1, the predominant species in groundwater changes with alkalinity under conditions of variable alkalinity and equilibrium with calcite. At low alkalinity values, $Ca_2UO_2(CO_3)_2$ is predicted to be the predominant species, accounting for greater than 84 percent of dissolved U(VI). Most of the remaining aqueous U(VI) is predicted to be present as $CaUO_2(CO_3)_2^{-2}$. Conversely, at an alkalinity of 24 meq/L, three species are important: $UO_2(CO_3)_2^{-4}$, $CaUO_2(CO_3)_2^{-2}$ and $Ca_2UO_2(CO_3)_2$, accounting for 37 percent, 31 percent and 23 percent, respectively, of the dissolved U(VI). The primary cause for this change in speciation is that the predicted calcium concentration decreases with increasing alkalinity, due to the imposed requirement that calcite remain in equilibrium with the aqueous phase.

5.3.3 Observed Breakthrough Behavior

Figure 5.4 illustrates Br, U(VI), and alkalinity concentrations observed at well A1 as a result of the injection of uncontaminated groundwater into well NAT25 (Tracer Test MT1). The observed Br concentration reached a maximum concentration of 7.0 mM at approximately 86 hr, which is within the range of the Br concentrations measured in the three injection containers. These observations correspond to an approximate velocity of 10 cm/hr (2.4 m/d). The Br concentration also exhibits significant tailing, suggesting that nonreactive transport is impacted by zones with varying velocities. The observation that the Br concentration in well A1 reached the injected concentration implies that if no U(VI) desorption occurred, the observed U(VI) concentration would have been equal to that in the injectate (0.04 μM). In contrast, the U(VI) concentration observed at 86 hr was 1.4 μM, indicating that a significant amount of U(VI) desorption had occurred even though the sediments had been in contact with elevated U(VI) concentrations for several decades (Davis and Curtis, 2003).

Figure 5.5 illustrates the Br, U(VI), and alkalinity concentrations observed in test MT2.

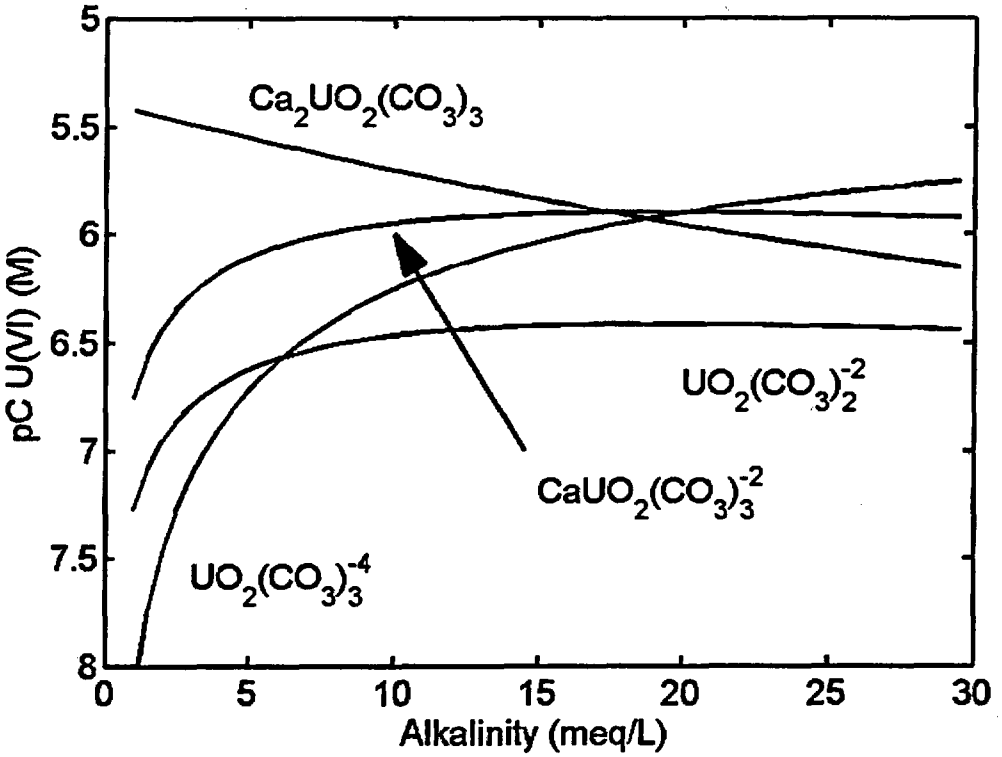

Figure 5.3. Speciation of 4 μM U(VI) in groundwater in equilibrium with calcite at pH 7.1 and with variable alkalinity.

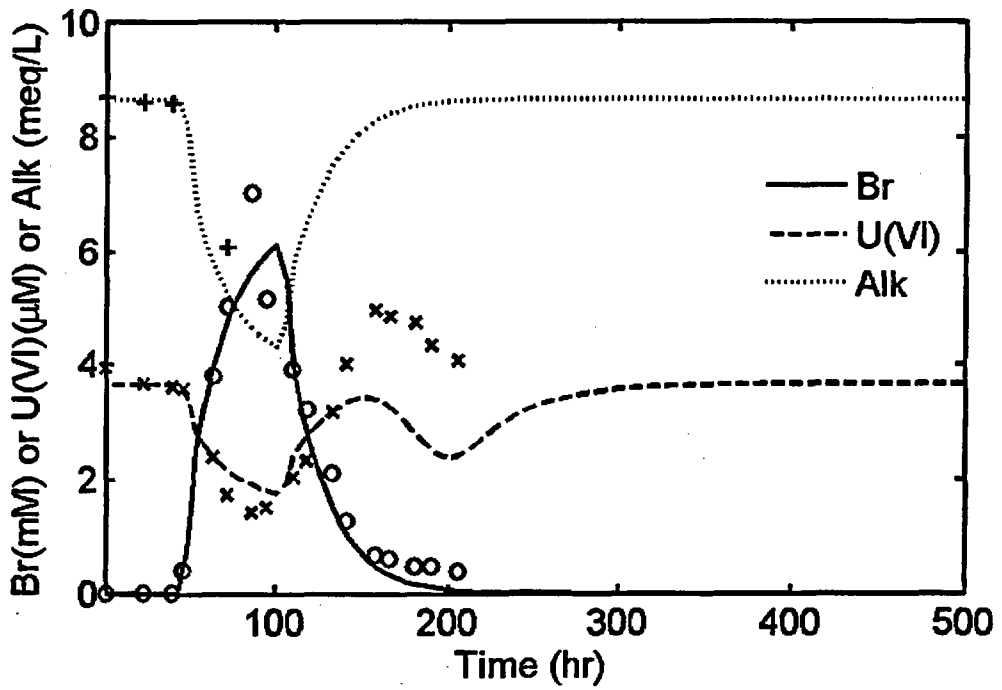

Figure 5.4. Observed and simulated bromide, U(VI) and alkalinity concentrations in migration test MT1 at observation well A1.

In this test, groundwater pumped from well NAT25 was treated to decrease the alkalinity to 2 meq/L as described above and then the sample was re-injected into the aquifer. The U(VI) concentration in NAT25 groundwater at the time of the experiment was 4.71 μM and the average U(VI) concentration of the injectate was 4.63 μM, demonstrating that loss of U(VI) to the container walls was insignificant (even with the decreased alkalinity). The observed Br concentration in observation wells A3, M2 and N2 reached maximum concentrations ranging from 4.7 to 5.5 mM, which corresponds to 71 to 83 percent of the injected concentration, and the peak concentrations were observed at between 66 and 91 hr. The peak Br concentration in well O1 was 5.3 mM, observed at 122 hr. The four Br breakthrough curves for test MT2 had varying amounts of tailing. The breakthrough at well A3 showed a modest amount of tailing, whereas the breakthrough at O1 was nearly symmetrical. The breakthrough observed in wells M2 and N2 both had a small increase in Br concentration between 200 and 300 hr, and then gradual decreases to background concentrations by 500 hr. These secondary peaks probably resulted from flowpaths that encountered zones of low hydraulic conductivity, but nevertheless were still captured by the sampling wells.

The U(VI) concentrations in each of the observation wells decreased from the initial concentration of 4.6 μM to minimum values that ranged from 1.2 to 1.9 μM. Moreover, the decreases in U(VI) concentrations coincided with the decrease in alkalinity and increase in Br concentration. Taken together, these data suggest that the alkalinity perturbation migrated nearly conservatively and that the U(VI) concentrations decreased in samples with decreased alkalinity because of increased adsorption. The observed U(VI) concentrations in each of the breakthrough curves (Figure 5.5) increased after the Br concentration had decreased to values near the background concentrations. Note that these results contrast markedly with results that would be predicted from a simple constant K_d model to describe U(VI) adsorption. The constant K_d would predict a constant U(VI) concentration during the breakthrough curve, because the U(VI) concentrations in the aquifer and in the injectate were nearly identical.

Br, U(VI), and alkalinity concentrations observed in test MT3 are shown in Figure 5.6. The observed Br in each of the 5 observation wells was similar to Br observed in test MT2. The alkalinity in each of the breakthrough curves increased and the location of the peaks coincided with the observed Br peak, again suggesting reactive processes did not significantly affect alkalinity. U(VI) concentrations increased in each of the experiments and the increase coincided with the Br and alkalinity peaks. After the Br concentrations had decreased to near background concentrations, the U(VI) concentrations decreased below the original ambient concentration of 4.7 μM to values ranging from 3 to 4 μM in each of the 5 breakthrough curves.

5.3.4 Quasi One-Dimensional Nonreactive Transport Modeling

In each of the cases discussed above, Br breakthrough curves were dominated by a single peak, although there was some tailing in many cases. Consequently, a quasi one-dimensional approach was used to simulate Br concentrations in the nonreactive and reactive transport simulations described below. In this quasi one-dimensional approach, it was assumed that the domain between the injection well and each individual observation well could be treated as a separate one-dimensional column, and that a pulse of high Br solution was introduced into the column over a finite period of time. The simulated injection period can be significantly longer than the actual injection time to compensate for high velocities that occurred during the actual injection. This approach is significantly simpler and more computationally efficient than the two-dimensional approach described in Sections 3 and 4 that attempted to simulation the injection, drift and extraction of the tracers in the push-pull simulations.

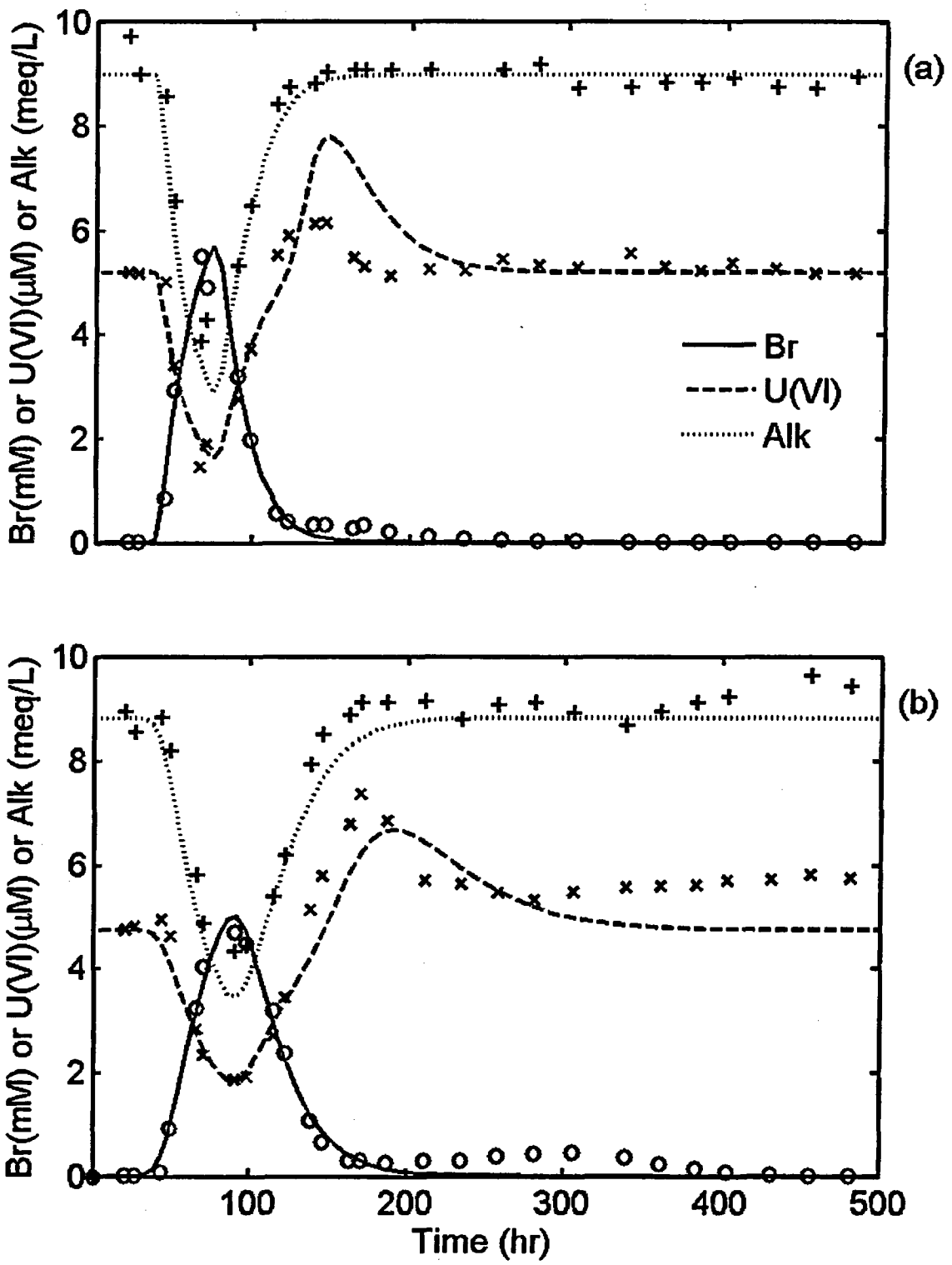

Figure 5.5. Observed and simulated bromide, U(VI) and alkalinity concentrations in migration test MT2 at observations wells (a) A3, and (b) M2.

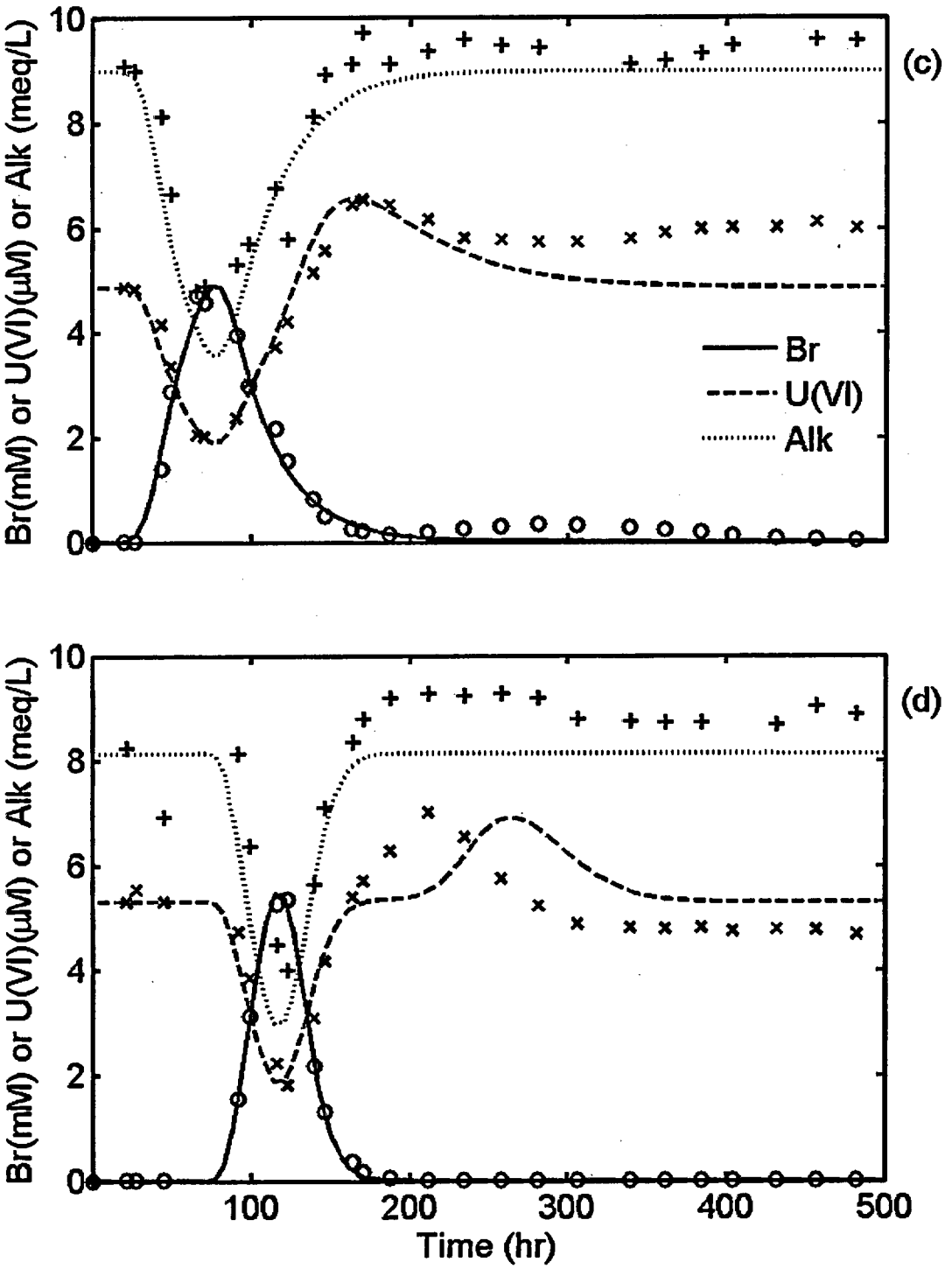

Figure 5.5 (cont). Observed and simulated bromide, U(VI) and alkalinity concentrations in migration test MT2 at observations wells (c) N2, and (d) O1.

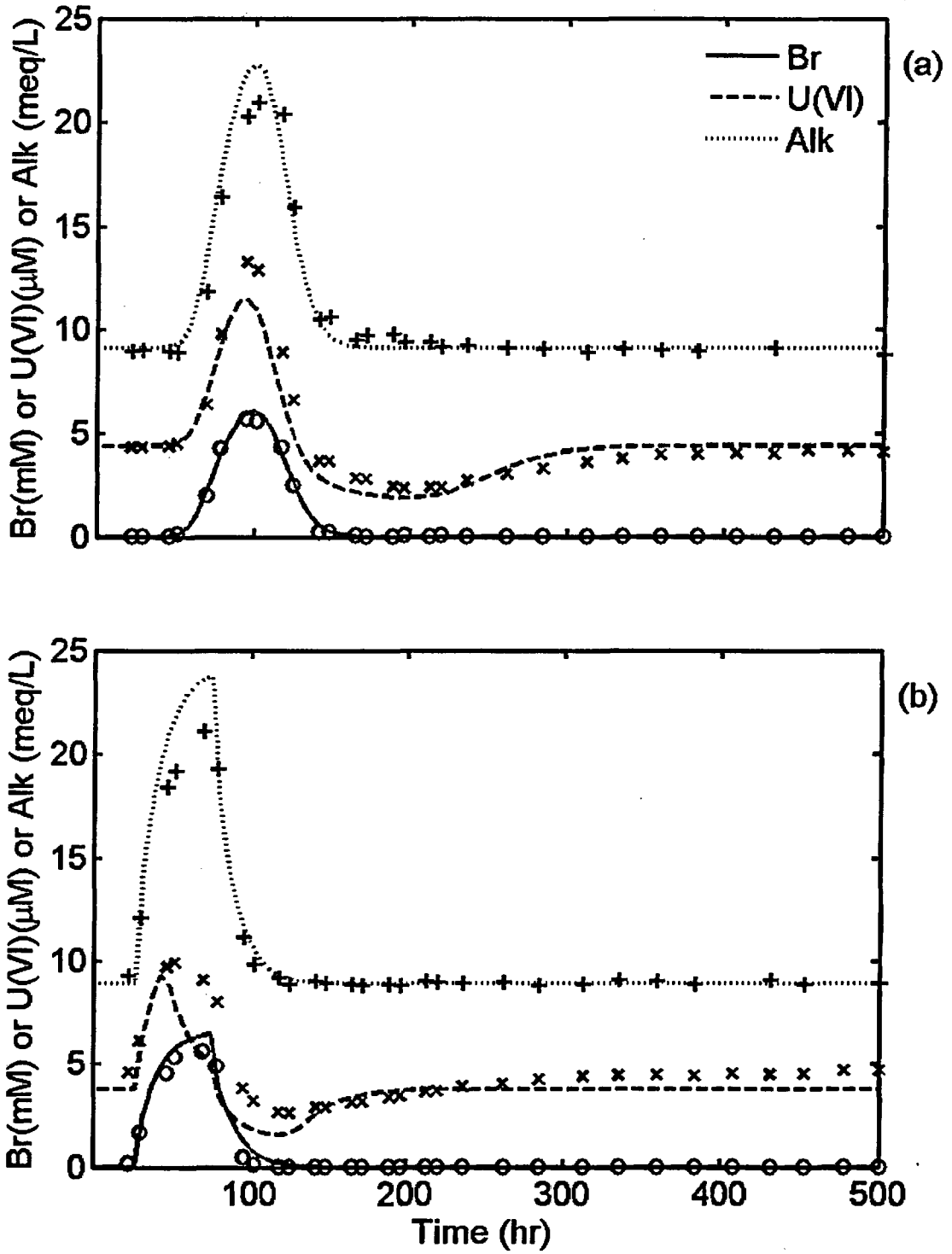

Figure 5.6. Observed and simulated bromide, U(VI) and alkalinity concentrations in migration test MT3 at observations wells (a) A3, and (b) D1.

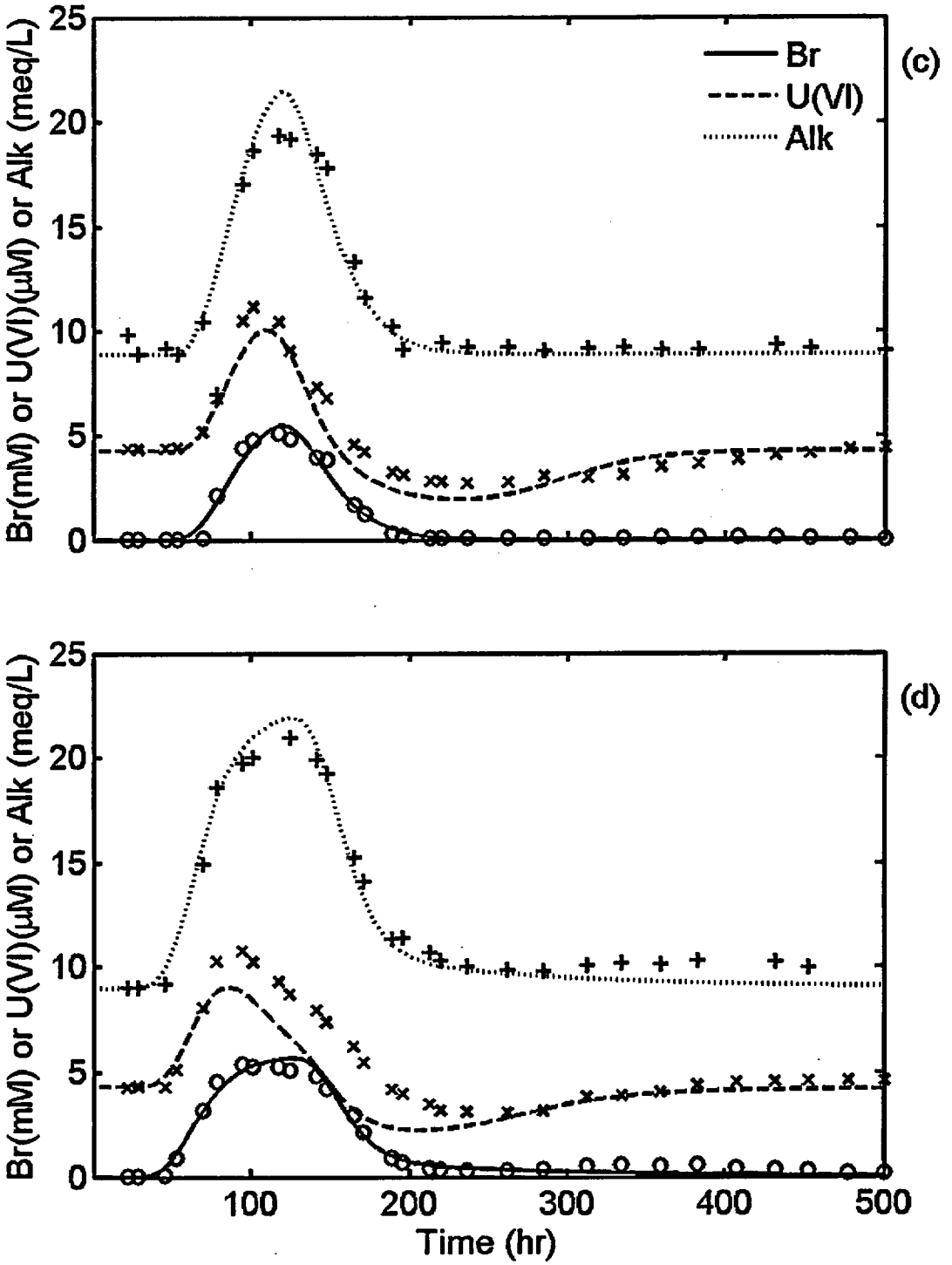

Figure 5-6 (cont). Observed and simulated bromide, U(VI) and alkalinity concentrations in migration test MT3 at observations wells (c) M2, and (d) N2.

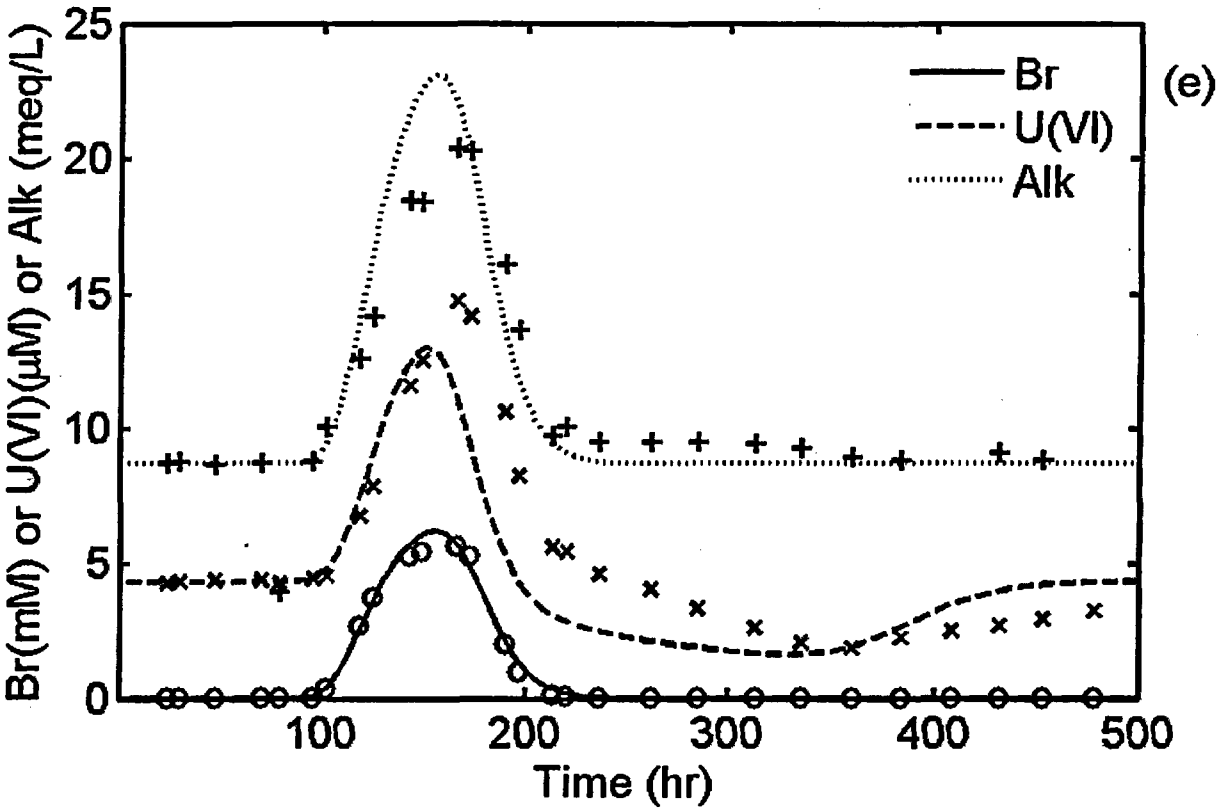

Figure 5-6 (cont). Observed and simulated bromide, U(VI) and alkalinity concentrations in migration test MT1 at observation well O1.

5.3.4.1 Modeling Approach

It was assumed that the one-dimensional domain could be approximated a simple mobile-immobile zone model. In this approach, transport of a nonreactive solute in the mobile zone is described by:

$$\frac{\partial(\theta_m C_m)}{\partial t} + \frac{\partial(\theta_{im} C_{im})}{\partial t} = \theta_m \alpha_L v \frac{\partial^2 C_m}{\partial x^2} - \theta_m v \frac{\partial}{\partial x} C_m \qquad (5\text{-}1)$$

where C_m is the concentration in the mobile zone, C_{im} is the concentration in the immobile zone, θ_m is the porosity of the mobile zone, θ_{im} is the porosity of the immobile zone, α_L is the longitudinal dispersivity, v is the groundwater velocity, t is time and x is distance. The concentration in the immobile zone is governed by:

$$\theta_{im} \frac{\partial C_{im}}{\partial t} = k_{La}(C_m - C_{im}) \qquad (5\text{-}2)$$

where k_{La} is a first order mass transfer coefficient.

The applicability of the semi-mechanistic SCM was assessed by comparing reactive transport simulations using the NABS SCM with the observed data. The groundwater velocity, dispersivity and mass transfer coefficient for exchange between the mobile and immobile porosity and the duration of the hypothetical injection were obtained by calibrating a one-dimensional nonreactive transport model to the observed Br breakthrough curves. The reactive transport of U(VI) was then predicted using the calibrated nonreactive transport model parameters together with the semi-mechanistic SCM described in Table 5.1. The concentration of adsorption sites was calculated from the measured surface area of the core sample of 4.0 m^2/g and the site density of $1.92 \cdot 10^{-6}$ sites/g (Davis et al., 2004b). The total porosity of the aquifer was assumed to equal 0.4, and it was further assumed that this porosity consisted of a mobile porosity of 0.3 and an immobile porosity of 0.1. The model simulations were conducted using the model RATEQ (Curtis, 2005) and the calibrations to the observed Br data were obtained using the optimization toolbox in Matlab.

5.3.4.2 Nonreactive Transport Modeling

The observed Br concentrations illustrated in Figures 5.4, 5.5, and 5.6 were fit to the mobile-immobile zone model. The final calibrated model simulations are shown on the figures and the model parameters are summarized in Table 5.3. In each case, it was possible to obtain a good fit to the observed data. The calibrated velocity values ranged by a factor of 2.5 from 0.00754 m/hr at well O1 in MT3 to 0.0189 m/hr at well D1 in MT2. In contrast, the dispersivity and k_{La} values ranged more widely: the dispersivity values ranged from 0.00066 to 0.064 m (a factor of 100) and the k_{La} values ranged from 0.00035 to 0.107 hr^{-1} (a factor of 300). Separate calculations showed that simulations with k_{La} values less than 0.002 hr^{-1} gave concentration breakthrough curves that were nearly identical to simulations that did not consider mass transfer (results not shown). The results in Table 5.3 also suggest a weak inverse relation between the dispersivity and the k_{La} values. Given that increases in both values increases peak spreading, it is possible that the parameter combinations in Table 5.3 are not unique values. However, for the purposes of this work, the primary objective was to account

Table 5.3. Summary of Nonreactive Transport Model Parameters

Tracer Test	Observation Well	Velocity (m/hr)	Dispersivity (m)	k_{La} (hr^{-1})	Pulse Length (hr)
MT1	A1	0.0112	0.000664	0.00263	57.7
MT2	A3	0.0127	0.00309	0.00461	37.3
MT2	M2	0.0102	0.0318	0.00287	48.5
MT2	N2	0.0118	0.0645	0.00194	48.3
MT2	O1	0.00928	0.000325	0.0144	34.3
MT3	A3	0.00965	0.0229	0.107	46.0
MT3	D1	0.0189	0.000749	0.00545	47.9
MT3	M2	0.00787	0.0169	0.00397	59.0
MT3	N2	0.00816	0.0637	0.000350	92.9
MT3	O1	0.00754	0.00118	0.0107	58.8

for the observed Br concentration breakthrough, even if only empirically, in each of the breakthrough curves.

5.3.4.3 Reactive Transport Modeling

Simulated U(VI) concentrations and alkalinity for test MT1 are illustrated as the solid lines in Figure 5.4. The model simulations agree very well with observed decrease in U(VI) concentrations up to 110 hr. This is particularly encouraging because, as described above, the observed changes in U(VI) concentration result from the opposing effects of dilution, which decreases the U(VI) concentration, and desorption, which increases the U(VI) concentration. After 110 hr, the predicted U(VI) concentrations do not agree as well with the observed data; the observed U(VI) concentration increased above the background concentration of 3.9 μM to 5 μM, whereas the simulated concentrations did not increase above background.

For test MT2, the decrease in alkalinity caused U(VI) adsorption to increase, which in turn caused the aqueous U(VI) concentration to decrease. The decrease in concentration is predicted very well in each of the four breakthrough curves shown in Figure 5.5. The model simulations also predicted the decrease in alkalinity very well, which occurred simultaneously with the appearance of Br tracer. After the Br and alkalinity concentrations returned to the initial values at approximately 200 hr, the U(VI) concentrations increased above the initial concentration. The increase can be attributed to desorption and retardation of the U(VI) that adsorbed when the alkalinity values were small. This trend is predicted in each of the breakthrough curves, although there are some discrepancies between the data and the model in each case. In observation well A3 (Fig. 5.5a), the model over-predicted the peak in U(VI) concentration that appeared at 120 hr by approximately 25 percent. In contrast, the predictions for U(VI) concentrations were closer to the observed data at wells M2 and N2, although concentrations were under-predicted after 250 hr. The alkalinity values observed in M2 and N2 after 200 hr were also slightly under-predicted. The small Br peaks between 200 and 500 hr in Figures 5.5b and 5.5c suggest that there was a minor, slow flowpath sampled by these wells, and this may have also increased the alkalinity and U(VI) slightly at longer times. In Figure 5.5d, the simulated U(VI) concentration reproduced the decrease in observed values in the first 120 hr. At longer times, the simulated peak in U(VI) concentration that occurred at 260 hr matches the shape of the observed U(VI) concentrations, but the observed peak is centered at 210 hr. The observed alkalinity after 210 hr was larger than the initial alkalinity, and the increased alkalinity is consistent with the observed earlier arrival of the U(VI), but the cause for these observations is unknown.

The model predictions were also good for test MT3 in which the alkalinity was increased. The model simulations demonstrate that the increase in alkalinity caused U(VI) to desorb, and therefore increase the aqueous U(VI) concentration. After the alkalinity peak passed through the aquifer, native groundwater that flows into the test site from upgradient encounters sediments with less adsorbed U(VI) than was present initially. Some of the dissolved U(VI) adsorbs to re-establish equilibrium, which causes the U(VI) concentration to temporally decrease. All of the simulated U(VI) breakthrough curves match the shape of the observations. However, all of the simulations under-predict the observed U(VI) concentrations.

5.3.4.4 Sensitivity Calculations

First-order sensitivity analyses were calculated for the simulated U(VI) concentrations. The scaled sensitivities (Poeter and Hill, 1998) were defined by:

$$SS_i = \frac{\partial Y}{\partial b_i} b_i \qquad (5\text{-}3)$$

where SS_i is the scaled sensitivity, Y is the simulated quantity, and b_i is the i'th parameter value. The scaling normalizes the sensitivity by the parameter values so that sensitivities with respect to widely varying parameter values can be compared. Equation 5-3 was approximated by finite differences, and the parameters were

perturbed by 0.1 log units. The parameters included in this simple sensitivity analysis were: 1) the formation constants for the aqueous species $UO_2(CO_3)_2^{-2}$, $UO_2(CO_3)_3^{-4}$, $Ca_2UO_2(CO_3)_2$ and $CaUO_2(CO_3)_2^{-2}$ and, 2) the equilibrium constants for the U(VI) surface reactions.

The sum of the absolute values of the scaled sensitivity values is illustrated in Figure 5.7 for the simulated U(VI) breakthrough curve at well A1 in test MT1 and at wells A3 in tests MT2 and MT3. The simulated U(VI) concentration is most sensitive to the formation constant for aqueous $Ca_2UO_2(CO_3)_2$ in each of the three cases. This is the predominant species in background water at the test site and is also the predominant species in the injectate for tests MT1 and MT2, as illustrated in Figure 5.3. The simulated U(VI) concentrations are also sensitive to the equilibrium constants for the reactions resulting in formation of both $>WOUO_2^+$ and $>SOUO_2^+$. These species were the predominant adsorbed species in Naturita plume scale simulations (Curtis et al., 2006) and are also the predominant species in the migration test simulations. The simulated U(VI) concentration is approximately equally sensitive to the constants for each of the two surface species. Overall, Figure 5.7 suggests that the model was more sensitive in the simulations for test MT3, but this is because the U(VI) concentrations increased to relatively high values (~12 μM), but the sensitivity calculations were not normalized by U(VI) concentration.

5.3.5 Complex Breakthrough Behavior

Breakthrough curves at well 25P1 were collected for tests MT2 and MT3 and the results are shown in Figure 5.8. In both cases, the breakthrough curves for each of the solutes were quite complex. In both tests, the breakthrough observed for Br had two distinct peaks that were observed at approximately 120 and 200-300 hr. These observations suggest that transport occurred along at least two unique flow paths, each of which was captured to some extent by the sampled well. The velocities along these flowpaths differed by only a factor of 3 or less, which is relatively small compared to other heterogeneous aquifers (Zinn and Harvey, 2003).

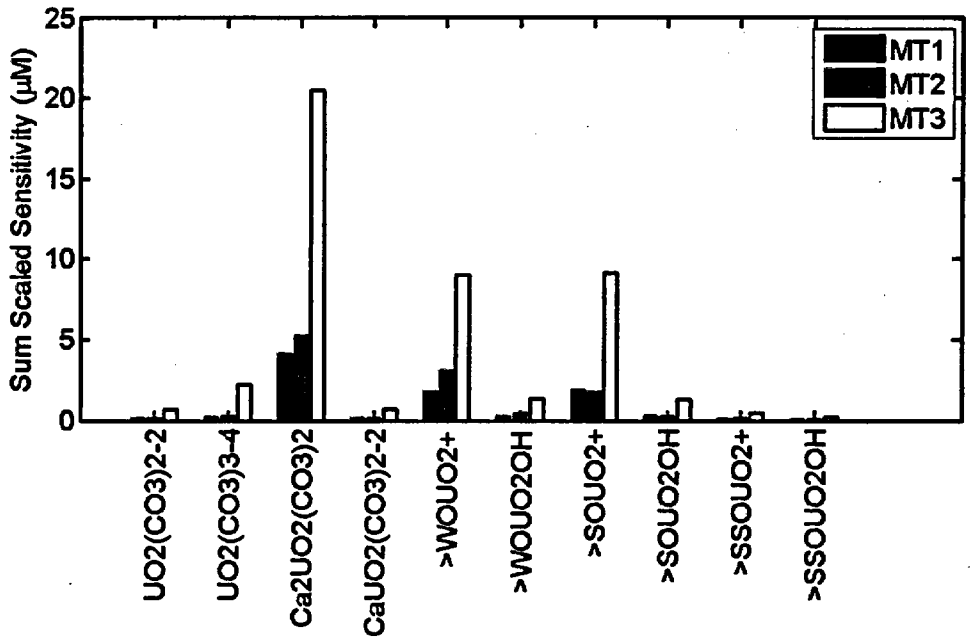

Figure 5.7 Sensitivity of simulated U(VI) concentration, at well A1 in test MT1 and well A3 in tests MT2 and MT3, to equilibrium constants for the predominant aqueous and surface species.

It was not possible to simulate this complex behavior with the quasi one-dimensional approach, which can only yield a single Br peak for a single injection (although the peak can be broad). However, it was possible to reproduce each of the two Br peaks observed in test MT2 by calibrating one quasi one-dimensional model to the first peak, using Br concentrations observed during the first 190 hr of the breakthrough, and then calibrating a second quasi one-dimensional model to the remaining data. Using this approach, a good fit to the observed Br data in test MT2 was obtained (Figure 5.8a) using the parameters listed in Table 5.4. Similarly, a good fit to the Br data was obtained for the MT3 test results as shown in Figure 5.8b. In both tests, the reactive transport models gave an excellent prediction of U(VI) concentrations, except for the U(VI) data collected after 200 hr in test MT2. In this latter case, the predictions show the observed temporal trends, but the U(VI) concentrations predictions are smaller than the observed data by approximately 1 μM. It is not clear why the U(VI) predictions were successful in test MT3 but apparently biased in MT2.

5.4 Conclusions

U(VI) that has been present in the Naturita aquifer for several decades can be readily desorbed by variable chemical conditions. In experiments where the alkalinity was increased from 8.8 to 24 meq/L (factor of 2.8), the U(VI) concentration increased from 4.3 to 14.7 μM (factor of 3.4). The cause of this increase in U(VI) concentration is the formation of aqueous $Ca\text{-}UO_2\text{-}CO_3$ complexes in the groundwater. The results clearly demonstrate that in environments where U(VI) concentrations are controlled by adsorption, dissolved U(VI) concentrations can be impacted by increases in alkalinity. Interestingly, increases in U(VI) concentration were also observed in experiments where the alkalinity was decreased. In experiments where the alkalinity was decreased from 8.8 to 2 meq/L (factor of 4.4), the U(VI) concentration initially decreased from 4.8 to 1.8 μM. Adsorption to the aquifer sediments causes this decrease in U(VI) concentration. However, when the alkalinity relaxed to its initial value, the additional adsorbed U(VI) desorbed, causing peak groundwater concentrations as high as 7 μM. Thus, a detailed understanding of U(VI) surface and aqueous speciation is required to predict changes in U(VI) concentration in the Naturita aquifer, and likely in other aquifers contaminated with U(VI).

The observed temporal changes in U(VI) concentration were reasonably well described by a reactive transport model that simulated adsorption reactions using the SCM approach. Although this model was previously shown to simulate U(VI) adsorption in long term, near steady-state experiments (Kohler et al., 2004; Curtis et al., 2004), the current results demonstrate the adequacy of the model for simulation of transient effects under the influence of a natural gradient. The model predicted both increases and decreases of U(VI) concentration reasonably well when the transport parameters were calibrated to observed Br transport. In contrast, a constant-K_d model would have predicted neither the observed increases nor decreases in U(VI) concentration

Table 5.4. Summary Of Nonreactive Transport Model Parameters for Bromide Breakthrough at Well NAT25P1

Tracer Test	Calibration Time(hr)	Velocity (m/hr)	Dispersivity (m)	k_{La} (hr^{-1})	Pulse Length (hr)
MT2	0-200	0.00658	0.0216	0.00135	29.5
MT2	200-500	0.00326	0.0510	0.00186	51.8
MT3	0-210	0.00576	0.00006	0.00198	34.0
MT3	210-500	0.00251	0.0389	0.00094	44.7

in tests MT2 and MT3, because the U(VI) concentration in the injectate was equal to that in the groundwater. This indicates that the uncertainty of predictions using the SCM approach were smaller than those that would have been obtained using a constant-K_d approach to model U(VI) sorption.

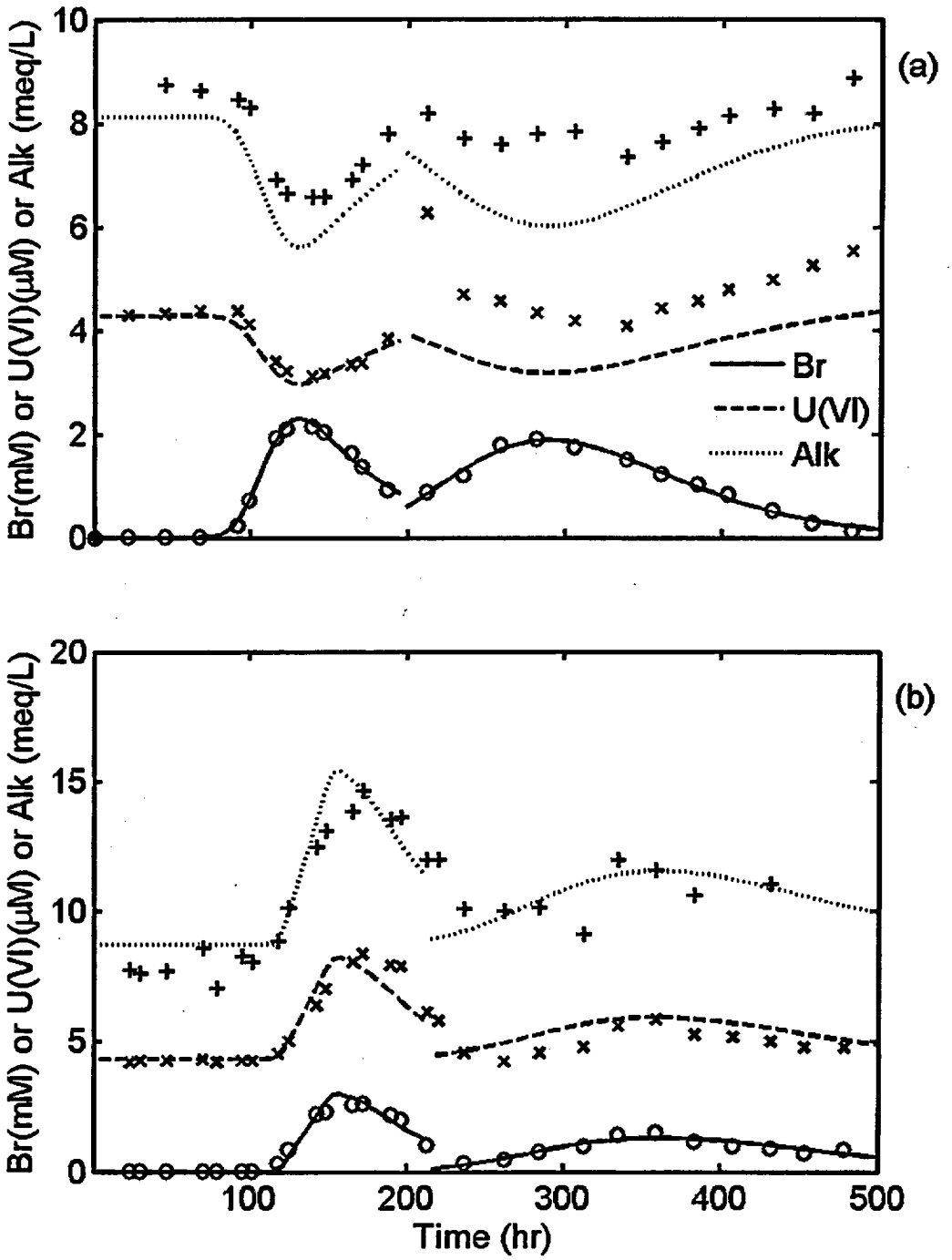

Figure 5.8. Observed and simulated bromide, U(VI) and alkalinity concentrations in migration tests MT2 and MT3 at observation well P1.

6 CONCLUSIONS

Simulations of reactive transport processes in groundwater often require many parameters as model inputs. These parameters include hydrologic parameters that describe flow and transport as well as reaction parameters that describe the chemical reaction network. While hydrologic parameters are most often determined from field tests such as pump tests, slug tests, or tracer tests coupled with model calibration, there is less agreement on how geochemical reaction parameters should be determined. For geochemical reaction processes, such as adsorption reactions, parameter values could be based on a variety of sources including tabulated thermodynamic data, laboratory experiments using site-specific materials, or field-determined values.

In this study, field-based techniques were tested for determining K_d values or for validating laboratory- or model-derived K_d values. The field site used for the study was the uranium mill tailings site at Naturita, Colorado (Davis and Curtis, 2003). The techniques included: 1) the use of downhole *in-situ* devices that held a sample of a single mineral or sediment that were deployed in the aquifer contaminated with uranium, 2) *in-situ* push-pull tracer tests conducted within the contaminated aquifer, and 3) small-scale U(VI) migration tracer tests conducted within the aquifer. The experiments were conducted on scales that ranged from centimeters for the downhole devices to several meters for the small-scale tracer tests.

6.1 Downhole *In-Situ* Devices

The use of downhole *in-situ* devices appeared to be quite successful in a previous application with mesh bags and uncontaminated Naturita sediments (Curtis et al., 2004). The experiments completed in this study were conducted as further tests of this method of measuring K_d values and as a measure of the applicability of surface complexation models to the field environment. The results suggest that either: a) the method or experimental approach needs further improvement, and/or b) current surface complexation models for kaolinite and hematite in the literature did not work well when applied to the aqueous chemical conditions in the Naturita aquifer. In particular, the ability of the kaolinite and hematite surface complexation models to predict U(VI) adsorption under conditions of high bicarbonate concentration is not well known. The quartz surface complexation model presented here was calibrated with data at high bicarbonate concentrations. However, the ability of this model to predict U(VI) adsorption could not be determined because of several factors, including the very low surface area of the quartz sample and the experimental error of the dialysis bag method related to entrained water collected with the sample. Improvements to the method and the deployment of larger quartz sample sizes in the well may solve some of these problems.

In-situ K_d values for U(VI) adsorption on samples of clinoptilolite and a 40-Mile Wash sediment composite were also made, but these values could not be compared with model-predicted values because of the lack of published models for these samples at present.

6.2 Push-Pull Tracer Tests

The experimental results illustrated that increases in groundwater alkalinity could quickly desorb U(VI) that had been present in the Naturita aquifer for several decades. Push-pull tracer tests that had contact times as little as 0.5 hr resulted in U(VI) concentrations that increased from an initial concentration of 0.05 μM in injected water to 2 μM in sampled groundwater. Higher concentrations, up to 17 μM, were observed in some experiments in which the alkalinity was increased.

It was concluded that push-pull test results were not useful in the Naturita aquifer for evaluating adsorption model parameters. This limitation results from the nearly reversible nature of the reactive transport simulations when applied to cases where sorption processes are probed by manipulating groundwater alkalinity. In

addition, the velocity and/or dispersive processes in this aquifer were sufficiently large that geochemical effects were dampened by dilution in most of the experiments. It is possible that push-pull tests would be more successful in environments where the groundwater velocity is small. In addition, push-pull tests may be useful for studying *rates* of sorption and desorption in aquifers.

6.3 Small-Scale U(VI) Migration Tracer Tests

U(VI) that has been present in the Naturita aquifer for several decades was readily desorbed by perturbing groundwater chemical conditions. In experiments where the alkalinity was increased from 8.8 to 24 meq/L (factor of 2.8), the dissolved U(VI) concentration increased from 4.3 to 14.7 μM (factor of 3.4). The cause of this increase in U(VI) concentration is the formation of aqueous Ca-UO_2-CO_3 complexes in the groundwater. The results clearly demonstrated that in environments where U(VI) concentrations are controlled by adsorption, dissolved U(VI) concentrations can be rapidly impacted by increases in alkalinity. Interestingly, increases in U(VI) concentration were also observed in experiments where the alkalinity was decreased. In experiments where the alkalinity was decreased from 8.8 to 2 meq/L (factor of 4.4), the U(VI) concentration initially decreased from 4.8 to 1.8 μM. Adsorption to the aquifer sediments causes this decrease in U(VI) concentration. However, when the alkalinity relaxed to its initial value, the additional adsorbed U(VI) desorbed, causing peak groundwater concentrations as high as 7 μM. Thus, a detailed understanding of U(VI) surface and aqueous speciation is required to predict changes in U(VI) concentration in the Naturita aquifer, and likely in other aquifers contaminated with U(VI).

The experimental observations in the U(VI) migration tests were reasonably well described by a reactive transport model that simulated adsorption reactions using the SCM approach. Although this model was previously shown to simulate U(VI) adsorption in long term, near steady-state experiments (Kohler et al., 2004; Curtis et al., 2004), the current results demonstrate the adequacy of the model for simulation of transient effects under the influence of a natural gradient. The model predicted both increases and decreases of U(VI) concentration reasonably well when the transport parameters were calibrated to observed Br transport. In contrast, a constant-K_d model would have predicted neither the observed increases nor decreases in U(VI) concentration in some of the tracer tests, because the U(VI) concentration in the injectate was equal to that in the groundwater. This indicates that the uncertainty of predictions using the SCM approach were much smaller than those that would have been obtained if a constant-K_d approach had been used to model U(VI) adsorption.

REFERENCES

Allison, J. D., Brown, D. S., and Novo-Gradac, K. J., "MINTEQA2/PRODEFA2, A Geochemical Assessment Model for Environmental Systems," Version 3.0 User's ManualEPA/600/3-91/021, 1991.

Anderson R. T. et al., "Stimulating the In-Situ Activity of Geobacter species to remove uranium from the groundwater of a uranium-contaminated aquifer," *Appl. Environ. Microbiol.*, Vol. 69, 5884-5891, 2003.

Arai, Y. et al., "Uranyl Adsorption and Surface speciation at the Imogolite-water Interface: Self-Consistent Spectroscopic and Surface Complexation Models," *Geochimica et Cosmochimica Acta*, Vol. 70, 2492-2509, 2006.

Bargar, J. R., Reitmeyer, R., and Davis, J. A., "Spectroscopic Confirmation of Uranium(VI)-Carbonato Adsorption Complexes on Hematite," *Environmental Science and Technology*, Vol. 33, No. 14, 2481-2484, 1999.

Barger, J.R. et al., "Characterization of U(VI)-Carbonato Cernary Complexes on Hematite: EXAFS and Electrophoretic Mobility Measurements," *Geochimica et Cosmochimica Acta*, Vol. 64, No. 16, 2737-2749, 2000.

Barnett, M.O. et al., "U(VI) Adsorption to Heterogeneous Subsurface Media: Application of Surface Complexation Model", *Environ. Sci. Technol*, Vol. 36, 937–942, 2002.

Barnett, M.O. et al., "Adsorption and Transport of Uranium(VI) in Subsurface Media," *Soil Sci. Soc. Am. J*, Vol. 64, 908–917, 2000.

Bernhard, G. et al., "Speciation of Uranium in Seepage Waters of a Mine Tailing Pile Studied by Time Resolved Laser-induced Fluorescence Spectroscopy (TRLFS)," *Radiochim. Acta*, Vol. 74, 87–91, 1996.

Bernhard, G. et al., "Uranyl(VI) Carbonate Complex Formation: Validation of the Ca2UO2(CO3)3(aq.) Species," *Radiochim. Acta*, Vol. 89, 511–518, 2001.

Bostick, B.C. et al., "Uranyl Surface Complexes Formed on Subsurface Media from DOE Facilities," *Soil Science Society of America Journal*, Vol. 66, No. 1, 99-108, 2002.

Brooks, S.C. et al., "Inhibition of Bacterial U(VI) Reduction by Calcium. Environ," *Sci. Technol*, Vol. 37, 1850–1858, 2003.

Caccavo Jr F. et al., "Geobacter Sulfurreducens Sp. Nov., a Hydrogen and Acetate-Oxidizing Dissimilatory Metal Reducing Microorganism," *Appl. Environ. Microbiol.*, Vol. 60, 3752-3759, 1994.

Crowley, K.D., and Ahearne, J.F., "Managing the Environmental Legacy of U.S. Nuclear Weapons Production," *Am. Sci*, Vol. 90, 514–523, 2002.

Curtis, G.P., Fox, P., Kohler, M., and Davis, J.A., "Comparison of In Situ Uranium KD Values with a Laboratory Determined Surface Complexation Model," *Appl. Geochem*, Vol. 19, 1643–1653, 2004.

Curtis, G.P., "Documentation and Applications of the Reactive Geochemical Transport Model RATEQ," Report NUREG CR-6871, *U. S. Nuclear Regulatory Commission*, Rockville, MD, 98, 2005.

Curtis, G. P., Davis, J.A., and Naftz, D.L., "Simulation of Reactive Transport of Uranium(VI) in Groundwater with Variable Chemical Conditions," *Water Resour. Res.*, Vol. 42, W04404, doi:10.1029/2005WR003979, 2006.

Davis, J.A., and Kent, D.B., "Surface Complexation Modeling in Aqueous Geochemistry: Mineral-water Interface Geochemistry," *Rev. Mineral*, Vol. 23, 177–260, 1990.

Davis, J. A. et al., "Application of the Surface Complexation Concept to Complex Mineral Assemblages," *Environ. Sci. Technol.*, Vol. 32, 2820-2828, 1998.

Davis, J.A. and Curtis, G.P., "Application of Surface Complexation Modeling to Describe Uranium(VI) Adsorption and Retardation at the Uranium Mill Tailings Site at Naturita, Colorado," Report NUREG CR-6820, *U. S. Nuclear Regulatory Commission*, Rockville, MD, 223, 2003 Available at:
http://www.nrc.gov/reading-rm/doc-collections/nuregs/contract/cr6820/cr6820.pdf,

Davis, J.A. et al., "Assessing Conceptual Models for Subsurface Reactive Transport of Inorganic Contaminants," EOS, Vol. 85, 449-455, 2004a..

Davis, J.A. et al., "Approaches to Surface Complexation Modeling of Uranium(VI) Adsorption on Aquifer Sediments," *Geochim. Cosmochim. Acta*, Vol. 68, 3621-3641, 2004b.

Davis, J.A. et al., "Processes Affecting Transport of Uranium in a Suboxic Aquifer," *Physics and Chemistry of the Earth, Parts A/B/C*, Vol. 31(10-14), 548-555, 2006.

Dong W. et al., "Influence of Calcite and Dissolved Calcium on Uranium(VI) Sorption to a Hanford Subsurface Sediment," *Environmental Science and Technology*, Vol. 39(20), 7949-7955, 2005.

Drever, J.I. and McKee, C.R., "The Push-Pull Test A Method of Evaluating Formation Adsorption Parameters for Predicting the Environmental Effects on In-Situ Coal Gasification and Uranium Recovery," *In Situ*, Vol. 4(3), 181-206, 1980.

Duff, M.C., and Amrhein, C., "Uranium(VI) Adsorption on Goethite and Soil in Carbonate Solutions," *Soil Sci. Soc. Am. J*, Vol. 60, 1393– 140, 1996.

Dzombak, D.A. and Morel, F.M.M., "*Surface Complexation Modeling: Hydrous Ferric Oxide*," John Wiley & Sons, New York, NY, 1990.

Fox, P.M., Davis, J.A., and Zachara, J.M, "The Effect of Calcium on Aqueous Uranium (VI) Speciation and Adsorption to Ferrihydrite and Quartz," *Geochimica et Cosmochimica Acta*, Vol. 70, 1379-1387, 2006.

Godsy, E.M., Warren, E., and Paganelli, V.V., "The Role of Microbial Reductive Dechlorination of TCE at a Phytoremediation Site," *International Journal of Phytoremediation*, Vol., 5, 73-88, 2003.

Grenthe, I. et al., *Chemical Thermodynamics of Uranium*, Amsterdam, North Holland, 715, 1992.

Guillaumont, R. et al., "Update on the Chemical Thermodynamics of Uranium, Neptunium, Plutonium, Americium, and Technetium," *Elsevier*, Amsterdam, 2003.

Haggerty, R. and Gorelick, S.M, "Multiple-Rate Mass Transfer for Modeling Diffusion and Surface Reactions in Media with Pore-Scale Heterogeneity," *Water Resources Research*, Vol. 31(10), 2382-2400, 1995.

Haggerty, R., Schroth, M.H. and Istok, J.D., "Simplified Method of "Push-Pull Test Data Analysis for Determining In Situ Reaction Rate Coefficients," *Ground Water*, Vol. 36, No. 2, March-April, 1998.

Hall, S.H., Luttrell, S.P., and Cronin, W.E., "A Method for Estimating Effective Porosity and Ground-Water Velocity," *Ground Water*, Vol. 29, No. 2, March-April, 1991.

Herbelin, A. L., and Westall, J. C., "FITEQL: A Computer Program for the Determination of Chemical Equilibrium Constants from Experimental Data," *Chemistry Department Oregon State University, Corvallis, Oregon*, Version 4.0, report 99-01, 1999.

Hsi, C.D. and Langmuir, D., "Adsorption of Uranyl onto Ferric Oxyhydroxides; Application of the Surface Complexation Site-binding Model," *Geochim. Cosmochim. Acta*, Vol. 49, No. 9, 1931-1941, 1985.

Istok, J.D. et al., "Laboratory and Field Investigation of Surfactant Sorption Using Single-Well, "Push-Pull" Tests," *Ground Water*, Vol. 37, No. 4, July-August 1999.

Istok, J.D. et al., "Single Well, 'Push-Pull' Test for In Situ Determination of Microbial Activities," *Ground Water*, Vol. 35, No. 4, July-August 1997.

Jeon, B-H. et al., "Chemical Reduction of U(VI) by Fe(II) at the Solid/Water Interface Using Natural and Synthetic Fe(III) Oxides," *Environ. Sci. Tech.*, Vol. 39, 5642-5649, 2005.

Kent, D.B. et al., "Modeling the Influence of Variable pH on the Transport of Zinc in a Contaminated Aquifer Using Semi-Empirical Surface Complexation Models," *Water Resources Research*, Vol. 36, 3411-3425, 2000.

Kohler, M. et al., "Experimental Investigation and Modeling of Uranium(VI) Transport Under Variable Chemical Conditions," *Water Resources Research*, Vol. 32, No. 12, 3539-3551, 1996.

Kohler, M. et al., "Methods for Estimating Adsorbed Uranium(VI) and Distribution Coefficients in Contaminated Sediments," *Environmental Science and Technology*, Vol. 38, 240-247, 2004.

Langmuir, D., *Aqueous Environmental Chemistry*, Prentice-Hall, Upper Saddle River, NJ, 1997

Leap, D. I. and Kaplan, P. G., "A Single-Well Tracing Method for Estimating Regional Advective Velocity in a Confined Aquifer: Theory and Preliminary Laboratory Verification," *Water Resources Research*, Vol. 24, No. 7, July 1988.

Lee, R.W. et al., "Phreatophyte Influence on Reductive Dechlorination in a Shallow Aquifer Contaminated with Trichloroethene (TCE)," *International Journal of Phytoremediation*, Vol. 2, 193-211, 2000.

Liger, E., Charlet, L., van Cappellan, P., "Surface Catalysis of Uranium(VI) Reduction by Iron(II)," *Geochim. Cosmochim. Acta*, Vol. 63, 2939-2955, 1999.

Liu C et al., "Influence of Sediment Bioreduction and Reoxidation on Uranium Sorption." *Environmental Science and Tech*nology, Vol. 39(11), 4125-4133, 2005.

Lovley D. R. et al., "Microbial Reduction of Uranium," *Nature*, Vol. 350, 413-416, 1991.

Morrison, S.J. and Cahn, L.S., "Mineralogical Residence of Alpha-emitting Contamination and Implications for Mobilization from Uranium Mill Tailings," *J. Contam. Hydrol.*, Vol. 8, 1-21, 1991.

O'Loughlin, E.J. et al., "Reduction of Uranium(VI) by Mixed Iron(II)/Iron(III) Hydroxide (Green Rust): Formation of UO_2 Nanoparticles," *Environ. Sci. Tech.*, Vol. 37, 721-727, 2003.

Pabalan, R.T., "Thermodynamics of Ion Exchange Between Clinoptilolite and Aqueous Solutions of Na+K and Na/Ca," *Geochim. Cosmochim. Acta*, Vol. 58, 4573-4590, 1994.

Pabalan, R.T. et al., "Uranium(VI) Sorption onto Selected Mineral Surfaces: Key Geochemical Parameters," *Adsorption of Metals by Geomedia*, Academic Press, 99-130, 1998.

Poeter, E. P. and Hill, M.C., "UCODE, a Computer Code for Universal Inverse Modeling," *U.S.Geological Survey, Water-Resources Investigations*, Rept. 98-4080, 1998.

Prikryl, J.D. et al., "Uranium(VI) Sorption Behavior on Silicate Mineral Mixtures," *J. Contam. Hydrol.*, Vol. 47, 241-253, 2001.

Qafoku N. et al., "Kinetic Desorption and Sorption of U(VI) During Reactive Transport in a Contaminated Hanford Sediment," *Environmental Science and Technology*, Vol. 39(9), 3157-3165, 2005.

Reinhard, M. et al., "In Situ BTEX Biotransformation under Enhanced Nitrate- and Sulfate-Reducing Conditions," *Environ. Sci. Technol.*, Vol. 31, 28-36, 1997.

Schroth, M.H., Istok, J.D. and Haggerty, R., "In Situ Evaluation of Solute Retardation Using Single-Well Push-Pull Tests," *Advances in Water Resources*, Vol. 24, 105-117, 2001.

Schroth, M.H. et al., "Spatial Variability in In-Situ Aerobic Respiration and Denitrification Rates in a Petroleum-Contaminated Aquifer," *Ground Water*, Vol. 36, No. 6, November-December 1998.

Senko, J.M. et al., "In-Situ Evidence for Uranium Immobilization and Remobilization," *Environ. Sci. Technol.*, Vol. 35, 1491-1496, 2002

Smith, R. M., and Martell, A. E., *Critical Stability Constants*, Volume 4, Inorganic Complexes, Plenum Press, New York, 1976.

Stollenwerk, K. G., "Molybdate Transport in a Chemically Complex Aquifer; Field Measurements Compared with Solute-transport Model Predictions," *Water Resour. Res.*, Vol. 34, 2727-2740, 1998.

Turner, G.D. et al., "Surface Charge Properties and UO22+ Adsorption of a Subsurface Smectite," *Geochim. Cosmochim. Acta*, Vol. 60, 3399–3414, 1996.

USEPA, "Understanding Variation in Partition Coefficient, K_d, Values," Vol. 1, *EPA* 402-R-99-0044A, Washington, DC, 1999.

USDOE, "Programmatic Environmental Impact Statement for the Uranium Mill Tailings Remedial Action Ground Water Project," *U.S. Department of Energy*, Grand Junction Office, Vol. I, No. DOE/EIS-0198, 314, 1996.

Valocchi, A.J., "Effect of Radial Flow on Deviations from Local Equilibrium During Sorbing Solute Transport Through Homogeneous soils," *Water Resources Research*, Vol. 22, 1693-1701, 1986.

Waite, T.D. et al., "Uranium(VI) Adsorption to Ferrihydrite: Application of a Surface Complexation Model," *Geochimica et Cosmochimica Acta,* Vol. 58, No. 24, 5465-5478, 1994.

Wang Z. et al., "Cryogenic Laser Induced U(VI) Fluorescence Studies of a U(VI) Substituted Natural Calcite: Implications to U(VI) Speciation in Contaminated Hanford Sediments," *Environmental Science and Technology*, Vol. 39, 2651-2659, 2005a.

Wang Z. et al., "Fluorescence Spectroscopy of U(VI)-Silicates and U(VI)-Contaminated Hanford Sediment," *Geochimica et Cosmochimica Acta*, Vol. 69(6), 1391-1403, 2005b.

Wersin, P. et al., "Interaction Between Aqueous Uuranium(VI) and Sulfide Minerals: Spectroscopic Evidence for Sorption and Reduction," *Geochim. Cosmochim. Acta*, Vol. 58, 2829-2843, 1994.

Zheng, Z., Tokunaga, T.K., and Wan, J., "Influence of Calcium Carbonate on U(VI) Sorption to Soils," *Environ. Sci. Technol*, Vol. 37, 5603–5608, 2003.

Zinn, B., and Harvey, C. F., "When Good Statistical Models Of Aquifer Heterogeneity Go Bad: A Comparison of Flow, Dispersion and Mass Transfer in Multigaussian and Connected Conductivity Fields," *Water Resources Research*, Vol. 39(3), 1051, 2003.

NRC FORM 335 (9-2004) NRCMD 3.7

U.S. NUCLEAR REGULATORY COMMISSION

BIBLIOGRAPHIC DATA SHEET

(See instructions on the reverse)

1. REPORT NUMBER (Assigned by NRC, Add Vol., Supp., Rev., and Addendum Numbers, if any.)

NUREG/CR-6911

2. TITLE AND SUBTITLE

Tests of Uranium(VI) Adsorption Models In A Field Setting

3. DATE REPORT PUBLISHED

MONTH	YEAR
August	2006

4. FIN OR GRANT NUMBER

Y6462

5. AUTHOR(S)

G.P. Curtis, J.A. Davis

6. TYPE OF REPORT

7. PERIOD COVERED *(Inclusive Dates)*

8. PERFORMING ORGANIZATION - NAME AND ADDRESS *(If NRC, provide Division, Office or Region, U.S. Nuclear Regulatory Commission, and mailing address; if contractor, provide name and mailing address.)*

Water Resources Division
U.S. Geological Survey
Menlo Park, CA 94025

9. SPONSORING ORGANIZATION - NAME AND ADDRESS *(If NRC, type "Same as above"; if contractor, provide NRC Division, Office or Region, U.S. Nuclear Regulatory Commission, and mailing address.)*

Division of Fuel, Engineering, and Radiological Research
Office of Nuclear Regulatory Research
U.S. Nuclear Regulatory Commission
Washington, D.C. 20555-0001

10. SUPPLEMENTARY NOTES

A. L. Schwartzman, NRC Project Manager

11. ABSTRACT *(200 words or less)*

Field-based techniques were tested for determining Kd values or for validating model-derived Kd values. The field site studied was a former uranium mill tailings site at Naturita, Colorado. The tests included: 1) in-situ devices that held a sample of a single mineral or sediment in the aquifer, and 2) small-scale tracer tests. The tracer tests demonstrated that, in aquifers where U(VI) concentrations are controlled by adsorption, dissolved U(VI) concentrations can be rapidly impacted by changes in alkalinity. In migration tests, U(VI) transport was reasonably well described by a reactive transport model that simulated adsorption with a semi-mechanistic surface complexation model. The results demonstrated the adequacy of the model for simulation of transient geochemical effects. It was concluded that push-pull test results were not useful in the Naturita aquifer for evaluating adsorption model parameters. Dispersive processes in the aquifer were sufficiently large that geochemical effects were dampened by dilution in most of these experiments. The results with in-situ devices for measuring Kd values indicated that the method needs further improvement. The experiments also suggested that surface complexation models for single minerals need to be calibrated in solutions with high dissolved carbonate concentrations in order to be applied to most aquifers.

12. KEY WORDS/DESCRIPTORS *(List words or phrases that will assist researchers in locating the report.)*

surface complexation model (SCM)
uranium mill tailings site
Naturita, Colorado
field techniques
U(VI)
Kd value
adsorption
in-situ

13. AVAILABILITY STATEMENT

unlimited

14. SECURITY CLASSIFICATION

(This Page) unclassified

(This Report) unclassified

15. NUMBER OF PAGES

16. PRICE

Federal Recycling Program